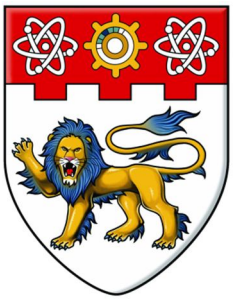

NANYANG TECHNOLOGICAL UNIVERSITY

First Principles Study on Silicon Nanostructures as Potential Anode Materials for Li-ion Batteries

Vadym Kulish

A Ph.D. thesis submitted to School of Materials Science and Engineering,
Nanyang Technological University

2013

ACKNOWLEDGEMENTS

I wish to express my gratitude to my supervisor Prof. Chen Zhong for the opportunity to study in Nanyang Technological University and the chance to learn from his expertise and experience. I am thankful for his guidance, continuous support, patience and inspiration over the years. I would like to thank my co-supervisor Dr. Ng Man-Fai for his notable suggestions and valuable advises. Many interesting ideas have been generated during our discussions. I want to thank Prof. Wu Ping for sharing his knowledge and experience in computer simulations. His advises and explanations were always helpful for me, and I am grateful for his enthusiasm in discussing many scientific problems and concepts with me. I wish to thank Prof. Andriy Gusak for introducing me into the world of scientific research. I am grateful to my teachers and friends from Cherkasy National University.

I am thankful to the members of my thesis advisory committee. The regular meetings, presentations and discussions with them have been very useful to me.

Many thanks go out to my colleagues and friends, Oleksandr Malyi and Matus Dubecky, for many interesting and useful discussions.

I wish to thank to my family and my wife for their love, care and support.

TABLE OF CONTENTS

LIST OF FIGURES

ABSTRACT

Rechargeable lithium-ion (Li-ion) batteries are the popular power sources in most of portable electronic devices, power tools and electric vehicles (EVs). Moreover, Li-ion batteries play an important role in the development of clean and efficient energy, serving as prominent energy storage devices for renewable energy sources, such as solar and wind. The emerging applications greatly raise the level of demands to batteries performance, however, existing Li-ion battery technology is reaching its limit, due to its relatively low Li storage capacity. The ever-growing demand for next-generation batteries requires electrode materials with larger capacity and higher power density, faster ionic diffusion and electronic transfer, lower cost and environmental friendliness. Silicon is among the promising novel anode materials for Li-ion batteries. The specific capacity of Si is an order of magnitude higher than that of conventional graphite anode, but the large volume expansion of bulk Si during lithiation and subsequent poor cycling behavior hinder its commercial use. The use of Si nanostructures was shown to be able to provide the means to overcome the abovementioned challenges. This thesis aims at the computational design and evaluation of novel Si-based nanostructures for their potential use in Li-ion battery anodes.

Firstly, we investigate silicon cluster/carbon nanotube (Si/CNT) hybrid nanostructures, where CNTs serve as a buffer and mechanical support for Si. The strength of Si/CNT interface is at the main focus here, in order to maintain electric contact and prevent Si particles from detachment and agglomeration. Since the interaction of Si cluster with pristine CNT is relatively weak, the functional groups (linkers) are introduced, aimed to enhance Si-CNT binding. We systematically evaluate the effects of the main components

(i.e. Si cluster, CNT support and linker) on the properties of hybrid system, such as morphology, interfacial bonding and electronic structure. From our calculations, we determine a suitable design strategy of Si/CNT hybrids, which not only increases the binding strength between Si clusters and CNT by 3 times under normal conditions, but also greatly contributes to the stability of hybrid material during lithiation.

Secondly, we theoretically study the properties of novel Si nanotubes of two structural types – hexagonal and gearlike. From our calculations, SiNTs show higher reactivity toward the adsorption of Li adatoms than CNTs and Si nanoclusters. Considering the importance of Li kinetics, we demonstrate that the interior of SiNTs may serve as a fast Li diffusion channel. The important advantage of SiNTs over its carbon analogues is 7 times reduction of energy barrier for the sidewall penetration of Li atoms into the nanotube interior. The improvements are attributable to the large void spaces, serving as fast Li diffusion pathways. This prepossesses the easier Li diffusion inside the tube and subsequent utilization of interior sites, enhancing the Li storage capacity of the system.

Finally, we use first principles calculations to investigate novel ultrathin silicon nanosheets (SiNSs) with a thickness of only few nanometres. Calculations show that binding energy of Li shows a strong dependency on the thickness of Si nanosheets; meanwhile, in all cases the surface sites are the most energetically favorable for Li insertion. Most importantly, our results show that Li diffusion on the surfaces of Si nanosheets is very fast (the activation barrier is more than 0.3 eV smaller on the surface than in the bulk). In addition, Li diffusion in nanosheets is very sensitive to their surface chemistry (e.g. passivation with hydrogen or halogens). Considering the high surface-to-volume ratio of nanosheets and fast Li surface diffusion, these results show a great

potential of these nanostructures as electrode materials for the next-generation Li-ion batteries.

In conclusion, detailed computational studies are performed which may serve as guidelines for the development of Si nanostructured anodes in the future. Novel nanostructures are investigated, and the correlation between structural features, dimensional effects, surface functionalization and Li insertion characteristics are established. This study demonstrates the viability of using computations to design novel electrode materials with improved properties. Similar computational methodology can be applied in the future studies of alternative electrode materials and other battery chemistries, such as sodium-ion and magnesium-ion.

Chapter 1

Literature Review

In this Chapter, the current research trends in rechargeable Li-ion batteries are reviewed. The main considerations about the choice of material for anodes are presented. Important literature findings from related studies are reviewed in order to show the main routes for structural design of Si nanostructures for Li-ion batteries application. The possible ways to improve the performance and cycle life of Si anodes are shown.

1.1. Rechargeable Li-ion batteries

Energy storage and conversion are among the most important challenges in the 21st century. As technology creates more complex machines and gadgets with increased portability, improved functionality and reduced size, there is a strong need in efficient energy systems that will power these devices. Thus there is a favor for environmental-friendly, high-performance and low-cost storage systems.

Rechargeable (or secondary) batteries are the electrochemical devices that convert the energy of chemical reactions into electrical energy.[1, 2] Since their invention, batteries have become a common power source for the many household and industrial applications. Currently, the most common types of rechargeable batteries are: lead-acid, nickel-cadmium (Ni-Cd), nickel-metal hydride (Ni-MH), lithium-ion (Li-ion) and lithium-air (Li-air).

The first rechargeable Li-ion battery was commercialized by Sony in 1991 and now it is the key-part of most portable electronic devices, such as laptops, cell phones,

and cameras. It provides several key advantages over other battery technologies (e.g. lead-acid and Ni-Cd): high energy density (energy-to-weight ratio), long cycle life, low toxicity, low self-discharge, and flexible design. The range of applications of Li-ion batteries is rapidly growing, covering new markets and setting higher performance demands. In telecommunication applications, rechargeable batteries had powered nearly 5 billion cellular phones by the end of 2009.[3] With respect to the expanded use of renewable energy resources, such as solar cells and wind power, the further development of this industry will rely on the rechargeable batteries as large scale energy storage. Moreover, a renewed interest in electric vehicles (EVs) in the 2000s is largely attributable to the technological developments in Li-ion batteries, as well as the reduction of their cost.[4] For instance, Tesla Motors was founded in 2003 to develop modern electric vehicles. By the year of 2009, the company was producing a high-performance sports car and planned to build a sedan. Most major automobile companies now have plug-in hybrid-electric and all-electric-vehicle programs, and some plan to produce EVs within the next few years. It is predicted that plug-in hybrid electric vehicles sales in the USA will increase to about 90 000 annually in 2015 and account for 1.7% of the total light-duty vehicle stock in 2030. Importantly, all main EV programs plan to use Li-ion batteries.[4]

Typical Li-ion battery is composed of the negative electrode (anode), positive electrode (cathode) and conducting electrolyte (Figure 1.1). The most popular anode material currently is graphite. There are three main choices for the cathode material: layered oxides such as $LiCoO_2$, transition metal phosphates such as $LiFePO_4$, or spinels such as $LiMn_2O_4$.[5] The two electrodes are separated by the ion conductive electrolyte, which consists of lithium salts, such as $LiPF_6$, $LiBF_4$, or $LiClO_4$, in an organic solvent such as alkene carbonates or mixtures of carbonates, amides, or imides.[6] Conductive additives (e.g. carbon black) are commonly added to the electrodes to enhance the electrical conductivity of the materials. A separator is used to prevent short circuit between the negative and positive electrodes and to provide abundant channels for the motion of Li ions. During the battery charging, Li ions are extracted from the cathode, transported through the conducting electrolyte and then inserted into the anode. On discharging, the Li ions migrate in the opposite direction (from anode to cathode) under the opposite electrical potential gradient. Physical, chemical, electronic properties of materials used in anode, cathode and electrolyte effect strongly the performance of the battery, its capacity, voltage and safety.

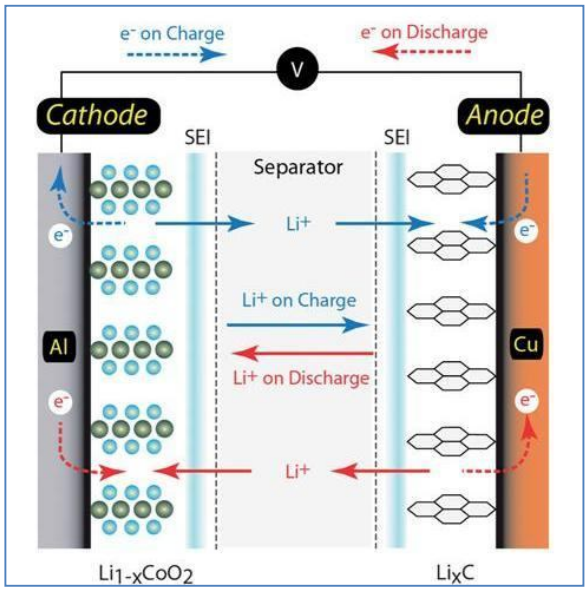

Figure 1.1. The schematic construction of Li-ion battery.[7]

The ever-growing demands for the improved performance of Li-ion batteries have motivated an extensive research interest and technological search for the new electrode materials and reactions. The main improvements are expected in terms of: (1) larger capacity; (2) higher reactivity, reversibility and structural stability during battery cycling; (3) faster ionic and electronic transfer; (4) lower cost and environmental friendliness. The behavior of any device depends critically on the properties of materials, on which it is built; therefore, in order to achieve the improvement in Li-ion battery performance, the advances in electrode materials science are strongly important.

1.2. The choice of anode material

To compare the advantages and disadvantages of different electrode materials, some general properties of electrodes are usually discussed. Thus, energy storage ability of battery is described with the terms *"specific energy"* (Wh/kg) and *"energy density"* (Wh/L). It is desirable that the amount of energy stored in a given mass or volume is as high as possible. The above properties depend on the *cell potential* (V) and

specific capacity (mAh/g), both of which are linked directly to the chemistry of electrode materials. Generally, the cell potential is also a function of the state of charge.

The ***specific capacity*** of an electrode can be calculated from the following expression:

$$Specific\ Capacity = \frac{\Delta x \cdot F}{M} \times \frac{1000}{3600}\ [mAh/g]$$

where Δx is the number of moles of Li that can participate in the electrochemical reaction, F is the Faraday constant and M is the molar mass of the electrode material. Here, Δx indicates how much Li can be stored in the electrode material and it depends on the number of Li insertion sites, energetically favorable and available in the crystal structure of electrode.

The ***rate capability*** of Li-ion battery is associated with *"specific power"* (W/kg) and *"power density"* (W/L), i.e. energy density divided by the time of battery discharging. The specific power and power density are strongly related to the rate of Li diffusion and electrons transport inside electrodes. The fast migration of Li and electrons is desirable to achieve high rate capability, and hence rapid charge/discharge rates.

Cycle life is defined as the number of charge/discharge cycles that can be performed before specific capacity of the electrode falls below a certain cut-off limit. To maintain a long cycle life, electrode materials should remain stable during insertion and deinsertion of Li ions. At the same time, electrode material should be stable in contact with electrolyte.

Reactions on electrodes should be highly reversible to maintain the specific charge during many charge/discharge cycles.

Finally, good electrode material is expected to have a low cost, easy fabrication procedure and be safe.

While keeping in mind the above requirements, various materials have been successfully examined as potential anode materials in Li-ion batteries, such as transition-metal oxides[8] (TiO_2,[9, 10] Fe_2O_3,[11] Co_3O_4,[12, 13] V_2O_5[14, 15]), lithium alloys,[16, 17] chalcogenides (TiS_2), polymers and others (Figure 1.2).

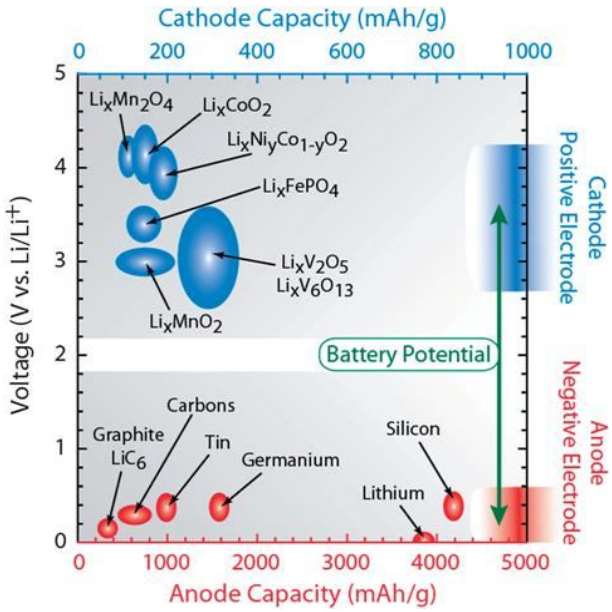

Figure 1.2. Comparison of different battery materials. Silicon possesses much higher theoretical capacity, than commercially used graphite.[7]

1.3. Silicon versus graphite

Graphite is currently used as a conventional anode material in Li-ion batteries. It has a high Coulumbic efficiency (the ratio of the extracted lithium to the inserted lithium is >95%) – which means that many repeatable lithium insertions and removals can occur in graphite anode without any significant loss in capacity over cycling.[18] However, its Li storage capacity is relatively low (372 mAh/g), which is not enough for the rapidly

developing Li-ion battery applications. Thus, there is a need to explore and develop alternative anode materials. In this respect, various candidates have been examined, such as Group IV materials (i.e. Si, Ge, Sn) and their compounds, transitional oxides, chalcogenides, etc.

Silicon is of particular interest as novel anode material for Li-ion batteries, because it has a low discharge potential (~370 mV vs. Li/Li+) and it is the second most abundant element in the Earth crust. Most importantly, Si has the highest theoretical capacity - 4200 mAh/g in $Li_{22}Si_5$ phase at high temperatures (Figure 1.2), and 3579 mAh/g in $Li_{15}Si_4$ at room temperature.[16, 17] Unfortunately, the enormous volume expansion (>300%) occurs in Si during insertion and extraction of lithium, which leads to the cracking of anode and fade of charge storage capacity with battery cycling. This is well illustrated in Figure 1.3a, which shows the change in specific capacity of amorphous Si film anodes with time.[19] The anodes show near theoretical capacity in the beginning, but after several cycles the capacity starts to decrease dramatically. Figures 1.3b-c show the evolution of Si anode with time: Si film breaks to the small islands, forming cracks, what eventually leads to the loss of electrical contact and severe capacity fading. Several strategies were proposed recently to overcome the above-mentioned problems, the main being reducing Si particle size to nanoscale dimensions and building Si-based composites. Both strategies will be discussed in the following sections of this report.

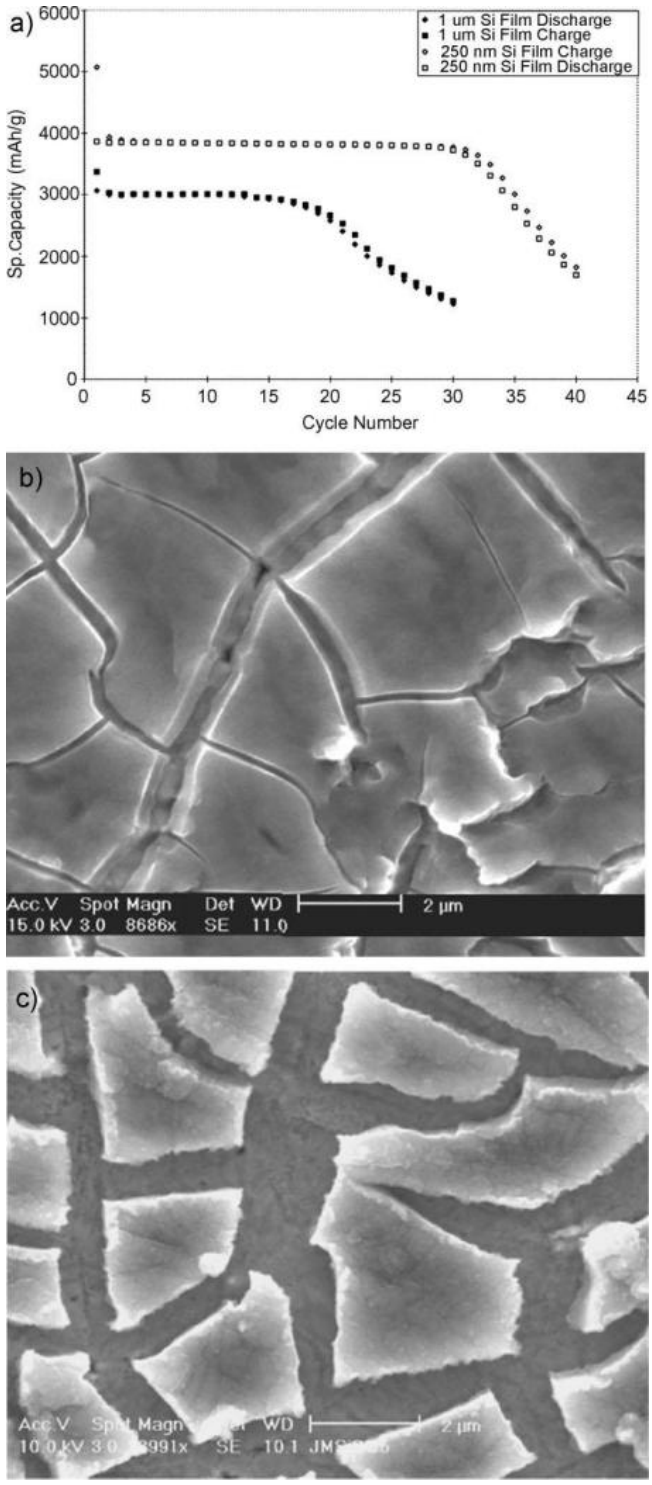

Figure 1.3. Characterization of amorphous Si films as the battery anode. a) Specific capacity plotted as a function of cycle number. b-c) Stress-induced cracking of the film during cycling.[19]

1.4. Silicon Nanostructured Anodes

Nanostructured electrodes offer a wide range of potential advantages,[20-22] as compared to the bulk materials:

(i) Better accommodation of strain/stress associated with the Li insertion, improving cycle life;

(ii) New reactions not possible with bulk materials (as demonstrated on the example of nanoparticles of transition metal oxides);

(iii) Short path lengths for Li diffusion, improving charge/discharge rates of Li-ion battery;

(iv) Enhanced electronic transport;

(v) Larger electrode/electrolyte contact area, leading to higher Li-ion flux across the interface.

The above benefits motivated extensive research studies, particularly, in the field of Si-based anodes for Li-ion batteries. It has to be noted that the capacity, reversibility and cycle life can vary widely between nanostructured silicon materials of similar morphology and size. The differences may appear from the variations in synthesis conditions; binder and conductive additives; the ratio of active/inactive material; charge/discharge rates during cycling; voltage cut-offs, etc. The wide variation of controllable parameters and, as a result, reported electrochemical performance makes it difficult to directly compare and conclude which particular morphology is superior over others. Instead, the focus of many recent works has been on the general trends in anode performance.[23]

1.4.1. Silicon 0-D nanoparticles

Electrodes comprised of 78-nm Si powder showed improved reversible capacity of 1700 mAh/g over 10 cycles.[24] Graetz et al. prepared Si anodes made of nanocrystalline particles (12 nm mean diameter), which exhibited specific capacity of 1100 mAh/g with a capacity retention of 50% after 50 cycles.[25] It has been shown that there is a critical Si nanoparticle diameter of ~150 nm, below which the particles neither cracked nor fractured upon first lithiation. In another work, it has been successfully demonstrated that 10 nm sized Si particles showed higher charge capacity as compared to 20 nm ones. Moreover, when carbon coating was applied to 10 nm sized Si nanoparticles, both Coulombic efficiency and capacity retention were significantly improved, to 89 and 96%, respectively.[26] It was suggested that electrical contact between the particles can be maintained via the use of surface coating (i.e. carbon, aluminum), as well as use of conductive additives or binders. The above studies demonstrate improved anode performance, however, it has been reported that nanoparticles tend to agglomerate after Li insertion/extraction and increase in size, resulting in poor Li kinetics and pulverization during cycling.[27] An attractive solution to this problem is to disperse nanoparticles on the rigid conductive support, such as carbon nanotubes, graphene, etc.[28-30]

1.4.2. Silicon 1-D nanowires

One dimensional (1-D) nanostructures offer a wide range of beneficial properties, when used as electrodes in Li-ion batteries. One of the most successful examples has been recently reported by Chan et al.[31] In their work, the authors reported synthesis and subsequent electrochemical testing of Si nanowires (SiNWs), grown directly on current collector substrates using the vapor-liquid-solid (VLS) technique. The electrochemical performance of SiNWs is remarkable – Chan et al. achieved the theoretical charge capacity for Si anodes and maintained a discharge capacity close to 75% of the maximum,

with little fading during cycling.[31] The average diameter of pristine, unreacted SiNWs was ~89 nm, while after charging with Li, it increased to ~141 nm. Despite the volume changes, the nanowires remained intact and did not break into smaller particles. In this case, the volume expansion of Si can be well accommodated by the space between adjacent nanowires. Besides, the 1-D geometry of SiNWs offers several key advantages over the bulk and nanoparticle-based counterparts. First, nanowires provide direct 1-D electronic pathway, which promotes efficient charge transport. Second, each individual nanowire is directly connected to the metallic current collector, ensuring a robust electrical contact to be maintained. Third, small diameter of SiNWs allows for a facile volume relaxation and deformation without fracturing. Finally, no binders or conducting additives are needed, which add extra weight and lower the overall specific capacity of the battery.[31]

The improved battery performance of Si nanowire-based anodes has been reported in many recent studies. For instance, Chockla et al. prepared a nonwoven fabric of crystalline SiNWs with a specific capacity of 800 mAh/g after 20 cycles.[32] Liu et al. presented a method for prelithiating a SiNW anode by a facile self-discharge mechanism, which can be further used in pairing with sulfur cathode for the preparation of Li-free electrodes in future Li-ion batteries.[33] Improved cycling life and capacity retention were obtained in electrodes, comprised of highly interconnected SiNWs.[34] A high specific capacity of 1600 mAh/g after 250 cycles at a current rate of 1C was achieved in porous Si nanowires fabricated by Ge et al.[35] The studies demonstrate that the electrochemical performance of SiNW-based electrodes depends on a wide range of factors, such as coating,[36-38] size,[37] electronic conductivity,[39] crystallographic orientation,[40-43] etc. The tremendous advances in the understanding of lithiation behavior of Si nanostructured anodes can be obtained from the recent *in situ* TEM studies.[36, 40, 44-46]

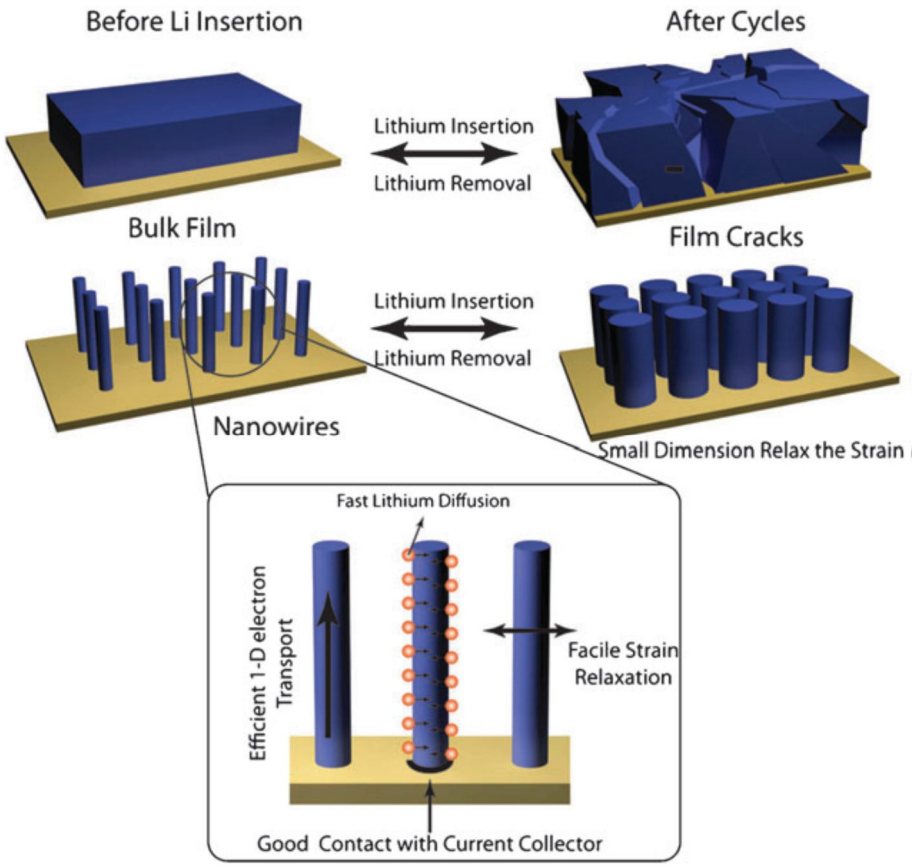

Figure 1.4. Advantages of using arrays of 1-D nanomaterials vs. their bulk counterparts as electrode materials for Li-ion batteries.[47]

In order to fully enjoy the benefits of 1-D architecture, it is possible to design a wide range of possible Si nanostructured anodes. For instance, it was found that Si crystalline/amorphous core/shell nanowires show significant improvements in both power density and cycle life when used as anodes.[48, 49] Generally, amorphous silicon (a-Si) has better cycling performance than crystalline (c-Si) since volume expansion in a-Si upon lithiation is homogeneous and exhibits less pulverization. Another important feature is that a-Si reacts with Li at a slightly higher potential than c-Si does. When limiting the charging potential, it is possible to utilize only the amorphous shell as active material while using the crystalline core as a mechanical support. To verify this idea, Chan et al. tested c-Si/a-Si core-shell NW samples at 150 mV cutoff and achieved a reversible

capacity of 1060 mAh/g with a stable NW morphology retention after more than 15 cycles.[48]

1.4.3. Silicon 1-D nanotubes

Another possibility is designing Si tubular nanostructures as Li-ion battery anodes. Si nanotubes (SiNTs) can be fabricated by a chemical vapor deposition (CVD) of Si onto a template of dense nanorods (i.e. ZnO, Ge, etc.), following by selective removal of this template. By utilizing this method, it is possible to produce silicon nanotubes with uniform, well-controllable wall thickness and inner diameter (down to as small as 1.5 nm).[50, 51] The first SiNT anodes have been reported in 2009 by Park et al. and demonstrated impressive reversible capacities of 3200 mAh/g and capacity retention of 89% after 200 cycles at a rate of 1C in practical Li-ion cells.[52] The superior performance can be rationalized by the fact that SiNTs possess a high surface area accessible to the electrolyte, which allows the Li ions to intercalate both at the exterior and interior of the nanotubes. Furthermore, Song et al. have developed a theoretical mechanics model, describing the stresses that occur in SiNTs during lithiation.[53] Theoretical analysis of the mechanics suggested that the additional free surfaces at the interior space of nanotubes improve the ability of these nanostructures to accommodate Si volume expansion without mechanical fracture. Song and co-workers further confirm their theoretical model with experimental testing. In their work, arrays of Si nanotubes exhibit high initial Coulumbic efficiencies (>85%) and stable capacity retention (>80% after 50 cycles).[53] Scalable and versatile fabrication of Si nanotubes through surface sol-gel reaction was reported by Yoo et al., as well as their further application in Li-ion battery anodes.[54]

The idea of using empty space to store the volume changes of Si has been realized in hollow or porous Si nanomaterials. For instance, 3D porous Si particles can maintain a

specific capacity of more than 2800 mAh/g even at a high rate of 1C due to fast intercalation kinetics and transport of Li ions, as well as accommodation of volume expansion inside the pores.[55] A high initial discharge capacity of 2725 mAh/g with less than 8% capacity degradation every hundred cycles for 700 total cycles (which is the longest ever for silicon anodes) has been achieved in interconnected Si hollow nanospheres.[56] Encapsulation of Si nanoparticles inside the rigid carbon matrix has proven to be another successful electrode design strategy. In such case, the void space between the nanoparticles and the carbon shell allows for Si expansion, meanwhile, carbon shell enhances the electronic conductivity of anode without preventing Li transfer to Si particles. Cui et al. and Yushin et al. reported easy and scalable fabrication of SiNP@carbon yolk-shell[57] and Si@carbon nanotube[58, 59] based electrodes, exhibiting a high stability after 1000 and 200 cycles, respectively.

1.4.4. Silicon 2-D thin films

Silicon thin films have also demonstrated improved capacity and reversibility during cycling. For instance, Si films with a thickness of 100 nm exhibit stable capacity retention of 2000 mAh/g over 50 cycles.[25] Maranchi et al. reported the electrochemical properties of amorphous 250 nm and 1 μm silicon films deposited by radio-frequency magnetron sputtering on copper foil,[60] meanwhile, Ohara et al. tested Si films vacuum-deposited on Ni surface.[61] These works revealed an important observation that the decreasing the Si film thickness significantly enhances its stability. As shown by Maranchi et al., 250 nm-thick films maintain steady capacity for 30 cycles, while thicker 1 μm films fade substantially just after 12 cycles.[60] Li et al. have suggested that there is a critical thickness for amorphous Si thin film, below which the material would not crack. By reducing the thickness below this critical value, it may be thus possible to create

crack-free electrode materials.[62] The performance of Si thin films can be further improved, if the rigid substrates (e.g. stainless steel current collectors) that constrain the "free" expansion/contraction of the Si anodes during charge/discharge are replaced by soft substrates. The main mechanism for stress relaxation here is that the volumetric strain in Si that is induced by charge/discharge cycling can buckle the flat Si thin films when they are on soft, flexible substrates, which in turn releases the stress in the Si films.[63]

Although high capacities were reported in Si films, but the above studies also demonstrate that it is very necessary to use extremely thin films to achieve reasonable cycle lifetimes of Li-ion batteries. Keeping in mind the recent advances in fabrication of ultra-thin (from 2 nm down to few-layer) Si nanosheets,[64-67] it makes sense to examine the possibility of their application as anodes. At the moment, such studies are very rare,[68] nevertheless, the successful implementation of nanosheets of other materials (e.g. MoS_2,[69] TiO_2,[10, 70, 71] SnO_2,[72, 73] SnS_2[74]) in Li-ion batteries demonstrate a great potential of these nanostructures. In this respect, theoretical density functional theory (DFT) calculations can serve as a useful tool for the evaluation of Si nanosheets as future anode materials.

1.5. Silicon Nanocomposite Anodes

Another attractive strategy towards the performance improvement of Si anodes is constructing Si-based nanocomposites and hybrid structures. The basic idea of active/inactive nanocomposite is to mix to materials, one (e.g. silicon) reacting with lithium, while the other acting as a buffer and mechanical support. Following the concept of Wilson and Dahn,[75] the nano-Si/C composites have attracted tremendous research attention, since they combine the benefits of Li-Si alloy with the reversibility of the

carbonaceous hosts. For example, a mixture of pure Si powder (78 nm in size) and carbon black exhibited a reversible capacity of 1700 mAh/g after 10 cycles.[24] Dispersion of nanocrystalline Si powder inside carbon matrix demonstrated a good reversible capacity of 1450 mAh/g when used as battery anode.[76] Two common strategies for the synthesis of Si/C composites have been mechanical ball milling of the active and matrix materials, or pyrolysis of silicon and carbon precursors to yield silicon embedded in a carbonaceous matrix. The prolonged ball milling and uniform carbon deposition during pyrolysis may result in a better contact between carbon and silicon, enhancing electronic conduction and surface passivation. The typical reversible capacities of ball milled Si/C nanocomposites range from 500 – 1000 mAh/g.[77-79] The improved capacities of ball milled composites may be attributed to the small particle sizes (typically on the order of a few tens of nm), and may also benefit from the dispersion of conductive additives such as graphite, carbon blacks, and carbon nanotubes. On the other hand, Si/C nanocomposites fabricated via pyrolysis of organic precursors mixed with silicon nanoparticles demonstrate slightly lower reversible capacities,[80] which may be attributed to the higher percentage of the inactive species that does not contribute to the anode capacity. Other factor may be the larger size of silicon particles (100 nm or greater in diameter) which then agglomerate into even larger particles leading to further fracture and pulverization during cycling. It has to be noted that the common problem with the above mentioned Si-composites has been the agglomeration of Si particles with the subsequent fracture and pulverization. Although the improved reversible capacities have been demonstrated, but the cycle life of Si/C composites was still far from satisfactory. From this point of view, a simple mixing of large-size Si nanoparticles with carbon may be not the ideal choice, and significant research attention was attracted by other morphologies, such as hybrid nanostructures, which will be described later.

Adding carbon nanotubes (CNTs) as effective conductive additives in anodes or using them as a matrix support led to the improvements in overall electrode performance.[81, 82] Indeed, CNTs possess excellent physical properties, such as superior mechanical strength (e.g. Young's modulus ~1.0 TPa) and electrical conductivity (e.g. resistivity $<10^{-4}$ Ω·cm), and have high aspect ratio (e.g. ratio of length to diameter - up to 10^7) and structural flexibility.[83] Due to these unique properties, CNTs can form a nanoscale matrix, which will buffer the volume changes of Si particles, thus preserving the structural integrity of the anode during cycling. Moreover, as electronic conductivity of Si is rather low, then the implementation of CNTs is expected to improve the electronic conductivity of the anode. All these reasons make CNT to be a good candidate for a matrix material in Si-based composites.

More recently, a new concept was proposed for the design of various kinds of heterogeneous electrode materials, such as MnO_2/CNT,[84] Sn/SnO_2,[28] CNT/TiO_2[85] and other. This new design involves the combination of two materials, both at the nanoscale, in the form of coaxial nanowire/nanotube, nanotube/nanotube or nanoclusters supported on nanowires or nanotubes.[47] Such hybrid structures improve the efficiency of the battery electrodes, as they, firstly, provide the access to the benefits of 1-D nanostructures and, secondly, can fully exploit the functionalities of both component materials.

Hybrid nanostructures may provide an attractive solution to the main drawbacks of Si anodes. For instance, as it was mentioned earlier, agglomeration and further pulverization of Si particles may cause a severe capacity fading in particle-based electrodes. However, uniform dispersion of Si nanoparticles over a rigid support with well-defined spacing between the nanoparticles can effectively circumvent the Si agglomeration and improve the cycle life of the battery. This design principle has been successfully applied on Sn/SnO_2,[28] Sn/graphene,[86] TiO_2/graphene,[29] FeF_3/CNT,[30]

MnO_x/CNT[87] systems. Hu et al. prepared Si nanoparticle-decorated Si nanowire networks for Li-ion battery anodes, which exhibit good cycling performance and structural integrity.[88] Novel carbon nanomaterials, i.e. CNTs and graphene, currently attract tremendous research attention as possible supports in hybrid nanostructures. That is due to the excellent mechanical strength of both CNTs and graphene. Besides, both CNTs and graphene are good electronic conductors and can form a fast conduction network, improving the anode performance. Si/graphene hybrid nanostructures have been prepared by Kung and co-workers.[89, 90]

Hybrid nanostructure made of Si-clusters on the CNT surface[91] showed high capacity of 2050 mAh/g on the first cycle, but also exhibited a rapid fade in capacity during 25 and 50 cycles, when the capacity dropped to around 1000 mAh/g. The reasons for such behavior were not understood enough, although Wang and co-workers suggested that one of the reasons may be the weakening of the Si-CNT interface leading to the detachment of Si droplets from the CNT. At the same time the improved performance (1500 mAh/g for 30 cycles) was observed for the composite made of silicon nanowires, mixed with carbon nanotubes or amorphous carbon.[92]

These findings from literature prove the high potential of Si/CNT electrodes, and also demonstrate the importance of the further work in this field, both in exploring the nature of Si-CNT interface, structural stability and other issues.

1.6. Summary

In order to improve the properties of silicon anodes, several approaches have been developed, of which the main are nanostructuring and mixing with the secondary phase in the form of composite or hybrid nanomaterial. The volume expansion problem can be

reduced by using small Si nanoparticles.[26] The improved cycle life can be achieved in such way, but it is essential to prevent nanoparticles from agglomeration with each other. This can be done by dispersing them over a rigid support, such as CNTs or graphene.[28] Strong interfacial interaction between Si and support is essentially important here and needs further research efforts. The electronic conductivity of anode can be improved by mixing Si nanoparticles with conductive nanomaterials, such as CNTs. Alternatively, one may design Si nanostructures in the form of 1-D Si nanowires or nanotubes, providing fast 1-D electronic pathways.[31] The Li diffusion rates can be enhanced by creating hollow or pore nanomaterials.[56]

Chapter 2

Computational Studies on Nanostructured Anode Materials

First principles calculations can be a useful tool in evaluating the properties of potential anode materials for Li-ion batteries. In this Chapter, we provide some examples from the recent literature on how theoretical studies are used to gain the insights on different nanomaterials, such as carbon- and silicon-based, for their prospective application in Li-ion battery anodes.

2.1. Carbon nanotubes

In search of alternatives to conventionally used graphite electrode, researchers firstly looked at other allotropes of carbon. The superior properties of carbon nanotubes (CNTs), such as excellent electronic conductivity and mechanical strength, make them promising anode materials for Li-ion batteries. Moreover, the unusual tubular structure of CNTs is expected to provide more intercalation sites for Li ions, enhancing the total anode capacity. Using first principles calculations, Zhao and co-workers studied Li intercalation sites, binding energies and electronic structures of Li-intercalated CNTs.[93] Results of their theoretical work showed that: (1) a strong charge transfer occurs between

Li atom and CNT host; (2) the structural deformation of CNT due to Li intercalation is very small; (3) both the exterior and the interior of CNT are energetically favorable for Li insertion; (4) the Li intercalation energy in CNT is comparable to that in graphite and independent of Li density. The above findings suggested that a high Li storage capacity of LiC_2 can be achieved in CNTs by utilizing sites at both outside and inside the nanotube. However, the subsequent theoretical simulations demonstrated that penetration of Li atoms through the CNT sidewalls is forbidden in pristine, untreated CNTs, because Li atom has to overcome the energy barrier of as high as ~10 eV.[94, 95] Therefore, for the practical application of CNTs in anodes, one has to introduce sidewall topological defects or tube open ends (i.e. by ball milling technique), which would reduce the Li diffusion barrier (Table 2.1).[94, 95] The results of these theoretical studies find an excellent agreement with the recent experiments – in particular, the capacity of ball-milled or chemically-etched CNTs is nearly two times larger, than that of untreated nanotubes, namely, 1000 and 400 mAh/g, respectively. Another possible strategy to reduce the Li migration barrier is doping. As reported by Zhou et al.,[96, 97] composite nanotubes, such as BC_3NTs, possess two times smaller energy barriers for Li motion through the sidewall six-member ring (in comparison to those in CNTs), namely, ~4.6 eV. Moreover, due to the strong propensity of boron to accept electrons from Li, the electron-deficient BC_3 nanotubes adsorb Li very favorably.[96, 97]

Table 2.1. Diffusion barrier for Li penetration through the sidewalls of (5,5) CNT with *n*-member ring defects and formation energy of the corresponding defects on (5,5) CNT, as calculated by Nishidate et al.[95] and Meunier et al.[94]

	Diffusion barrier (eV)		Formation energy (eV)	
	GGA (Ref.[95])	LDA (Ref.[94])	GGA (Ref.[95])	LDA (Ref.[94])
Defect free	10.12	13.5	0.0	0.0
Heptagon *(n=7)*	5.72	7.5	4.23	3.5
Octagon *(n=8)*	3.58	3.0	7.60	6.2
Enneagon *(n=9)*	0.96	0.5	9.66	9.5

2.2. Hybrid Structures: C_{60}/CNT and Sn/CNT

Besides serving as an active material in Li-ion batteries, CNTs have also been widely used as a buffer material, mechanical support in hybrid electrodes, because of their excellent strength and electronic conductivity. However, in order to fully enjoy all the benefits of hybrid electrode architecture, it is important to ensure a strong connection between the active material nanoparticles and CNT support. Strong interaction is important due to the following reasons: (i) to prevent the nanoparticles from agglomeration and retain the well-defined space between them; (ii) to maintain electrical contact and enhance the overall electronic conductivity of the electrode.

There have been recent theoretical studies on different hybrid nanostructures as potential anode materials, such as C_{60}/CNT,[98, 99] Sn/CNT,[100, 101] SiNW/graphene,[102] etc. Moreover, there have been extensive studies on the various hybrid nanostructures for other applications, such as hydrogen storage, sensing, etc.[103-107] For the practical application of hybrid structures in Li-ion batteries, it is important to ensure a strong

interaction between different components, as well as structural stability. For instance, Ng et al. evaluated thermodynamically and energetically stable models for Sn-CNT structures, such as Sn nanowire@CNT[101] and Sn cluster/CNT.[100] In case of SnNW encapsulated CNT (SnNW@CNT), it was found that for each SnNW size there is an optimal CNT diameter, at which the interaction energy between SnNW and CNT is the lowest. However, SnNW@CNT hybrid has to be made ultrathin in order to effectively accommodate the volume expansion of SnNW. Importantly, SnNW@CNT has higher conductivity than its standalone counterparts, which is beneficial for anode application.[101]

The Li adsorption mechanism on hybrid fullerene/nanotube system (C_{60}/(5,5)CNT) has been investigated using first-principles calculations by Koh et al.[98, 99] Due to the high electron affinity of C_{60}, the lithium adsorption energy on C_{60}/CNT hybrid system (-2.11 eV) is found to be larger than that of the pure SWCNTs (-1.72 eV). From the calculations, Li atoms preferably occupy the mid-space between C_{60} and CNT, then C_{60} side and subsequently the CNT side. Furthermore, the authors also calculate the Li adsorption energy, as well as the electronic properties of the C_{60}/CNT system as a function of the number of adsorbed Li atoms.

2.3. Silicon: bulk and nanowires

In order to optimize the performance of Si anodes, it is necessary to establish the understanding of interactions between Li atoms and covalently-bonded Si host. In this respect, there has recently been a good progress in theoretical studies of energetics and dynamics of Li-Si compounds, at both early and late stages of lithiation. In particular, Wan et al.[108] and Kim et al.[109] studied the insertion process of single Li atom into the host

Si matrix. Both groups concluded that tetrahedral interstitial (*Td* site) is the most stable position for Li atom inside Si crystal, which agrees well with the early experiments.[110] Figure 2.2 shows the most stable positions for Li atom in Si bulk crystal. The insertion of Li atom results in noticeable outward displacement of the four Si first neighbors by ~0.08 Å[109] from their crystalline positions. Calculations demonstrate an accumulation of charge in the region of Li-Si bonds with a shift toward the Si atoms. The amount of charge transfer from the inserted Li to the Si host is calculated to be 0.83*e* from the Bader charge analysis.[109] Importantly, there is noticeable charge depletion nearby Si-Si bonds, especially between the first and second nearest Si atoms. The charge depletion in the region between two Si atoms indicates the weakening of the corresponding Si-Si covalent bonds. The above findings indicate that the Si host can be easily destabilized by Li insertion, consistent with experimental studies.

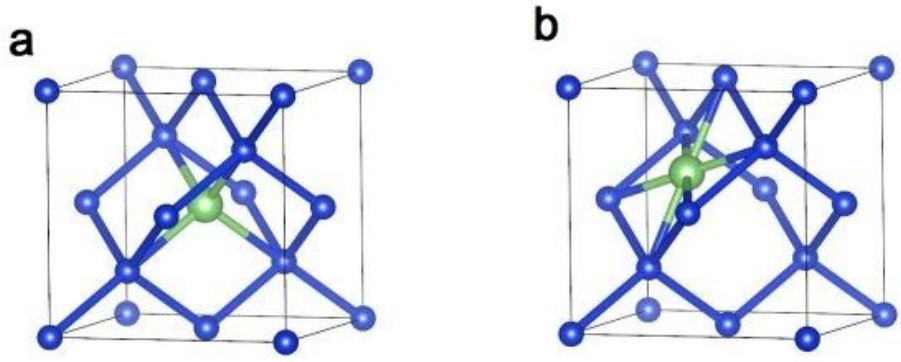

Figure 2.2. Stable Li insertion sites in bulk Si: (a) tetrahedral *(Td)*, and (b) hexagonal *(Hex)*.

Lithium insertion in silicon nanowires (SiNWs) follows similar trends as that in the Si bulk, but also represents a more complicated picture of Li binding sites and energies due to anisotropy between bulk, subsurface and surface states. Recently, Zhang et al. reported an *ab initio* study of Li insertion in small-diameter SiNWs of different size

and growth orientation.[111] The results of this study suggest that the lithiation in SiNWs occurs layer by layer from the outer surface towards the inner region, consistent with the Finite Element Analysis (FEA) by Liu et al.[40]

Chapter 3

Motivation & Objectives

Silicon is an attractive novel anode material for Li-ion batteries, because of its ultra-high specific capacity and large abundance. It has the highest theoretical capacity of 4200 mAh/g at $Li_{22}Si_4$ phase or 3579 mAh/g in $Li_{15}Si_4$, about ten times larger than that of conventional graphite anode (372 mA/g). However, its practical use is hindered by an enormous volume change that silicon undergoes during lithiation/de-lithiation (up to 400%), which leads to cracking of anode and significant fade in specific capacity.

The early studies demonstrated that nanometer-sized Si powder exhibits improved specific capacity and cycle life, as compared to the bulk material.[25] However, it has been reported that Si nanoparticles tend to agglomerate and increase in size during Li insertion/extraction, resulting in poor Li kinetics and pulverization during cycling.[27] The agglomeration problem can be avoided by dispersion of nanoparticles on the rigid conductive support, such as carbon nanotubes, graphene, etc. Recently synthesized hybrid Si-cluster/CNT nanostructures were shown to be able to maintain high capacity of more than 1000 mAh/g for 25 cycles.[91] This result has been very encouraging, however, the capacity of Si-cluster/CNT system exhibited a rapid fade during 25 to 50 cycles. The reason for such irreversible loss is not well understood yet. One of the possible reasons may be the weakening of Si-CNT interface leading to the detachment of Si droplets from the CNT. As such, further work is required in this field, especially on the properties of Si-

CNT interface and the stability of Si/CNT hybrid. In this thesis, we systematically address this issue by using first-principles calculations. We introduce and compare several functional groups, such as -NH_2, -OH, -COOH, in order to find the suitable strategy to strengthen the Si-CNT interfacial interactions.

Nanostructuring has played a fundamental role in the recent advances in Li-ion battery science. However, there is still room for improvement in battery performance and design of novel nanostructures for the battery application. For instance, there have been only few studies on the ultra-thin few nm-thick Si nanosheets as possible anode materials. Experimentally, Si nanosheets with a thickness of 2 nm down to a single-layer can be synthesized now by CVD process, exfoliation or template-based methods.[64-66, 68] They possess several important benefits, such as very large surface area, shortened Li insertion/deinsertion paths, possibility of carbon coating and constructing of stacking structure, etc. The latest studies on nanosheets of other materials (e.g. MoS_2, TiO_2, etc.) for Li-ion battery application are very encouraging. Nevertheless, the study of Si nanosheets for Li-ion application remains less explored in the literature to date. In this thesis, we use first-principles calculations to evaluate the potential of Si nanosheets as anode materials. We study the important Li insertion properties, such as Li binding energy and diffusion barriers, as a function of Si nanosheet thickness and surface chemistry.

For certain Li-ion battery applications, such as in hybrid electric vehicles (HEV), or power tools, the rate capability of the battery is crucial in addition to the high energy density. In turn, the rate capability of the Li-ion battery depends on how fast Li ions and electrons can move in the electrode material. Unfortunately, experimental studies of intrinsic Li diffusion in materials experimentally is often quite complicated due to many external factors involved such as grain size distribution, morphology, and the presence of

defects in the structure. Due to these factors, systematic studies of Li diffusion are complex. In investigating the intrinsic Li diffusion, first principles calculations have proven to be quite successful. By providing accurate and reliable energy surfaces one can identify and characterize possible Li motion pathways and their kinetics. In this thesis, we theoretically study Li diffusion in Si nanostructures, such as nanotubes and nanosheets. We show that Li diffusion rates can be greatly improved by the means of materials design, particularly by increasing the void size (in nanotubes) or utilizing fast surface diffusion pathways (in nanosheets).

The more specific objectives can be identified as:

- Evaluate the structural stability of Si/CNT hybrids: Si atoms and clusters, adsorbed on carbon nanotubes; explore the effect of Si doping site, nanotube diameter, cluster size on the adsorption energy of Si on CNT;
- Theoretically suggest a suitable strategy to strengthen the Si-CNT interface in Si/CNT hybrids;
- Evaluate the potential of novel Si nanostructures (Si nanotubes and Si nanosheets) as potential anode materials for Li-ion batteries;
- Study Li insertion and diffusion properties in Si nanotubes and Si nanosheets. For this purpose, the adsorption energies of Li at different insertion sites will be compared, and the diffusion pathways and energy barriers for the diffusion of Li will be investigated;
- Explore the effects of surface modification on the Li diffusion kinetics in Si nanosheets.

Chapter 4

Computational Methods

4.1. Ab Initio Simulations with Quantum Espresso

First-principles calculations are performed within the DFT framework, as implemented in *Quantum Espresso* package.[112] Quantum Espresso is a powerful and widely used tool for electronic-structure calculations and materials modelling based on density-functional theory, plane waves basis sets and pseudopotentials to represent electron–ion interactions. It is free, open-source software distributed under the terms of the GNU General Public License (GPL). In the presented work, the exchange-correlation potential is approximated by generalized gradient approximation (GGA)[113] using Perdew-Burke-Ernzerhof (PBE) functional generated using the Rappe-Rabe-Kaxiras-Joannopoulos (RRKJ) method.[114] The ultrasoft pseudopotentials are used for the description of electron–ion interactions. Before any property calculations, the converging tests are performed from which the kinetic-energy cutoffs for valence electron wave functions and charge density are set as 37 Ry and 370 Ry, respectively (more details are presented in Appendix A). In all calculations, the optimized structures are obtained by relaxing all atomic positions using the Broyden-Fletcher-Goldfarb-Shanno (BFGS) quasi-newton algorithm until the interatomic forces are less than 0.01 eV/Å.

For Si/CNT calculations, we use a Monkhorst-Pack mesh with 1×1×6 *k*-point sampling. A denser *k*-point mesh of 1×1×12 sampling is performed in the case of density of states (DOS) calculations. Periodic boundary conditions and a tetragonal supercell approximation are used in this study. The unit cell dimensions of the CNT are 25Å×25Å×17.22Å, with the CNT lying along the *c*-axis. The vacuum spaces along *a*- and *b*-axes are set to be larger than 15 Å, which are large enough to ensure that Si/CNT system does not react with its periodic images though the periodic boundary in the *a*- and *b*-axes, while the *c*-axis dimension is determined by the length of the CNT. Large cells of (5,5) CNTs with 140 carbon atoms are used in our calculations in order to reduce interactions between the adsorbate and its periodic images. We chose metallic (5,5) CNT rather than semiconducting CNT because we are interested in its electron conduction capability. In case of Si_n/graphene, the unit cell dimensions are set to 17.22Å×17.22Å×20Å.

For calculations on Si nanotubes (SiNTs), a Monkhorst-Pack 1×1×6 *k*-point sampling is used for geometry optimizations, and 1×1×12 sampling is performed for density of states (DOS) calculations. Periodic boundary conditions and a 25Å×25Å×15.58Å tetragonal supercell approximation with a vacuum spacing of about 15 Å in lateral directions are used to prevent the interaction of SiNT with its periodic images.

For calculations on Si nanosheets (SiNSs), the Brillouin zone is sampled by 6×6×1 and 6×6×6 Monkhorst-Pack *k*-points grid for the 2-D Si nanosheets and bulk Si, respectively. All structures are treated with periodic boundary conditions, and Si nanosheets in the periodic supercells are separated by a vacuum spacing greater than 12Å.

The accuracy of used pseudopotentials has been carefully checked. The calculated bulk lattice constants for Si and Li are 5.48 and 3.52 Å, respectively, which are in good

agreement with the experimental values of 5.43 and 3.49 Å. For the Li_2 molecule, the bond length and binding energy are 2.75 Å and 1.07 eV, respectively, close to the experimental data (2.67 Å and 1.03 eV).

4.2. The Nudged Elastic Band Method

Activation barriers for Li diffusion are calculated using the climbing-image nudged elastic band (CI-NEB) method.[115, 116] The NEB method is an efficient technique to find the minimum energy path (MEP) between given initial and final states of a transition. The MEP describes the mechanism of diffusion, and the energy barrier along this path can be used to calculate the diffusion rate. This path passes through at least one first-order saddle point. The MEP has the property that any point on the path is at an energy minimum in all directions perpendicular to the path.

In the NEB method, a set of images (i.e. geometric configurations of the system) is constructed to describe a diffusion pathway. The number of images is typically of the order of 8-20. The initial guess of the diffusion trajectory is generated by linear interpolations between initial and final points of the pathway. When an intermediate state of the diffusion is known, an initial path can be constructed considering this particular intermediate. A spring interaction between neighboring images is added to ensure continuity of the path, thus mimicking an elastic band. An optimization of the band, including the minimization of the forces acting on the images, brings the band to the MEP. The images along the NEB are relaxed to the MEP through a force projection scheme in which potential forces act perpendicular to the band, and spring forces act along the band. To make these projections, the tangent along the path is defined as the unit vector to the

higher energy neighboring image. An efficient strategy to find a saddle between known states is to roughly optimize a NEB calculation and then perform a following saddle point search from the highest energy image to find the transition state. Alternative approach, which avoids running two separate optimizations or interpolating to find the saddle, is the climbing-image NEB (CI-NEB), which is used in our study.

NEB method has been used successfully in the previous studies to determine Li diffusion rates in silicon nanostructures,[109, 117] as well as other electrode materials.[118-121]

Chapter 5

Silicon/Carbon Nanotube Hybrids

5.1. Introduction

Nanostructuring provides an elegant and efficient way of producing Li-ion battery electrodes with unique properties and improved performances. A variety of Si nanoparticles (SiNPs) have been tested as anode materials and showed improved specific capacities and cycle life. However, agglomeration of SiNPs during battery cycling and a need to maintain good electric contact between them represents important technological challenges. Dispersing nanoparticles on a rigid and conductive support affords promising means to overcome the above issues. Recently, Wang and co-workers have reported the successful synthesis of Si/CNT hybrid, which is comprised of Si-clusters adsorbed on the outer surface of carbon nanotube (CNT), by a two-step CVD process.[91] In this nanostructure, the spacing between Si clusters is required to accommodate the volume changes of Si during the lithiation in order to prevent Si from agglomeration. On the other hand, CNT serves as a mechanical support and fast electronic pathway due to its excellent mechanical strength and good electrical conductivity,[83] while both Si clusters and CNT provide Li intercalation sites, which should enhance the total Li uptake.

The interface chemical engineering in hybrid materials has recently become the subject of both experimental and theoretical studies.[122-124] Tailoring the interfacial

interactions can lead to novel properties and functionalities,[125-127] as well as the promotion of various applications. For instance, Li et al. fabricated optoelectronic devices, which can switch between two distinct and reversible photosensing behaviors (relative increase and decrease of the hybrid conductivity under illumination) by simple chemical modulating of the CdS/CNT interface.[127] More recently, Zhou et al. demonstrated that it is also true for Li-ion battery materials and enhancing the interfacial interaction between Fe_3O_4 nanoparticles and graphene nanosheets has a direct impact on the specific capacity and cycling life-time of hybrid metal oxide anodes.[128] In the light of the above studies, it is desirable to address the properties of Si-CNT interface in the design of hybrid Si/CNT anodes. Understanding the interaction between Si and CNT surface is an important step towards improving the Li-ion battery performance.

We perform a study on the Si cluster/CNT nanostructures for their application as anode material in Li-ion batteries using density functional theory (DFT) calculations. We first investigate the adsorption characteristics of Si clusters on CNT in terms of the structural stabilities and electronic properties. We aim to predict the main trends in Si adsorption and explore the possible reaction mechanism between Si clusters and nanotube support. Then, we take into account the interfacial properties of such hybrid material upon chemical functionalization on CNT, i.e. to compare the interactions between Si cluster/pristine CNT and Si cluster/functionalized CNT. Finally, we explore the Li uptake ability of Si/CNT system by calculating the adsorption energy of Li on this hybrid nanostructure. The effects of Li insertion on the strength of Si-CNT interface with and without surface functionalization are also examined. Our results support the recent experimental findings[129] and suggest that tuning the interfacial interaction between Si and CNT may lead to the improved anode's stability under both normal and lithiated conditions.

5.2. Results & Discussion

5.2.1. Single Si atom Adsorption on CNT

We begin with the study of single Si adatom adsorption on the carbonaceous supports (e.g. armchair, zigzag CNTs and graphene). We use these results for the comparison with the respective properties of adsorbed Si clusters and also for the judgment about the validity of our model and pseudopotentials. The four high-symmetry adsorption sites on the surface of CNTs have been considered as shown in Figure 5.1: center of hexagon (H); the midpoint of C-C bond 1 (B1); the midpoint of C-C bond 2 (B2) and top of C atom (T). It has to be noted that B1 and B2 sites on graphene are equivalent to each other, and, therefore, can be joined into one B site. From our calculations, the interaction between (5,5) CNT and single Si atom, adsorbed on its outer surface, is found to be quite strong. The most favorable adsorption sites is B1, consistent with the previous study.[130] For the adsorption of single Si atom on the graphene support, the most favorable site is found to be bridge (B), while the center of hexagon (H) is the least stable for Si adsorption, which agrees well with the trends, observed for Si and Ge in the recent studies.[131, 132] The consistency of the above results with existing literature supports the validity of our model and chosen pseudopotentials.

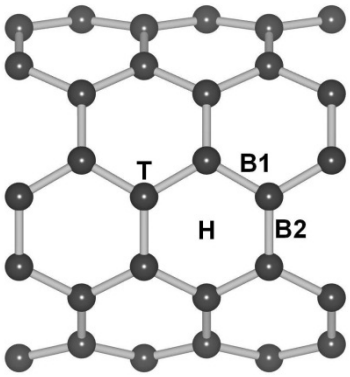

Figure 5.1. High-symmetry adsorption sites on metallic (5,5) CNT: center of hexagon *(H)*; the midpoint of C-C bond 1 *(B1)*; the midpoint of C-C bond 2 *(B2)* and top of C atom *(T)*.

5.2.2. Si Cluster Adsorption on CNT: Size and Orientation Effects

The small Si_n clusters (n=2-20) have received remarkable attention in past years, because of their potential applications in silicon-based nanoelectronics and photovoltaic cells. Theoretical[133-138] and experimental studies[139-141] have gained important advances in the knowledge about geometrical shape and structural properties of gas-phase silicon clusters. It has been reported that the 2D – 3D transition in Si_n clusters occurs very early - the clusters, having five or more atoms prefer three-dimensional shape.[142] This happens due to the preference for sp^3 hybridization in silicon, and, as a result, Si favors formation of 3D, compact structures.

In the present work, we use small Si clusters adsorbed on CNTs and graphene as models of Si/CNT and Si/graphene hybrid nanostructures. In literature, similar M_n/CNT (n < 10) models have been successfully employed in computational investigations of metal nanocatalysts, hydrogen media, sensors, etc.[100, 143, 144] We study the possible short range ordering of Si clusters, allowing us to predict the main trends in Si adsorption and

explore the possible mechanism of interactions between Si clusters and nanotube support. In order to consider different possible ways of covering the support surface, we study both planar (2D) and three-dimensional (3D) Si_n cluster shapes. We investigate the relaxed structures of Si_n/(5,5) CNT by setting up various starting configurations, considering both parallel and perpendicular Si cluster orientations towards the CNT surface. The possible adsorption configurations of CNT-supported Si clusters can be summarized into the three different types: (i) one Si atom in direct contact with the CNT support labeled as *Si_n-Per1*, (ii) two Si atoms in direct contact with the CNT support labeled as *Si_n-Per2*, (iii) three Si atoms in direct contact with the CNT support labeled as *Si_n-Par*. The initial configurations are further optimized without any symmetry constraints.

The adsorption energy (E_a) of Si_n-cluster on CNT is calculated from the following equation:

$$E_a = E(Si_n + CNT) - E(CNT) - E(Si_n) \tag{5.1}$$

where $E(Si_n + CNT)$ is the total energy of the hybrid system (Si_n+ CNT), $E(CNT)$ is the total energy of pristine CNT, and $E(Si_n)$ is the total energy of free silicon cluster. In this equation, $E_a < 0$ represents an attractive interaction between Si_n and CNT. While $E_a > 0$ corresponds to the adsorbed structures, which are unstable thermodynamically relatively to the host CNT and separated Si cluster. The low-energy structures of Si_n/(5,5) CNT and the respective adsorption energies obtained from our calculations are shown in Figure 5.2.

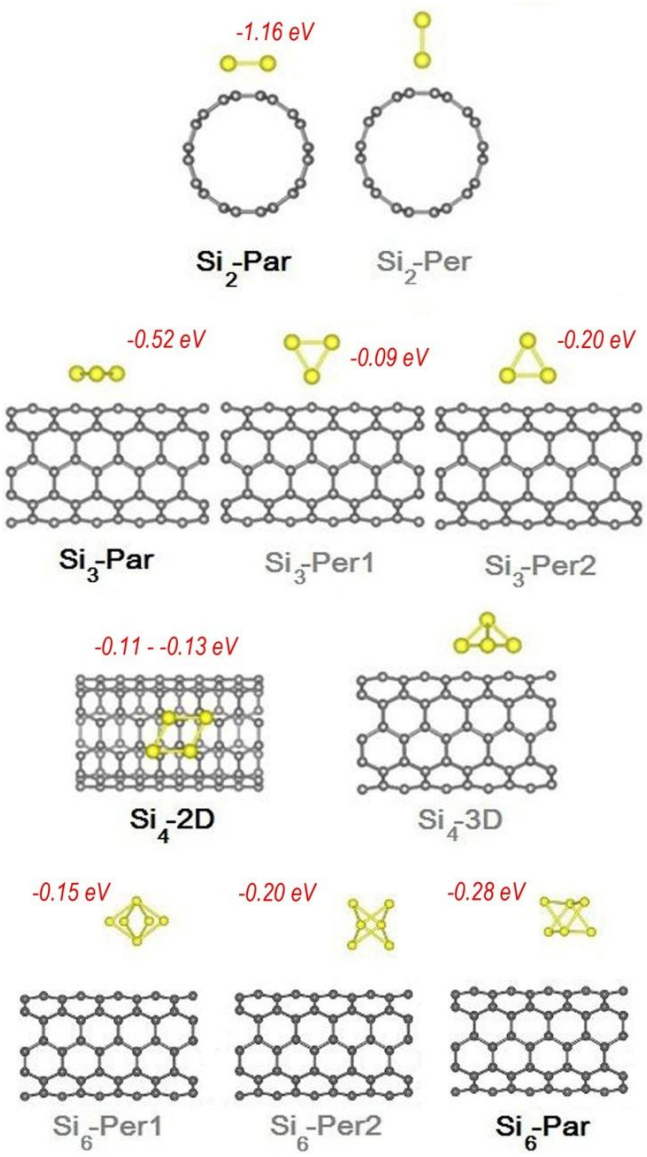

Figure 5.2. Optimized adsorption configurations of small Si clusters on the outer (5,5) CNT surface. The most stable configurations are shown in bold. The adsorption energies are shown in red.

We start with the adsorption of the smallest Si clusters (i.e. Si_2 and Si_3) on CNT support. Our calculations suggest that free-standing Si_2 dimer has a bond length of 2.23 Å, in agreement with previous literature.[135] The ground structure of free-standing Si_3 cluster is isosceles triangle with two equal Si-Si bond lengths of 2.18 Å, and the Si_1-Si_2-

Si_3 angle of 80º. When adsorbed on (5,5) CNT, both Si_2 and Si_3 clusters prefer the orientation parallel to CNT surface (*Si_2-Par* and *Si_3-Par*, respectively). For Si_2/CNT, the configuration with both Si atoms adsorbed at the bridge sites is the most energetically favorable with the adsorption energy of -1.16 eV and minimum Si-C distance of 2.11 Å. Interestingly, the initial perpendicular (*Si_2-Per*) configuration of Si_2-dimer eventually transforms into parallel (*Si_2-Par*) after geometry optimization. When Si_3 cluster is adsorbed on (5,5) CNT, it energetically favours parallel orientation (*Si_3-Par*) with all 3 Si-atoms of Si_3 located on the top of C atoms in the same C_6 ring of (5,5) CNT. The adsorption energy is equal to -0.52 eV, which is lower than that of Si_2 cluster, indicating the decreasing stability. The Si-C bond lengths are about 2.3 Å, which are larger than those for the single Si atom and Si_2 adsorptions. Si cluster changes its shape to equilateral triangle with the Si-Si-Si angles at 60º and Si-Si bond length of 2.29 Å. The C atoms in the underlying hexagonal ring move up, which leads to the increase of the average C-C bond length from 1.426 to 1.476 Å.

The character of binding between the cluster and the CNT has been examined by calculating the charge-density difference. For the fully relaxed, minimum total-energy configuration, we calculate the charge-density difference:

$$\Delta\rho = \rho(Si_n + CNT) - \rho(CNT) - \rho(Si_n), \tag{5.2}$$

where $\rho(Si_n + CNT)$, $\rho(\mathrm{CNT})$, and $\rho(\mathrm{Si_n})$ are charge densities of Si_n/CNT system, pristine CNT, and Si_n cluster with C and Si atoms in the same positions as they occupy in Si_n/CNT system. Taking Si_3 as an example as presented in Figure 5.3, our results indicate that charge is generally transferred from Si to CNT, which can be easily understood by the electronegativities of the two elements[145] (1.90 and 2.55 on Pauling scale for Si and C, respectively). The electrons transferred from Si to C atoms mainly distribute in the region

nearby Si–C bonds. Note the slight charge depletion in the CNT region nearby Si cluster, suggesting a possible weakening of the corresponding C-C bonds, consistent with their aforementioned elongation.

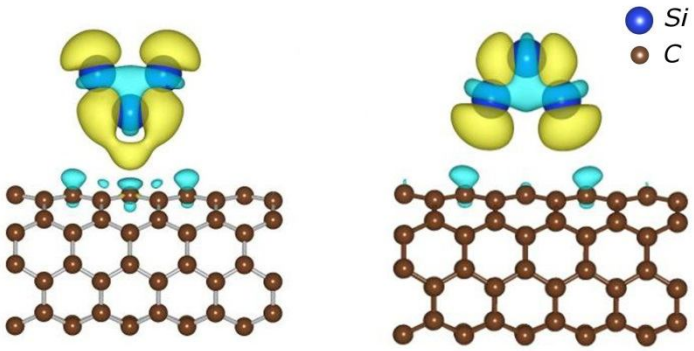

Figure 5.3. Contour plots of charge-density difference in Si_3/CNT nanostructures. Yellow color indicates positive regions (charge accumulation), while blue – negative (charge depletion).

The ground-state structure for Si_4 cluster is planar rhombus, formed by edge-capping the Si_3 triangle. Such planar shape is considerably more stable in the gas-phase than the 3-D Si_4. Nevertheless, we considered both of these forms as the initial configurations for the adsorbed Si_4 clusters on the carbonaceous support (Figure 5.2). The calculated adsorption energies of 2-D Si_4 layer on the outer surface of (5,5) CNT lay in the range of -0.11 to -0.13 eV with the minimum Si-C distance of 3.67-3.92 Å. In its most stable adsorption configuration four Si atoms are located above the C atoms. Meanwhile, initially three-dimensional Si_4 cluster after adsorption transforms into the planar form. In this aspect, the adsorption of Si_4 cluster represents an interesting case, since the flat 2-D layer with such number of Si atoms has a poor stability on the CNT surface, however, on the other side, the 2-D – 3-D transition in Si clusters has not taken place yet. Therefore,

Si_4 cluster has smaller adsorption energy than both of its neighbors in the size space (Si_2, Si_3 and Si_5).

Next, we study the adsorption of Si_6 clusters on the outer surface of (5,5) CNT as a model of stable supported 3D Si cluster. Here, Si_6 was chosen because it is especially stable among small Si_n clusters (n=2 to 13)[146] and alongside Si_{10}, it is found abundantly in experimental mass spectra.[141] Due to its high stability compared to the other small silicon clusters, Si_6 is characterized as one of the "magic-number" clusters.[141] In our study, Si_6 cluster initially has a shape of tetragonal bipyramid (D_{4h} symmetry) and the interatomic distances of six Si atoms are chosen in accordance with the Si_6 gas phase equilibrium structure.[135, 140]

After adsorption, Si_6 cluster preserves its 3D structure. Parallel cluster orientation *Si_6-Par* is generally the most stable with the adsorption energies in range of -0.25 to -0.28 eV. Meanwhile, configuration *Si_6-Per1* with only one Si atom attached to CNT is the least stable one. The above suggests that Si_6 cluster prefers to adsorb on the CNT with three CNT-adjacent Si atoms. At the most stable *Si_6-Par* position, three Si-atoms of Si-Si-Si face in contact with CNT are located on the top of C atoms in the same C_6 ring. In such case, the adsorption energy is equal to -0.28 eV and the minimum Si-C distance is 3.17 Å, which is larger than that in the Si_2 dimer adsorption of 2.11 Å. The adsorption process slightly changes the geometrical shape of Si_6 cluster: the Si-Si bond lengths in the triangular face just above the CNT are enlarged from 2.34, 2.34, 2.70 to 2.37, 2.37, 2.86 Å, respectively, which indicates the slight weakening of the corresponding Si-Si bonds.

Adsorption energy of Si_6 cluster on the outer surface of (5,5) CNT is smaller than those of Si_2 dimer and Si_3 trimer (-1.16 eV and -0.52 eV, respectively). This result shows that increasing the cluster size would reduce the adhesive strength, and hence Si may be

unable to produce continuous coatings on the outer surface of pristine CNT, most likely forming discrete particles.[147] Nevertheless, interaction between Si particles and CNT can be enhanced via preliminary functionalization (pre-treatment) of pristine CNT surface with chemically active groups.

5.2.3. Support Dependent Adsorption: CNTs vs. Graphene

Adsorption on carbonaceous supports is greatly affected by the dimensionality and electronic properties of nanocarbon. Our calculations show that Si clusters produce stronger interaction with CNTs, than with graphene (for instance, -0.52 and -0.10 eV for Si_3 on (5,5) CNT and graphene, respectively). Keeping in mind that nanotubes differ from graphene sheet by curved and non-planar sp^2 bonding configuration, this makes curvature as one of the main factors affecting Si adsorption. As the curvature of CNT decreases (i.e. CNT's diameter increases), the adsorption energy of Si clusters becomes smaller. Therefore, adsorption energy of Si clusters on graphene has the smallest value, compared to CNTs. Moreover, this trend holds for all studied cluster sizes. Such behavior is expected since curvature effect has been observed in the other systems (e.g. Ti/CNT, Al/CNT, etc.) in literature.[130, 148-150] The enhanced adsorption on the CNT surface may be attributed to the enhanced hybridization between the molecular orbitals of C and adsorbate at small tube radius.[150] For instance, as described by Ciraci *et al*,[148] Al atom is not bound to the graphite surface, but its binding on the nanotube surface is relatively strong.

5.2.4. Functionalization of CNT: the Linker Effect on Si Adsorption

Our results indicate that increasing the Si cluster size would reduce the adhesive strength between Si clusters and CNT support. In practical applications (such as in Li-ion batteries), mechanical integrity and stability of Si/CNT hybrid anodes play an important role. Therefore, it is highly necessary to establish ways to strengthen the Si-CNT binding. One of the strategies is through chemical functionalization, which is performed by attaching active groups at the sidewalls of CNTs, so that these groups would serve as a link between the cluster and CNT. The choice of optimal functionalization strategy plays a crucial role, since different functional groups on the CNT surface show significantly distinct interface chemistry, as well as cluster-support binding. For instance, Au nanoparticles actively decorate thiol-treated CNTs, while carboxyl treatment leads only to small adsorbed Au amounts, as observed by Chopra *et al.*[151] In their work, thiol-functionalized end of CNT had an estimated Au nanoparticle density of ~526 nanoparticles μm^{-1}, in contrast to only 80 particles μm^{-1} at the carboxyl-functionalized CNT end.[151] These results suggest that in order to sufficiently tailor the hybrid materials, it is desirable to develop the understanding of interfacial cluster-support interactions, as well as to investigate the role of different chemical elements inside the functional groups.[152]

We modify the CNT surface with three functional groups, namely, amino ($-NH_2$), hydroxyl (-OH) and carboxyl (-COOH). Amine molecules and amino-based groups have been used to link CdS[127] and Fe_2O_3[153] nanoparticles to the CNT surface for optoelectronic and magnetic applications. Meanwhile, hydroxyl and carboxyl groups are the main products in oxidative acid treatment of carbon nanotubes.[154] Such pre-treatment of carbon nanotubes in oxidative acids (e.g. nitric acid) increases the solubility of CNTs, creating

the possibility of further development of nanocomposites.[155] In order to find the minimum-energy atomic configuration for functionalized CNTs, we considered different initial adsorption sites and various initial orientations of each functional group with respect to (5,5) CNT. Each starting structure was further optimized without any symmetry constraints. The most stable configurations of (NH_2)-(5,5)CNT, (OH)-(5,5)CNT and (COOH)-(5,5)CNT are shown in Figures 5.4a-c, respectively. We found the each functional group prefers to bind to (5,5) CNT at the on-top C site with the bond lengths of 1.49, 1.47 and 1.57 Å for (-NH_2), (-OH) and (-COOH) radicals, respectively. The adsorption leads to a change in local geometry, and the C atom underneath the functional group is pulled out of its initial position. As a result, the C-C bond lengths between the C atom at an adsorption site and its neighbors increase from 1.42 to ~1.52 Å.

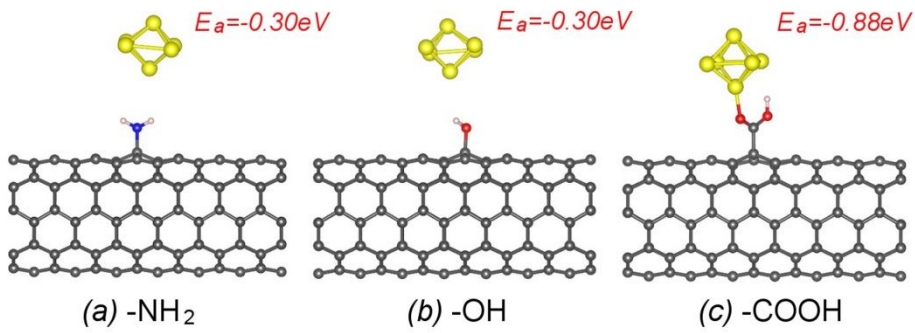

Figure 5.4. Adsorption of Si_6 cluster on the CNT surface, functionalized with (-NH_2), (-OH) and (-COOH) active groups.

We then introduce the Si clusters to the functionalized CNTs in order to study the effect of functionalization on the interfacial interactions. The comparison of the adsorption of Si_3 and Si_6 clusters on the pristine and functionalized (5,5) CNTs is given in Table 5.1. The interaction of Si_6 with (-NH_2)-functionalized (5,5) CNT (Figure 5.4) is found to be weak with the adsorption energy of -0.30 eV (Table 5.1), almost the same as

on the pristine nanotube. The minimum Si-H distance is 3.25 Å, which lies beyond the range of chemical bonding and represents only a little improvement over the pristine (5,5) CNT case. The pre-treatment of CNT with hydroxyl (-OH) group gives a slightly stronger adsorption, although still weak. The minimum Si-H distance is 3.21 Å in Si_6-(OH)-(5,5) CNT.

Table 5.1. Adsorption Energies *(E_a),* Minimum Distances (d_{min}) for Si_3 and Si_6 Clusters Adsorption on Pristine and Functionalized (5,5) CNT

Configuration	***E_a, eV***	***d_{min}, Å***
Si_3-(5,5)CNT	-0.52	2.05
Si_3-*(NH_2)*-(5,5)CNT	-0.55	2.00
Si_3-*(OH)*-(5,5)CNT	-0.56	2.00
Si_3-*(COOH)*-(5,5)CNT	-1.32	1.66
Si_6-(5,5)CNT	-0.28	3.50
Si_6-*(NH_2)*-(5,5)CNT	-0.30	3.25
Si_6-*(OH)*-(5,5)CNT	-0.30	3.21
Si_6-*(COOH)*-(5,5)CNT	-0.88	1.67

In contrast, the strongest binding has been achieved after the functionalization of CNT surface with the carboxyl molecule (-COOH) (Figure 5.4). The adsorption energy of Si_6 cluster on the outer surface of (COOH)-(5,5) CNT is -0.88 eV, which is ~3.1 times improvement over the adsorption energy on pristine (5,5) CNT. Similar results are obtained for the adsorption of Si_3 cluster - the introduction of (-COOH) contributes to the

~2.5 times increase in binding strength (from -0.52 to -1.32 eV). Si clusters in the Si/(COOH)-CNT structure prefer to adsorb on the carbonyl (-C=O) side of the carboxyl group. The minimum Si-O distance is ~1.67 Å, suggesting that Si-O bond has been formed. The enhanced interaction due to functionalization is further confirmed by Bader charge analysis. The amount of electron transfer from the Si atom of Si_6 in contact with (-COOH) radical is estimated to be 0.85*e*, much larger than that of 0.08*e* in case of Si_6 cluster on pristine (5,5) CNT. Therefore, the oxygen in carbonyl side promotes more active charge transfer from the adsorbed Si to the CNT, enhancing the binding at Si-CNT interface. These results show the different role of the elements in carboxyl group: with oxygen being the main element responsible for strong Si-support binding. The hydrogen side is less active, which explains the weak interaction of Si clusters with amino ($-NH_2$) and hydroxyl (-OH) functionalized CNTs. Moreover, although oxygen is also present in hydroxyl molecule, its chemical activity is hindered by the electron deprivation by hydrogen. The above results show the importance of oxygen for the strong binding of Si with CNT. From our studies, we suggest that carboxyl groups may be used in the preparation of Si/CNT hybrids.

5.2.5. Li Uptake in Si Cluster/CNT

Both CNTs and Si are known for the ability to store large amounts of Li ions (theoretical capacities of CNT and Si are >1116 mAh/g,[7, 93] and 4200 mAh/g,[17] respectively). The use of hybrid Si/CNT anodes, possessing two different lithium storage mechanisms simultaneously, may enhance the total specific capacity of the Li-ion battery. In order to study the interaction of Li atoms with Si/CNT complex, we first investigate where Li atoms "sit" in the Si/CNT. The Si_6 cluster, adsorbed on the outer surface of (5,5)

CNT with three CNT-adjacent Si atoms, was used as Si/CNT model, since Si_6 is especially stable among small Si_n clusters (n=2 to 13)[146] and it is found abundantly in experimental mass spectra.[141] We consider 5 typical initial positions for Li atom insertion (Figure 5.5): face (F), long Si-Si bridge (~2.70 Å) (LB), short Si-Si bridge (~2.34 Å) (SB), Si atom (A), hollow site on CNT (N). The adsorption energy (E_a) of Li at these sites is defined as follows,

$$E_a = E(Li + Si_6/CNT) - E(Si_6/CNT) - E(Li), \tag{5.3}$$

where $E(Li + Si_6/CNT)$ is the total energy of optimized system (Li-Si_6/CNT), $E(Si_6/CNT)$ is the total energy of Si_6/CNT, and $E(Li)$ is total energy of Li atom.

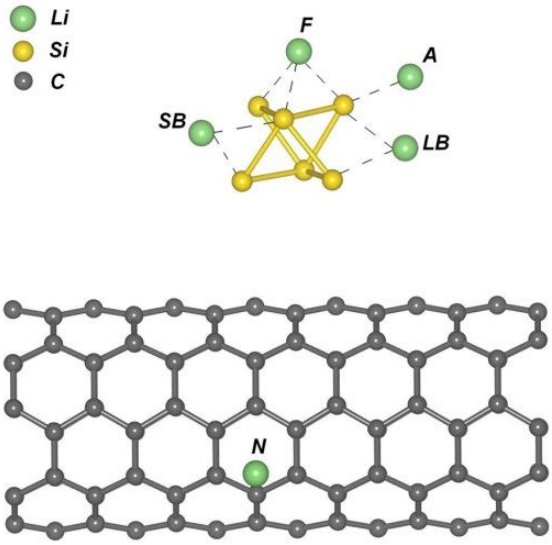

Figure 5.5. Li adsorption sites on Si_6/CNT: face (F), long Si-Si bridge (LB), short Si-Si bridge (SB), Si atom (A), and hollow site on CNT (N).

The Li adsorption energies and geometrical parameters of Li-Si_6/CNT system are listed in Table 5.2. From our calculations, all adsorption positions are found to be energetically favorable for Li insertion. The rich Li adsorption sites indicate that Si/CNT

anodes can potentially achieve high energy densities. The adsorption energy depends on the number of Si atoms neighboring to Li atom. The triangular face of Si cluster is preferable for Li adsorption, while Li atom in contact with only one Si atom is energetically the least favorable. The adsorption energies of Li in all considered positions vary from -1.41 to -1.60 eV, which is close to the respective values in bulk Si and Si nanowires.[111] Next, we increase the number of Li atoms by putting one Li atom at each Si-Si-Si face of the Si_6 cluster, except the face that connects cluster to the CNT. This gives a stoichiometry of Li_7Si_6. The average adsorption energy per Li atom in optimized Li_7Si_6/CNT is -1.56 eV, which is slightly smaller than that of a single Li atom, indicating the decreased thermodynamic stability with the increase in Li concentration.

Table 5.2. Adsorption Energies *(E_a)* and Minimum Li-Si ($d_{Li\text{-}Si}$) Distances for One Li Atom Adsorption on Si_6/CNT Hybrid Nanostructures

Li Adsorption Site	***Adsorption Energy (eV)***	***Li-Si Distance (Å)***
Face (F)	-1.60	2.55
Long Si-Si	-1.53	2.58
Short Si-Si	-1.51	2.61
Si atom (A)	-1.41	2.66
Nanotube (N)	-1.53	$d_{Li\text{-}C}$ = 2.24

When Li is adsorbed on the hollow site on CNT far from the Si cluster, the adsorption energy is found to be -1.53 eV. Energy values from our calculations are close to the experimental binding energies[156] of 1.70±0.14 eV in Li-C_6H_6 system. This indicates

that the Li uptake ability of CNTs is preserved in Si/CNT hybrid structure. Thus CNTs not only serve as buffer material, accommodating Si expansion, but also provide additional intercalation sites for Li.

5.2.6. Effect of Li Insertion on the Strength of Si Cluster/CNT Interface

One more important issue is: how does insertion of lithium affect the strength of Si/CNT interface? To answer this question, we compare the adsorption energies of Si_6-cluster and lithiated Si_6-cluster on the outer surface of pristine and (COOH)-functionalized (5,5) CNTs, i.e. (1) Si_6/CNT, (2) $LiSi_6$/CNT, (3) Si_6/(COOH)-CNT and (4) $LiSi_6$/(COOH)-CNT systems.

From our calculations, the adsorption energy of pure Si_6 on the outer surface of (5,5) CNT ($E_{1\text{-}pristine}$) is -0.28 eV, while the adsorption energy of the corresponding Li-Si_6 complex ($E_{2\text{-}pristine}$) is -0.14 eV. This result indicates that the insertion of lithium into the system (alloying of Li with Si) would weaken the adhesion of Si on the pristine CNT surface. The decrease in adsorption energy becomes even more obvious when more Li atoms are added. The adsorption energy of the optimized Li_7Si_6 alloy is only -0.12 eV, which is lower than the both cases above ($E_{1\text{-}pristine}$ and $E_{2\text{-}pristine}$). Such behavior may lead to the detachment of Si droplets from the pristine CNT during cycling, which, in turn, may lead to the agglomeration of free Si particles and contribute to the capacity fade in practical Si/CNT anodes. In contrast, the adsorption energy of the pure Si_6 cluster on the outer surface of (COOH)-functionalized (5,5) CNT ($E_{1\text{-}func}$) is -0.88 eV, and the adsorption energy of the corresponding Li-Si_6 complex ($E_{2\text{-}func}$) is -0.86 eV. The change of adsorption energy in this case is not critical, and functionalized hybrid system still preserves its integrity upon lithiation. This significant improvement in stability upon

lithiation in functionalized Si/CNT hybrids, as compared to the pristine case, may result in the improved cycle life of battery anode.

5.3. Summary

In summary, we reveal that in all adsorbed Si_n clusters, the structure of free-standing cluster is preserved, although slightly distorted. The smallest Si_n clusters (n = 2 – 4) energetically prefer to form planar, parallel to the support surface orientations with all Si atoms bonded to CNT. Both Si_2 and Si_3 clusters form strong Si-C bonds with the underlying CNT support. Once Si_n cluster becomes larger, the Si-C interactions are weakened and the adsorbed Si cluster starts to favour 3D structures. The Si_4 cluster can be treated as a transition size between 2D and 3D adsorbed configurations. Moreover, the interaction between Si clusters and CNT support shows a strong dependence on the CNT surface chemistry. From our calculations, the interfacial bonding between Si and pristine, ammonia- or hydroxyl-functionalized CNTs is quite weak. In contrast, the bonding can be significantly improved by carboxyl-functionalization of the CNT.

The Li adsorption energy depends on the number of Si atoms neighbouring to Li atom, namely, the triangular faces of Si clusters are energetically preferable for Li insertion over edges and corners. Both CNT and Si cluster in the resulting Si/CNT structure preserve their Li uptake ability with the Li adsorption energies (-1.4 to -1.6 eV) close to those in bulk Si and Si nanowires. More importantly, we show that Li insertion leads to the weakening of Si/CNT interface, which could be a main reason for the experimentally observed capacity fade in hybrid Si/CNT anode. Nevertheless, the structural integrity of Si/CNT hybrid upon lithiation is improved after the

functionalization of CNT surface, potentially leading to the longer cycle life of the hybrid anode. Our findings reveal the importance of surface engineering in the design of hybrid nanomaterials for potential applications in Li-ion batteries and other fields, such as supercapacitors, catalysis and sensing.

Chapter 6

Silicon Nanotubes

6.1. Introduction

Silicon nanostructures exhibit many unusual properties as compared with bulk material, such as direct band gap, reduced thermal conductivity, etc.[157-160] Silicon nanoclusters (SiNCs) and nanowires (SiNWs) have long been in the mainstream of nanoscience, serving as important building blocks of functional devices.[161, 162] The discovery and success of C_{60}, CNTs and graphene in the past decades inspired a strong interest in developing their silicon-based analogues, Si being the next group IV element in the periodic table after carbon. For instance, silicon fullerenes have been theoretically studied as promising hydrogen storage media.[163, 164]

A two-dimensional honeycomb lattice of Si, named *silicene*, is proven to be stable with a characteristic low-buckled (LB), puckered structure.[165] Silicene monolayer has a graphenelike electronic band structure with charge carriers behaving as massless Dirac fermions.[165-168] As reported by Chen et al., quasiparticle interference (QPI) patterns have been observed in silicene suggesting both intervalley and intravalley scattering of charge carriers, and a large measured Fermi velocity of 10^6 m/s has been derived.[168] Compared with that of graphene, a stronger spin-orbit coupling in silicene may lead to a detectable quantum spin Hall effect (QSHE) and other attractive properties.[169-174] Importantly,

compatibility of silicene with existing silicon-based nanotechnology favors its potential device applications. Experimentally, single-layer silicene sheet has been grown on Ag(111) by chemical vapor deposition method.[175-177] Functionalized Si monolayers have been produced by by the exfoliation of layered polysilane (Si_6H_6) precursor.[65, 66]

Silicon nanotubes (SiNTs) represent another interesting nanostructure, which drew attention of the scientific community in recent years. The possibility of the existence of tubular shapes of silicon has been firstly suggested theoretically. On the experimental side, successful synthesis of SiNTs has been reported by several groups in recent years utilizing hydrothermal process,[178, 179] dc-arc plasma method,[180] laser ablation[181] and plasma treatment.[182] These studies report the experimental observations of SiNT features, which resemble those observed in CNTs, such as rounded tips,[182] multiple walls,[178] different chiralities or atomic arrangement compatible with a puckered structure,[180, 181] suggesting the possible formation of helical tubes of Si. Although the exact experimental atomic arrangement of SiNTs remains controversial, the theoretical studies have proposed stable structural models for Si nanotubes (SiNTs), and their electronic properties have been carefully tested.[183-187] In many studies, Si nanotubes exhibit semiconducting or metallic behavior depending on the tube diameter, chirality, similar to CNTs.[187, 188] Importantly, the nanostructures of Si can gain extra stability by puckering (buckling)[165] or metal encapsulation.[189] A significant interest has been paid to various potential applications of single-wall SiNTs in magnetic nanodevices,[190] nanoelectronics,[191] hydrogen storage[192] and chemical sensors.[193] These studies also inspire us to investigate the Li intercalation behavior in Si nanotubes, especially taking into account the great promise of silicon as high-performance anode material in Li-ion batteries.

In this Chapter, we present our density-functional-theory calculations on Li insertion behavior in Si nanotubes of two structural types – hexagonal and gearlike. The

Li adsorption energies for single and multiple Li atoms insertion are calculated, while the mechanism of Li-SiNT interaction is studied by charge-density and density of states analysis. We address the Li diffusion in SiNT by calculating the energy barriers along several diffusion pathways. Importantly, we make a comparison between SiNTs and their structural analogues (e.g. CNTs, Si nanowires and Si nanoclusters) in terms of the main Li insertion properties. The predicted advantageous properties of Si nanotubes, such as large Li adsorption energy and low Li diffusion barriers, demonstrate great potential of these nanomaterials as Li-ion battery anodes.

6.2. Results & Discussion

6.2.1. Structural Properties of Si Nanotubes

Single-wall SiNTs can be viewed as the rolled-up single layers of Si, similarly to CNTs. Rolling the hypothetical 2-D graphite-like silicon sheet will form a hexagonal SiNT (*h*-SiNT) with a structure identical to CNT (Figure 6.1a). On the other hand, by rolling the Si (1 1 1) sheet of diamond structure one can obtain the gearlike SiNTs (*g*-SiNTs) (Figure 6.1b). The unique feature of the latter type of SiNTs is that its sidewalls are not smooth, but exhibit "gearlike" distortion, resulting from the initial non-flat shape of Si (1 1 1) sheet. Therefore, the local coordination of each atom in *g*-SiNT is not planar but slightly pyramidalized, with mixed sp^3-sp^2 hybridization. The presence of sp^3 configuration (which is more natural for silicon) results in the higher stability of *g*-SiNTs over smooth-walled *h*-SiNTs, as confirmed by previous theoretical studies.[183, 188] Moreover, Zhang et al. showed that armchair *g*-SiNTs are more stable than zigzag ones due to the efficient overlap of p_z orbitals and delocalized π bonds.[186]

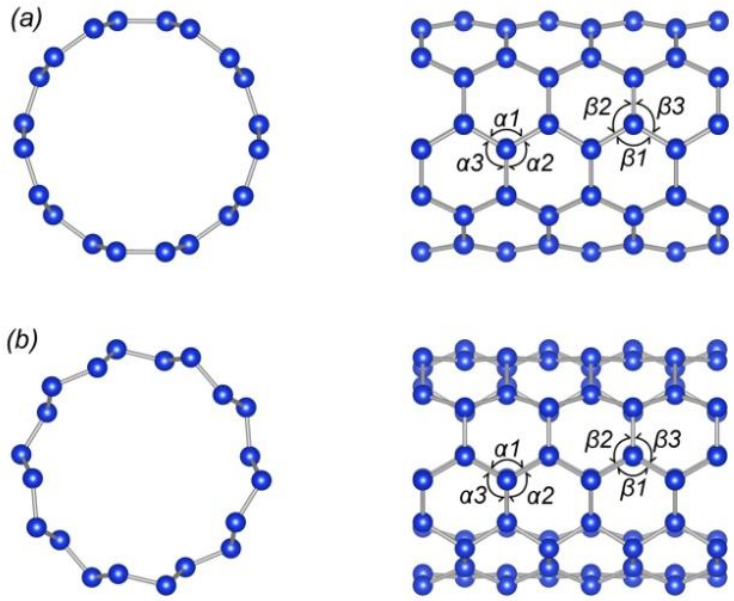

Figure 6.1. Optimized structures of (a) hexagonal and (b) gearlike (5,5) SiNTs.

We compare the structural and energetic properties of *h*-(5,5)SiNTs and *g*-(5,5)SiNTs by fully relaxing the supercells containing nanotubes with 80 Si atoms. The optimized structures are shown in Figure 6.1. The formation energy per atom of SiNTs in our study is defined as follows,

$$E_{form} = E_{total}(SiNT)/N_{atoms} - E(Si), \tag{6.1}$$

where $E_{total}(SiNT)/N_{atoms}$ is the total energy of SiNT per atom and $E(Si)$ is the total energy of the isolated single Si atom. The formation energy per atom for *g*-(5,5)SiNT is found to be 0.003 eV lower than that for *h*-(5,5)SiNT, consistent with previous studies for Si nanotubes of this diameter.[188] The sum of bond angles at each Si atom in *h*-(5,5)SiNT is nearly equal to 360°, corresponding to sp^2 planar configuration. The Si-Si bond lengths in *g*-(5,5)SiNT are 2.28 Å for the bonds perpendicular to the axis and 2.30 Å for the bonds in other directions. There are two types of local configurations for the Si atoms in

g-(5,5)SiNT, labeled as *"α"* and *"β"*. The calculated sums of angles surrounding atoms of types *"α"* and *"β"* are 355° and 329°, respectively, close to the idealized values of 360° and 328.4° for planar *(sp^2)* and tetrahedral *(sp^3)* structures, respectively. The latter suggests the presence of mixed sp^3-sp^2 hybridization in *g*-SiNTs. Thereby, puckering in *g*-SiNTs induces the dehybridization of sp^2 hybrid orbitals and subsequent formation of sp^3-like orbitals, which, in turn, enhance the stability of nanotubes, similarly as in 2-D honeycomb silicon nanoribbons.[165, 194]

6.2.2. Stability of Si Nanotubes upon Li-insertion

Next, the structural stability of nanotube host during Li insertion is tested. We place one Li atom at the initial Li-Si distance of 2 Å and perform a full relaxation of all Si and Li atomic positions. As shown in Figure 6.2a-b, the optimized structures of Li/*h*-(5,5)SiNT show significant local distortions after the introduction of Li atom. After relaxation, Li atom hardly changes its initial coordinates, while the local Si atoms are "pressed" inside of the nanotube. Therefore, if hexagonal CNT-like SiNTs are synthesized, the pristine nanotubes could not be used as battery anodes due to the host instability and structural changes upon reaction with Li, leading to the limited cycling life. However, the stability of *h*-SiNTs may be potentially improved via doping or encapsulating metal atoms.[189]

In contrast, the optimized structures of *g*-SiNTs preserve its local order after the insertion of Li atom (Figure 6.2c-d). Such result is logical, since *g*-SiNTs are more stable over disturbance.[188] The nanotube preserves its shape and the maximum deformation of the tube radius *($\Delta R/R$)* is only 1.72% from our calculations. From the prospect of host

stability, *g*-SiNTs are much more suitable than *h*-SiNTs for the Li-ion battery application. Based on this conclusion, we focus on the study of the properties of *g*-(5,5) SiNTs.

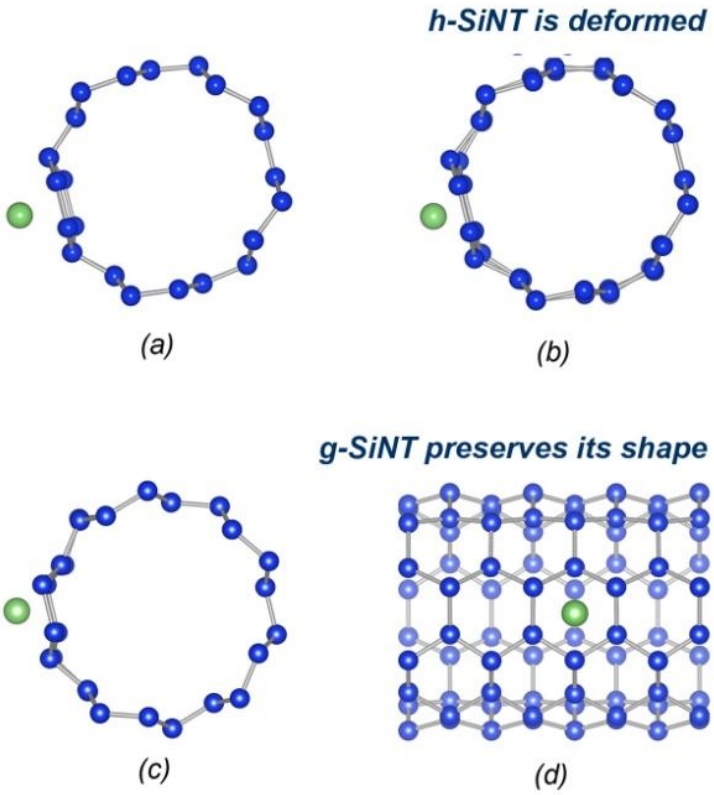

Figure 6.2. Optimized structure of (a, b) Li-*h*-(5,5) SiNT and (c, d) Li-*g*-(5,5) SiNT. Only g-SiNT preserves its structure during Li insertion.

6.2.3. Lithium Adsorption Energies

The adsorption energy of Li at the outer/inner surface of *g*-SiNT is defined as follows,

$$E_a = E(Li + SiNT) - E(SiNT) - E(Li), \tag{6.2}$$

where $E(Li + SiNT)$ is the total energy of optimized system (Li + SiNT), $E(SiNT)$ is the total energy of gearlike Si nanotube, and $E(Li)$ is the total energy of single Li atom. By

definition, $E_a < 0$ corresponds to exothermic reaction and attractive interaction, while $E_a > 0$ indicates the system that is thermodynamically unstable compared to its standalone parts.

The adsorption of Li atom both outside and inside of *g*-(5,5)SiNT is exothermic with the negative adsorption energies of -2.28 and -2.45 eV, respectively. The minimum Li-Si distances in these cases are 2.67 and 2.68 Å, respectively. The average Si-Si bond length in the Si_6 ring underneath the Li atom is slightly enlarged from 2.29 to 2.30 Å, indicating the slight weakening of the respective Si-Si bonds. Most importantly, the Li adsorption energies on *g*-(5,5)SiNT are much larger than in (8,8) CNT (-1.46 eV) and even other nanostructured forms of silicon – Si_6 nanoclusters (-1.68 eV) and [1 1 0] Si nanowires (-1.73 eV).[111] We found that Li adsorption is more favorable on the faces of Si_6 nanoclusters rather than its edges and corners. Therefore, Li should adsorb even stronger on the six-member Si ring. The large adsorption energies in *g*-(5,5)SiNT represent an advantage, because the strong interaction between Li and host tube can effectively compensate the electrostatic repulsions among adsorbed Li ions. Hence, the stability of the host system may be enhanced under high Li concentrations during battery cycling.

We further study the Li insertion at different densities by gradually increasing the Li concentration in the system. We begin with placing the second Li atom at various positions with respect to the first adsorbed Li atom. The initial configurations include: (1) two Li atoms located above the centers of the nearest neighboring Si_6 rings (NN site); (2) above the centers of the next nearest neighboring Si_6 rings (NNN site); (3) from the opposite sides of *g*-(5,5) SiNT (Far site). The respective Li adsorption energies at the above sites are listed in Table 6.1. The computed average Li adsorption energy per Li atom shows a clear dependence on the distance between Li atoms. The configuration with the smallest Li-Li distance (NN) has the smallest adsorption energy, being the least

energetically favorable. As the distance between two Li atoms increases, the adsorption energy becomes larger and approaches that of a single Li atom on *g*-(5,5)SiNT (-2.23 eV). The adsorption behavior of Li atoms is quite similar for both inside and outside the SiNT, showing the same trends. In all configurations, the Li adsorption energy is larger than the binding energy in Li_2 dimer (-1.07 eV). Therefore, we can assume that Li clustering is not expected at low Li concentrations in SiNT. The above findings confirm that the overall Li adsorption energy in *g*-(5,5)SiNT results from the repulsive forces between the adsorbed Li atoms and the interaction between Li and the nanotube host.

Table 6.1. Li Adsorption Energies (E_a) and Nearest Li-Li Distances ($d_{Li\text{-}Li}$) for Multiple Li Insertion in *g*-(5,5)SiNT

Configuration	Adsorption Energy (eV)	Li-Li Distance (Å)
Outside:		
2 Li atoms – NN	-2.12	3.89
2 Li atoms – NNN	-2.17	7.79
2 Li atoms – Far	-2.23	13.51
10 Li atoms	-2.02	7.79
Inside:		
2 Li atoms - NN	-2.34	3.89
2 Li atoms -NNN	-2.37	7.79
2 Li atoms - Far	-2.41	8.98
10 Li atoms	-2.17	3.95

The *g*-(5,5) SiNT with 10 adsorbed Li atoms was constructed by placing Li atom above each next nearest neighboring (NNN) Si_6 ring. After optimization, Li atoms outside the *g*-SiNT rearrange over the cylindrical surface of radius 7.34 Å (while the outer/inner radius of *g*-(5,5)SiNT is 5.60/5.06 Å) (Figure 6.3a). The average adsorption energy per Li

atom is -2.02 eV, decreasing with the increase of number of Li atoms. Similarly, when all 10 Li atoms are placed in the interior of the SiNT, they relocate over the cylindrical surface of radius 3.37 Å (Figure 6.3b). In the stable structure, all Li atoms remain isolated and keep their positions above the centers of hexagons. The insertion of 10 Li atoms changes the shape of nanotube to a greater extent than in the case of single Li atom adsorption. Herein, the maximum deformations *(ΔR/R)* are 2.71 and 4.16 % for the outside and inside adsorption, respectively. Both exterior and interior are nearly equally favorable for Li insertion, as the energy difference of 10 Li atoms all outside or inside the *g*-(5,5)SiNT is only 0.15 eV per Li atom.

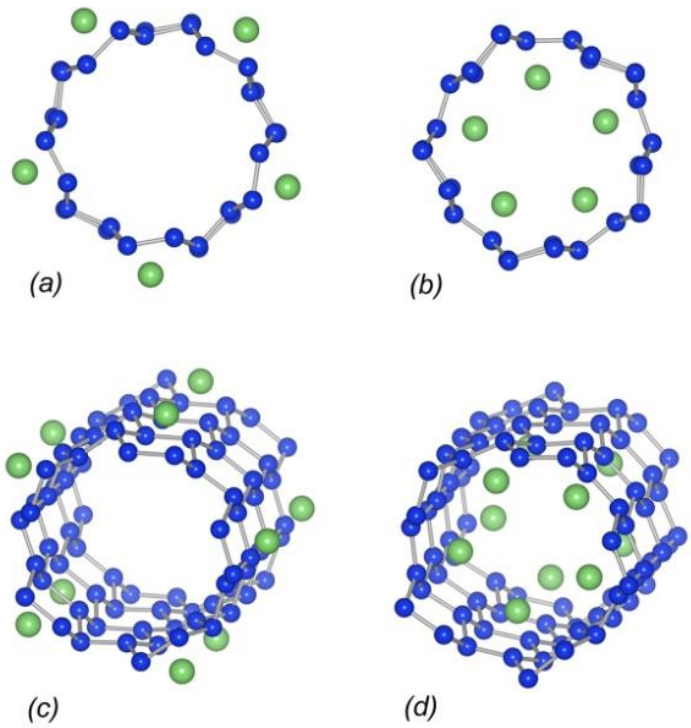

Figure 6.3. Front and diagonal views of optimized g-(5,5)SiNT structures with 10 Li atoms, adsorbed (a, c) outside and (b, d) inside the nanotube.

6.2.4. Electronic Properties of g-SiNTs

Next, the binding mechanism between Li atom and *g*-(5,5)SiNT is examined. Figure 6.4 shows charge density difference plot for Li-*g*-(5,5)SiNT system, where Li

atom is adsorbed above (Fig. 6.4a) or below (Figure 6.4b) the center of hexagonal ring. The charge density difference ($\Delta\rho$) is defined as

$$\Delta\rho = \rho(Li + SiNT) - \rho(SiNT) - \rho(Li), \tag{6.3}$$

where $\rho(Li + SiNT)$, $\rho(SiNT)$, $\rho(SiNT)$ are the total electron densities of the Li-SiNT system, pristine SiNT and single Li atom, respectively. Our analysis shows that there is a charge transfer from the Li atom towards the Si nanotube. This can be understood by the larger electronegativity of Si compared to Li (1.90 and 0.98 on the Pauling scale, respectively).[145] The chemical binding between Li and SiNT has a positive ionic character. Bader charge analysis confirms that the Li atom stays as a cation. Note that the slight charge depletion on the Si_6 ring underneath the Li atom can be associated with the weakening of the corresponding Si-Si bonds.

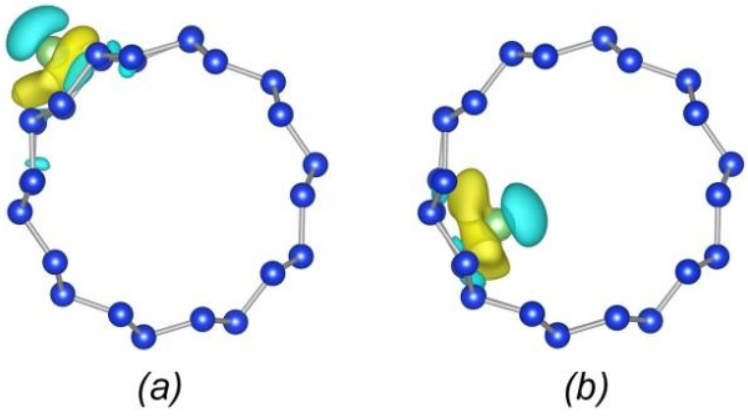

Figure 6.4. Charge density difference plot for the *g*-(5,5) SiNT with Li atom adsorbed (a) outside and (b) inside the nanotube. The blue and yellow isosurfaces represent charge depletion and accumulation, respectively.

The total density of states of pristine and Li-adsorbed *g*-(5,5) SiNTs are shown in Figure 6.5. Previous theoretical studies concluded that pristine armchair *g-(n,n)* SiNTs are semiconductors with the small band gap of 0–1 eV.[166, 183, 188] From our calculations, *g*-(5,5) SiNT is semiconductor with a gap of 0.15 eV, as shown in Figure 6.5a. It has to be

noted that standard GGA calculations usually underestimate the band gap of semiconductors as in the case of bulk Si. The TDOS of Li-*g*-(5,5) SiNT (Figure 6.5b) closely matches that of the pure nanotube, showing that it mainly comes from the Si states.

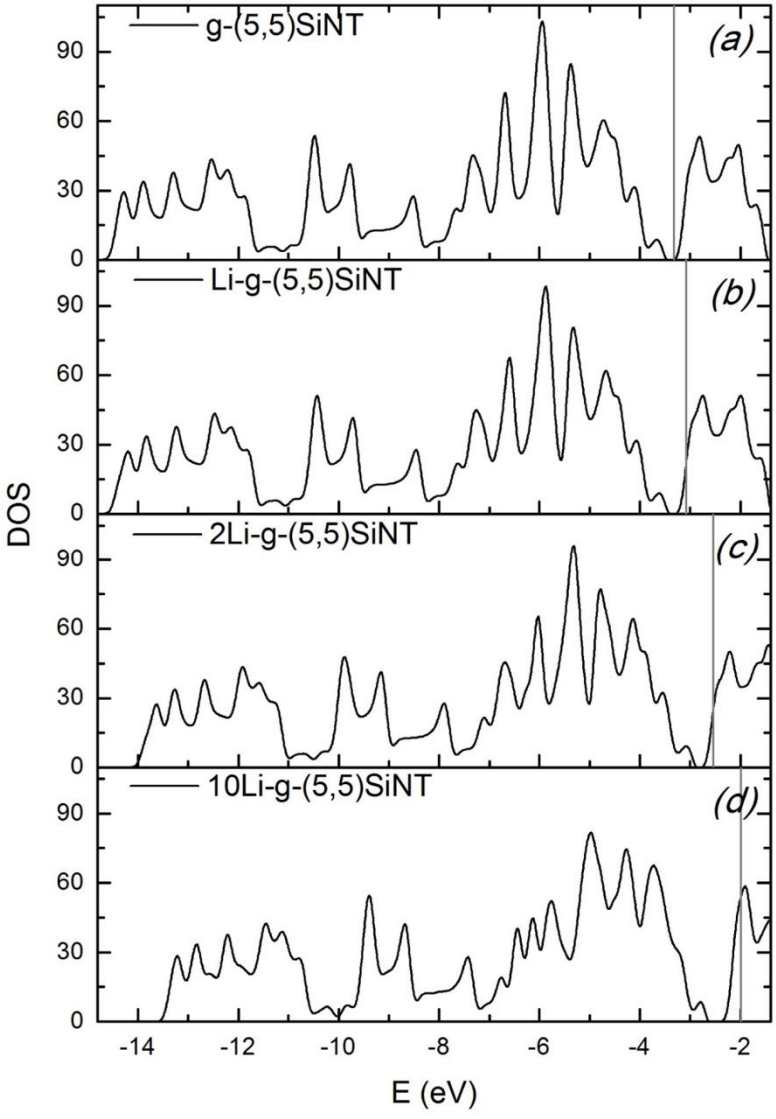

Figure 6.5. Total density of states (TDOS) of the *g*-(5,5)SiNT with (a) no Li, (b) 1 Li atom, (c) 2 Li atoms, and (d) 10 Li atoms. The grey vertical line indicates the Fermi level.

Adsorption of Li atom raises the charge transfer, shifting the Fermi level into the bottom of conduction band – from -3.32 eV in pristine to -3.08 eV in Li-adsorbed *g*-SiNTs. The adsorbed Li atom transfers its partial charge to Si but does not create an extra level inside

the band gap. Li makes two main contributions to the total DOS: one is located in the valence band while the other is around the Fermi level. Increasing the number of Li atoms also increases the amount of total charge transfer. Therefore, the Fermi level is shifted further, as shown in Figure 6.5c-d. These results suggest that Li-adsorbed *g*-SiNT becomes metal-like.

6.2.5. Lithium Diffusion in g-SiNTs

A critical issue that has to be addressed in the design of nanotubular anodes is how easy Li ions can penetrate into the nanotube interior, and hence fully utilize intercalation sites at both the outer and inner tube surfaces. For instance, the specific capacity of pristine CNTs is only 450 mAh/g,[195] barely larger than that of graphite. It is not surprising since the penetration of Li ions through the sidewalls of pristine CNT meets very high energy barriers of about 10 eV,[94, 95] suggesting that very few Li ions can actually reach the tube interior. Nevertheless, the experiments have shown that the specific capacity can be increased twice (up to 1000 mAh/g) after chemical etching or ball-milling treatment,[195, 196] which introduce sidewall defects and open ends into the nanotube. Subsequent theoretical calculations by Meunier et al.[94] and Nishidate et al.[95] demonstrated the significant reduction of energy barrier for Li motion through the created defective rings, which allows Li ions to enter the nanotube interior. Besides defect engineering, another strategy to reduce the penetration barrier is doping, as it has been shown in boron-carbon nanotubes.[96, 97] The above works highlight the effect of Li ion kinetics and, particularly, sidewall penetration barrier on the performance of practical nanotubular anodes. Therefore, it is highly necessary to address these issues in the design of SiNTs anodes.

The ability of Li ions to penetrate easily into the nanotube interior (and hence occupy more adsorption sites) greatly determines the Li storage capacity of nanotube anodes. Besides, fast Li diffusion is desirable for high charge/discharge rate in practical Li-ion batteries.

Herein, we investigate the energetics of two diffusion pathways in *g*-(5,5)SiNT:

(1) movement of Li atom in the channel inside the nanotube;

(2) penetration of Li atom into the interior through the center of sidewall Si_6 rings.

The energy barrier is defined as the difference in energy between the saddle point (i.e. the most unstable Li position) and the equilibrium state along the diffusion pathway. We firstly consider the movement of Li atom through the open-ended SiNT and subsequent diffusion inside the tube. In this case, we use the SiNT consisting of 80 Si atoms, having a length of 13.5 Å. All edge silicon atoms at both the nanotube ends are saturated by hydrogen atoms. From our calculation, we find that Li atoms tend to stay near the ends of nanotube after entering its interior. Interestingly, there is no energy barrier for Li atom to penetrate into the hydrogen-saturated SiNT due to the capillary action, likewise to the case of Li atom entering the CNT.[94, 197] The calculated energy barrier for the diffusion of Li atom inside the nanotube is 0.10 eV, implying that once Li atom can get into the interior of SiNT, the diffusion will become facile.

To evaluate the energy barriers for Li to enter through the nanotube sidewalls in *g*-(5,5) SiNT, we gradually moved the Li atom from the position outside the nanotube *(A)* through the ring *(O)* to the inside of nanotube *(B)*, and monitor the total energy changes along the diffusion path $A \rightarrow O \rightarrow B$ by means of nudged elastic band (NEB) method. The calculated energetics of this pathway is shown in Figure 6.6. The diffusion path has two

local minima positions, which correspond to the equilibrium positions of Li atom from both sides of the Si nanotube wall. Most importantly, even when Li is placed precisely at the center of the Si_6 ring, the adsorption energy still has a negative value, revealing that such situation is energetically accessible. The calculated energy barrier for Li to actually pass the sidewall ring is 1.41 eV. On the other hand, the computed energy barrier for Li penetration through the sidewall of (8,8) CNT is as large as 9.68 eV. The impressive 7 times reduction of the barrier in Si nanotubes in comparison to CNTs would result in the enhanced penetration rates into the interior through the sidewalls. Although the energy barrier remains higher than the optimal value for Li diffusion (0.4 – 0.8 eV) in the Li-ion batteries, we expect that it may be further reduced by doping[96, 97] or topological defects.

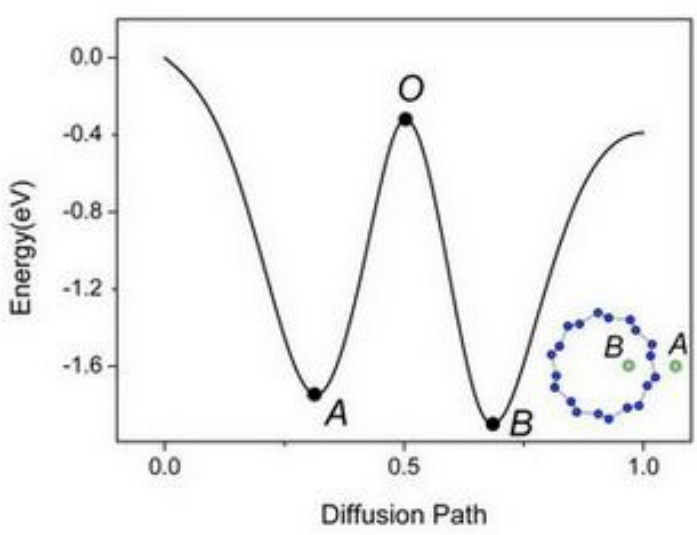

Figure 6.6. Energetics of the diffusion pathway A→O→B for Li penetration through the sidewall of *g*-(5,5) SiNT. Zero value of the distance corresponds to the center of the Si_6 ring.

The significant reduction of the energy barrier for Li penetration into *g*-(5,5) SiNT, as compared to (8,8) CNT, can be explained by the difference in the sizes of Si_6 and C_6 rings. As mentioned above, the Si-Si bond lengths are ≈1.6 times longer than

the C-C bonds, due to the larger atomic size of silicon. As the area of a regular hexagon with side length *a* is given by,

$$A = \frac{3\sqrt{3}}{2}a^2, \tag{6.4}$$

it makes Si_6 ring nearly 2.56 times larger than C_6, which facilitates Li diffusion through the ring. Moreover, when Li atom is located just at the center of the Si_6 ring, the minimum Li-Si distance is 2.34 Å, which is close to the equilibrium Li-Si value of 2.67 Å. For comparison, the minimum Li-C distance for Li atom, located at the center of the C_6 ring, and the equilibrium Li-C distance are 1.45 and 2.22 Å, respectively.

6.3. Summary

From the prospect of host stability, *g*-SiNTs are much more suitable than *h*-SiNTs for the Li-ion battery application. From our calculations, gearlike *(g-)* SiNTs remain stable with the deformations of only 1.72%; meanwhile, hexagonal *(h-)* SiNTs exhibit poor structural stability during Li insertion. Si nanotubes show higher reactivity toward the adsorption of Li adatoms than CNTs and Si nanoclusters. During multiple Li insertions, Li adsorption energy shows a dependence on the distance between adsorbed Li atoms, revealing the competition between Li-Li repulsions and attractive Li-host interaction. The binding between Li and *g*-SiNT has a positive ionic character with the electrons transferred from Li to the nanotube. This charge transfer subsequently leads to the shifting of the Fermi level to the conduction band in the total DOS, indicating that SiNT becomes metal-like, while the magnitude of the shift is proportional to the number of adsorbed Li atoms.

As fast Li diffusion is desirable for high charge/discharge rate in practical Li-ion batteries, we find that SiNT interior may serve as a fast diffusion pathway because of the low barrier of 0.10 eV, which is also true for CNTs and BC_3NTs. However, the important advantage of g-SiNTs is the significant reduction of energy barrier (nearly 7 times) for the penetration of Li atoms through the sidewall rings. Considering one of the key indications of a high performance anode is how easily Li atoms can move into the tube interior, the above findings favorably distinguish Si nanotubes from its carbon-based counterparts. Overall, the obtained results suggest that g-SiNTs are promising candidates as the anode material for Li-ion battery application. We expect that this work will promote the new applications of SiNTs, as well as contribute to the fundamental knowledge about novel Si nanostructures.

Chapter 7

Silicon Nanosheets

7.1. Introduction

Two-dimensional nanosheets (2-D NSs) with a thickness of only few nanometers have attracted tremendous attention recently because of their unusual properties, originating from the quantum size effects. For example, graphene – a famous 2-D material – exhibits high electron mobility, quantum Hall effect and remarkable mechanical strength.[198] The latest experimental advances have led to the exploration of ultrathin 2-D compounds of many materials, such as metals (e.g. Pd),[199] oxides (e.g. CeO_2, TiO_2),[200, 201] chalcogenides (e.g. MoS_2, WS_2, $MoSe_2$, TiS_2, CdSe, etc.),[202, 203] which have shown promising applications in catalysis, plasmonics, energy storage and high-k nanodielectrics.

Silicon has been a fundamental material in nanotechnology for many years, owing to its key role in modern nanoelectronics industry. Very recently, some methods for the synthesis of free-standing 2-D silicon nanosheets (SiNSs) have been reported.[64-66, 68, 204-206] For instance, using CVD technique, Kim et al. have prepared SiNSs with a thickness of just 2 nm,[64] which exhibit certain unique optoelectronic properties such as photoluminescence blue emission at 435 nm and the enhanced direct band gap transition. Moreover, Nakano and co-workers have prepared and investigated functionalized single-

layer nanosheets by the exfoliation of layered polysilane (Si_6H_6) precursor.[65, 66, 204-206] Furthermore, the synthesis of Si nanosheets with a thickness of ~3 nm using graphene oxide (GO) as the template has also been reported.[68] Nanosheets prepared by all these methods exhibit unique characteristics such as controllable thickness (single or few atomic-layers), crystalline structure with large surface area and the potentials of being functionalized by a wide range of molecules.

One of the emerging areas, where Si nanosheets can find its potential application, is the field of energy storage, particularly, as the anode of lithium-ion (Li-ion) batteries. Silicon itself is an attractive novel anode material with ultra-high Li storage capacity (4200 mAh/g), which has been suggested to replace the conventional graphite. However, the alloying reaction with Li leads to the enormous volume changes (>400%) for Si, resulting in the pulverization of the active material and large capacity fading with cycling.[207] Nevertheless, the improved anode performance has been achieved in nanostructured forms of Si, such as nanoparticles,[26, 208] nanowires,[31, 48, 209] nanotubes,[52, 53] thin films[25] and nano-composites.[24, 88, 90, 210, 211] A better understanding of the effects of size, surface structure, strain distribution, Li diffusion anisotropy, electrical conductivity is critical for further development of nanostructured Si anodes.

In this Chapter, the study on the 2-D form of Si – Si nanosheets – for its application as the anode material for Li-ion battery is presented. The large active surface area and shortened Li insertion/deinsertion paths make it attractive for such application. In fact, recent implementation of 2-D nanosheets of MoS_2,[69] TiO_2,[10, 70, 71] SnO_2,[72, 73] SnS_2[74] and graphene[212] as electrode materials have demonstrated a significant enhancement of lithium storage as compared to bulk or cluster counterparts. Owing to the unique structural features, the storage of lithium in these nanosheets mainly takes place on surface, which is different from the insertion mechanism of lithium in bulk materials.

More importantly, the effective surface storage provides remarkable improvement in high-rate charging and discharging.[71] The study of Si nanosheets for Li-ion application remains less explored in the literature to date.

We use first-principles calculations to study the ultrathin Si nanosheets as potential anode materials for Li-ion batteries. With the availability of synthesized Si nanosheets, theoretical studies can further enhance our knowledge about its properties and potential as the electrode materials. We first study the thickness dependent properties of Si nanosheets, ranging from single-layer up to 2 nm. Then, we determine the favorable binding positions of Li towards the nanosheets and more importantly, the Li diffusion rates within. In addition, we study the effect of different chemical passivations such as H, Cl, F, and I on SiNS in order to understand how the chemical surfaces affect the Li diffusion rates. Considering the high surface-to-volume ratio of nanosheets and fast Li surface diffusion rates, our results show a great potential of Si nanosheets as electrode materials for the next-generation Li-ion batteries.

7.2. Results & Discussion

7.2.1. Model of Energetically Stable (111) SiNS

The atomic structure of silicon nanosheets (SiNSs) was initially constructed by cleaving the surfaces of the bulk diamond structure of Si. Using this technique, it is possible to get nanosheets with a wide range of surface orientations and thicknesses. The thickness of the studied nanosheets varies from 0.1 to 2.0 nm, which corresponds to the thicknesses obtained in experiments.[64, 65, 68] The dangling bonds on the surfaces are passivated by hydrogen atoms. During geometry optimization, all atoms in the

constructed nanosheets are allowed to relax freely to their new equilibrium positions in order to obtain the lowest-energy configuration. A series of calculations is performed to find the equilibrium in-plane lattice constant for each Si nanosheet, corresponding to its minimum total energy. The optimized structures of SiNSs with the thickness of one, four and seven atomic layers are shown in Figure 7.1. After geometrical optimization, the atomic arrangements in the relaxed Si nanosheets preserve the features of sp^3 hybridization. The Si-Si bond lengths at the core of SiNSs are ~2.34 Å, while they are ~2.36 Å near the surfaces. The slight bond length difference is attributed to the surface relaxation effect. The Si-H bonds are ~1.50 Å. Our surface energy analysis reveals that SiNS with the (111) surface orientation has the lowest surface energy as compared to the (110) and (001) SiNSs. Therefore, the (111) orientation is expected to be the most favorable for Si nanosheets, in good agreement with experimental studies.[64, 65] Since the stability of the (111) SiNSs is confirmed by both experiment and theory, then we will focus on the nanosheets with this surface orientation in our study.

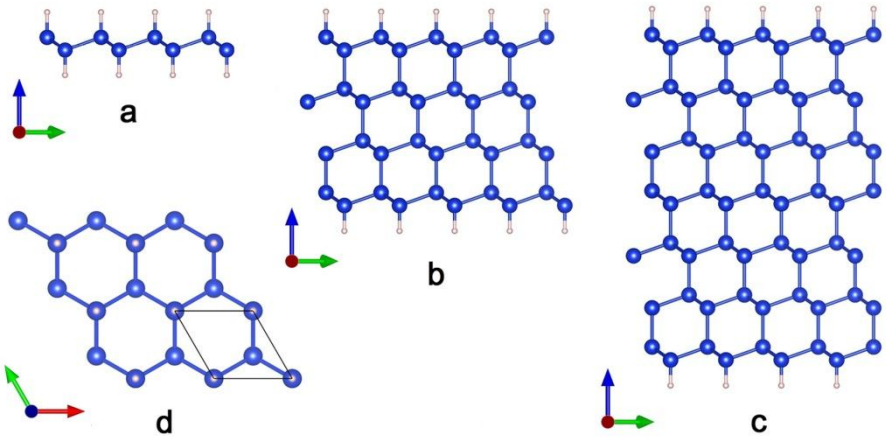

Figure 7.1. (a-c) Side views of optimized structures of hydrogenated (a) single-layer SiNS, (b) 1nm-SiNS, (c) 2nm-SiNS. (d) top view of single-layer SiNS. Blue and white balls represent Si and H, respectively.

7.2.2. Lithium Insertion Sites and Binding Energies in SiNS

To determine the preferred Li insertion sites, we calculate the binding energies of Li within Si nanosheets. The Li binding energy (E_b) is defined as:

$$E_b = E_{SiNS+Li} - E_{SiNS} - E_{Li} \tag{7.1}$$

where $E_{SiNS+Li}$, E_{SiNS} and E_{Li} are the total energies of Li-inserted SiNS, pristine SiNS and Li atom, respectively. By definition, $E_b < 0$ corresponds to exothermic reaction and attractive interaction, while $E_b > 0$ indicates the system that is thermodynamically unstable compared to its standalone parts.

From the previous literature,[108, 109] it has been concluded that tetrahedral (*Td*, see Figure 7.2a) interstitial is the most stable position for Li atoms inside the bulk silicon. Our first-principles calculations on 64-atoms Si crystal further confirm that. Tetrahedral site represents the total energy minimum with the calculated binding energy of -1.62 eV, while Li binding energy in hexagonal (*Hex*, see Figure 7.2b) site is -1.01 eV. The description of Li insertion in Si nanosheets is more complicated, because it involves non-equivalent Li positions between bulk and surface regions. We have tested all typical Li insertion sites in Si nanosheets and divided them into the following groups, as shown in Figure 7.2c: (1) surface *(S)*; (2) sub-surface *(SS)*, and (3) core *(C)*. The calculated Li binding energies in optimized Li-inserted Si nanosheets of different thickness are summarized in Table 7.1.

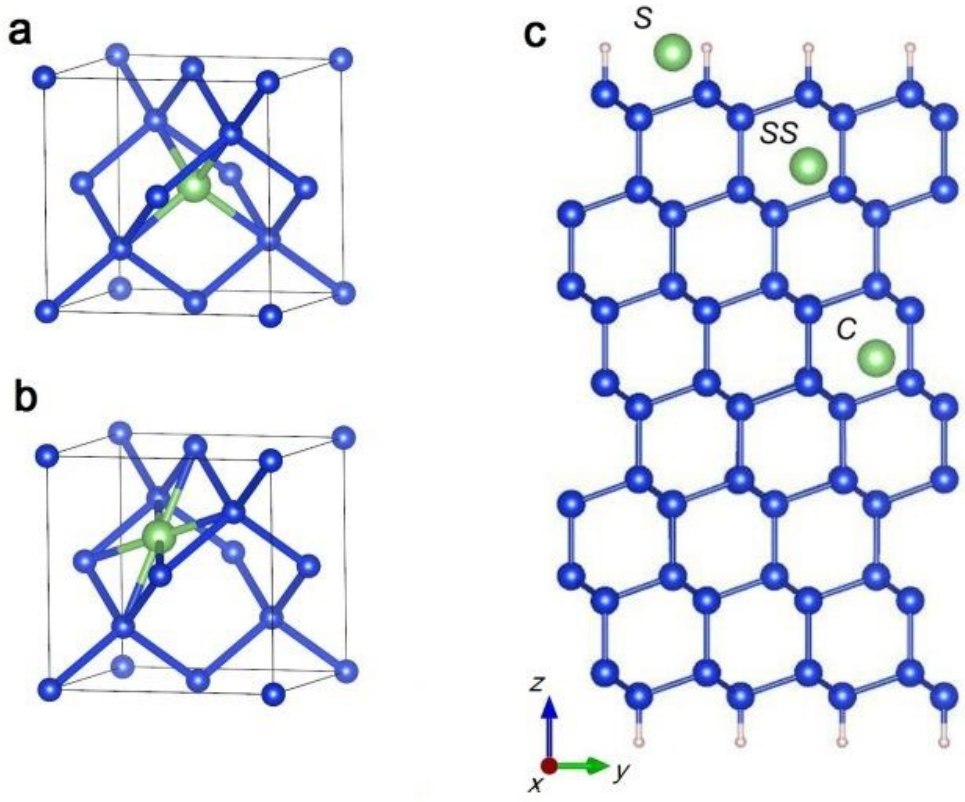

Figure 7.2. Li interstitial sites in Si: (a) tetrahedral *(Td)*, and (b) hexagonal *(Hex)*. (c) Typical Li insertion sites inside Si nanosheet: surface *(S)*, sub-surface *(SS)* and core *(C)*. Blue, green and white balls are Si, Li and H, respectively.

Table 7.1. Li binding energies (in eV) in (111) SiNS

Site type	***Single-layer***	***1 nm***	***2 nm***
Surface	-0.86	-1.47	-1.77
Sub-surface	-	-1.20	-1.43
Core	-	-1.28	-1.57

The calculated Li binding energies in all nanosheets are negative, denoting the favorable interaction between Li and the Si host. The most stable position for Li insertion is at the surface (S) site, and this trend holds for all nanosheet thicknesses. The higher Li binding energy at the surface site can be rationalized by a larger available space for Li atom at the surface, as compared to the core and sub-surface sites. In fact, the minimum Li-Si distances at the S site are ~2.66 Å, close to the sum of the Li and Si radii (i.e. 2.7 Å) and larger than those of 2.44−2.45 Å in C and SS sites. The more effective stress relaxation is responsible for the enhanced stability of Li atom at the SiNS surface. Li atoms will try to occupy all possible surface sites before proceeding to the sites in the core of nanosheet. The preference for Li insertion at the surface sites agrees well with the experimental studies, in which lithiation near the outer surface of Si nanowire proceeded faster than that near the core.[40]

We also observe a difference of 0.08-0.14 eV between the Li binding energies in core and subsurface regions of Si nanosheets (see Table 7.1). Our analysis shows that Li-Si bond lengths in the C and SS sites are identical and equal to 2.44-2.45 Å, suggesting similar stress and volume relaxation conditions. In such case, the binding energy difference is attributed to charge transfer and local environment of Si atoms. Interstitial Li atom forms four Li-Si bonds in both C and SS sites. At C site, all four Si neighbors belong to core Si atoms (Si_{core}). Meanwhile, at SS site, some of Si neighbors are surface Si atoms ($Si_{surface}$), which are passivated with hydrogen. Since H has larger electronegativity than Si, there is a charge transfer from $Si_{surface}$ to H. Charge redistribution reduces the electron density around $Si_{surface}$ atoms, which leads to weaker Li-Si interactions in the subsurface sites, as compared to core region. To confirm this idea, we use Bader charge analysis. We find a charge transfer of 0.24*e* and 0.12*e* in Li-Si_{core} and Li-$Si_{surface}$ atom pairs, respectively, suggesting weaker Li-Si bonds in the

subsurface sites. The above results show the important role of local environment of Si atoms in Li insertion process.

We also note that the thickness of the Si nanosheet has an effect on the Li binding energy. There is a trend of decreasing of Li binding energy with the decrease of nanosheet thickness. The smallest in magnitude Li binding energy has been obtained in single-layer (111) SiNSs. Moreover, the deformations of SiNS, caused by Li insertion, are also the largest in single-layers, as compared to thicker nanosheets.

7.2.3. Lithium Diffusion in SiNS: Penetration vs. Surface Pathways

Examination of the intrinsic Li ion mobility in SiNSs is of vital interest when considering its use as an anode material in lithium batteries. Simulations of such process can greatly enhance our understanding of ion diffusion pathways by evaluating the activation energies for various possible mechanisms at the atomic level.

As noted above, tetrahedral site is the most stable position for Li interstitial in bulk silicon structure. The diffusion of Li in bulk silicon occurs in the form of jumps between tetrahedral sites, while hexagonal position serves as the saddle point. The activation barrier along this diffusion pathway, calculated by the NEB method, is equal to 0.57 eV.

We now explore possible diffusion pathways for a single Li atom on Si nanosheet. When a Li atom adsorbs on the surface of (111) SiNS, two possible scenarios are considered: (1) Li atom penetrates inside the SiNS ***(penetrating diffusion)***; (2) Li atom moves along the surface of SiNS ***(surface diffusion)***. During the penetrating diffusion, Li atom motion occurs in the form of jumps between *Td* and *Hex* stable positions, similarly

to the bulk case. However, in SiNS, the Li sites are non-equivalent to each other, depending on the position inside the crystal. Figure 7.3 shows the variation of relative total energy along the diffusion pathway for penetrating Li diffusion in (111) SiNS. While moving from the *Td* site at the surface of (111) SiNS (the most stable Li position) to *Hex* site at the sub-surface (the most unstable), the Li atom has to overcome the maximum energy barrier along the diffusion pathway. Our calculated value of the energy barrier is 0.90 eV, close to the result of 0.88 eV for Si (100) surface reported by Peng et al.[213] However, once Li atom is inside the core region of nanosheet, then the diffusion barrier becomes smaller (~0.53 eV) and close to that during bulk Li diffusion.

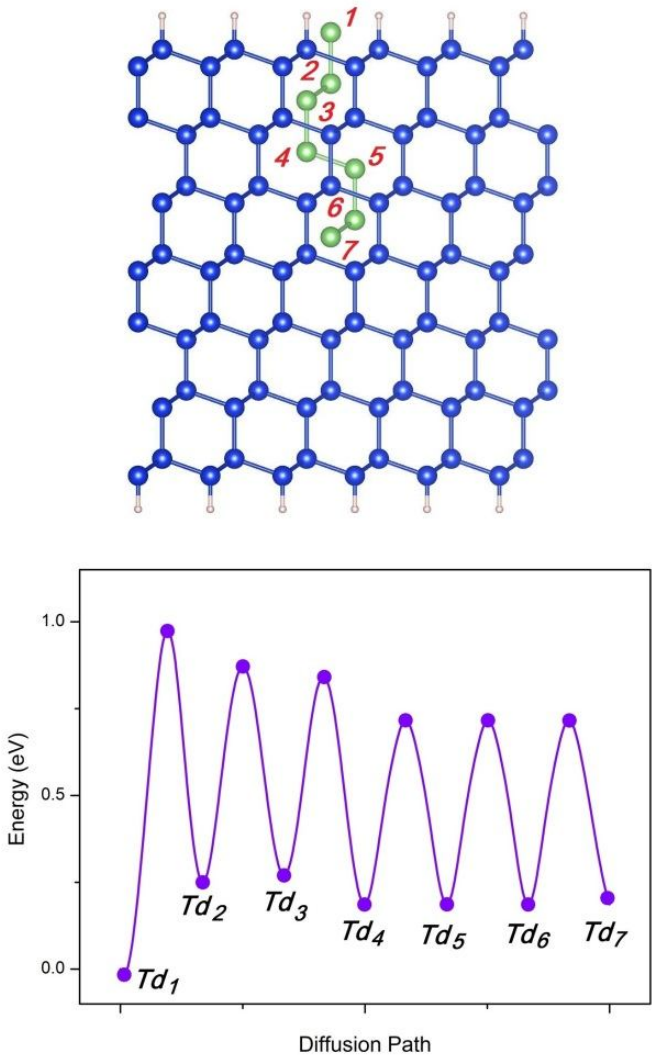

Figure 7.3. Li Penetration (surface-to-core) Diffusion. Diffusion barrier profile for Li penetrating diffusion from position 1→ position 7 as denoted above.

As the particle size is reduced to nanoscale, the ratio of surface atoms/bulk increases rapidly, and thus, the importance of the surface chemistry and surface processes becomes tremendous. Surface diffusion can play much more important role due to the increasing surface area in nanostructures (in CVD-synthesized SiNSs[64] the thickness is only few nanometers, while the width may reach several micrometers). Therefore, the impact of Li surface diffusion rates on the overall performance of SiNS-based anode material is critical. Previous theoretical studies on the Li diffusion in bulk Si,[108, 109] Si nanowires[111, 117] and Si thin films[213, 214] have mainly focused on the penetration of single Li atom into the bulk and subsequent bulk diffusion. The Li surface diffusion, on the other side, remains less explored.

The most stable positions for Li atom on surface of (111) SiNS are S_1 and S_2 sites (Figure 7.4). In S_1 site, Li atom sits on the top of a second-layer Si atom. Meanwhile, in S_2 site, Li sits on top of a first-layer Si atom. Both sites have equal Li binding energies with a difference of only 0.002 eV. The minimum Li-Si distances are 2.66 Å. We have investigated the Li surface diffusion path between two adjacent S_1 and S_2 sites on the outer surface of hydrogenated (111) SiNS. Li motion between S_1 and S_2 sites occurs through the neighbouring bridge (B) site. The Li surface diffusion path and the corresponding energy profile along this pathway are shown in Figure 7.4. The calculated energy barrier for Li diffusion on the nanosheet is only 0.13 eV, which is a significant improvement over that during bulk diffusion (0.57 eV). The difference of 0.44 eV between the energy barrier on (111) nanosheet and bulk may have a great effect on Li transport rates. Li diffusion coefficient is proportional to activation energy (energy barrier) according to Arrhenius equation:

$$D \propto exp\left(-E_{barrier}/k_B T\right), \tag{7.2}$$

where k_B is the Boltzmann constant and T is the temperature. The decrease of 0.44 eV in energy barrier for Li diffusion would result in the increase of diffusivity by a factor of 10^7 at room temperature.

In fact, an enhancement of diffusion rates in nanostructured anodes with 2D dimensionality has been demonstrated experimentally in ultrathin TiO_2 nanosheets.[71] Liu and co-workers[71] have achieved remarkable improvement in high-rate charging/discharging in the stacked TiO_2 NSs. In this structure, the storage of lithium mainly takes place on surface, maintaining rapid Li surface diffusion and electron transport and the elimination of the Li diffusion process in TiO_2 bulk. Therefore, due to large surface area of ultrathin Si nanosheets and low activation energy for Li surface diffusion, we can also expect a significant improvement of Li diffusion rates in Si nanosheets as potential anode materials for Li-ion batteries.

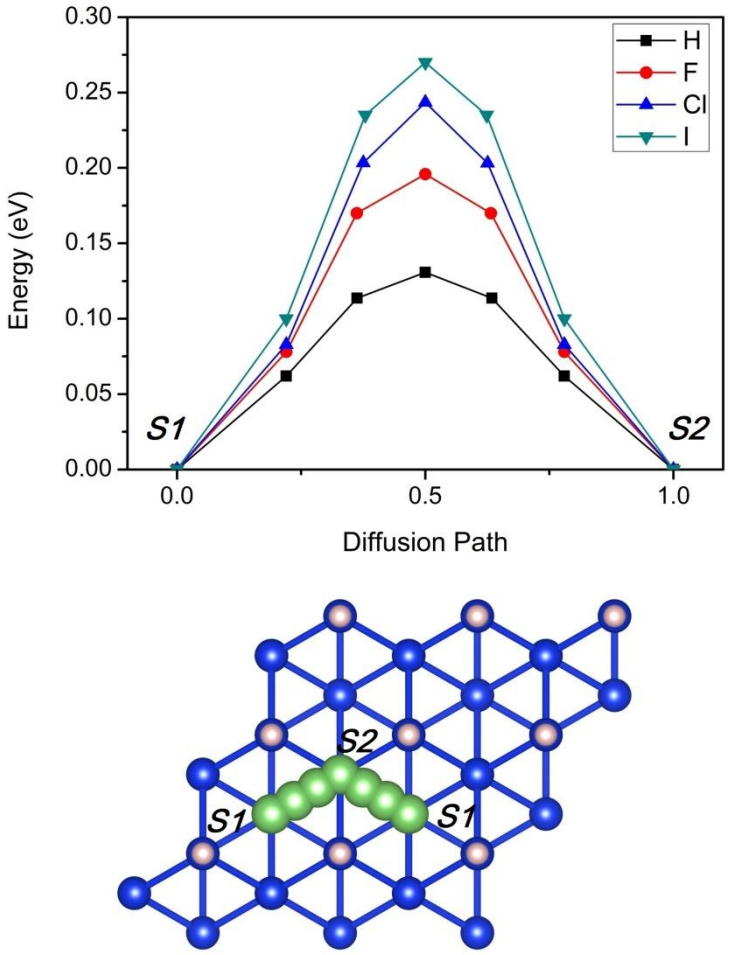

Figure 7.4. Li Surface Diffusion. Li diffusion pathway and corresponding diffusion barrier profile on the (111) SiNS-X (X = H, F, Cl, I).

7.2.4. Surface Functionalization of SiNS on Li Diffusion

In most theoretical studies of silicon nanostructures, the dangling bonds are passivated with hydrogen atoms. However, in real experiments silicon surface may also be capped with other species, such as oxides, metals, or organic molecules. Moreover, numerous studies have shown that surface passivation can tremendously change the structural and electronic properties of Si nanocrystals, nanowires or single-layer sheets.

In this respect, it is highly desirable and necessary to investigate and understand how surface chemistry may affect the properties of Si nanomaterials in Li-ion battery anodes, particularly, Li transport rates. We have modified the surface of Si nanosheets with halogen atoms (F, Cl, I) and evaluated the Li diffusion barrier in the modified nanosheets. The choice of these passivation elements has been motivated by the fact that: (1) passivation Si surfaces with halogens is an established experimental technique,[215] (2) it has been investigated in the recent model theoretical studies.[174, 216, 217]

The effect of surface species on Li surface diffusion rate is examined on the basis of Li-inserted (111) SiNS–X (X = H, F, Cl, I). The surface modification is performed by substituting the hydrogen atoms with different surface species and the resulting geometry is fully relaxed. In all the modified nanosheets, the diffusion path between two adjacent S_1 and S_2 sites on the outer surface of SiNS is investigated by CI-NEB method with 7 intermediate images. The variation of relative total energy along this diffusion path in (111) SiNS–X is plotted in Figure 7.4. We found that the energy barrier for Li diffusion is affected significantly by the surface modification. All the energy profiles corresponding to Li motion in (111) SiNS–X show a maximum at the middle between initial and final positions as in the case of hydrogenated SiNS. The value of energy barrier (activation energy for Li diffusion) changes with the change of surface species. We find that energy barrier increases with the increase in ionic radius of passivation atoms, being the lowest (0.13 eV) in (111) SiNS–H and the highest (0.27 eV) in (111) SiNS–I. The difference of 0.14 eV may result in a notable change in Li diffusivity by a factor of ~260 at room temperature since Li diffusion coefficient is exponentially proportional to activation energy as shown in eq. (7.2). Our results suggest that H passivated SiNS has the fastest Li diffusion rate. This study reveals the important effect of surface engineering on the Li transport rates in Si-based anode materials.

7.3. Summary

First-principles study on 2-D ultrathin silicon nanosheets (SiNSs) for their potential application as anode materials for Li-ion batteries is presented. From our calculations, Li binding energy is negative in all studied Si nanosheets, and it shows a strong dependence on the thickness of nanosheets. Li insertion is energetically the most favourable at the surface of Si nanosheets. As a result, lithiation near the outer surface of Si nanosheet would proceed faster than near the core. Using nudged elastic band technique, we investigate possible Li diffusion pathways and the respective activation barriers in Si nanosheets. Our results show that Li diffusion on the surfaces of Si nanosheets is very fast as compared to the bulk case (the activation barrier is 0.4 eV smaller on the surface than in the bulk). Moreover, we find that surface passivations (H, Cl, F, and I,) has a strong effect on the Li surface diffusion rate in Si nanosheets. Our results suggest H passivated SiNSs have the fastest Li diffusion rate. Considering the high surface-to-volume ratio of nanosheets and fast Li surface diffusion rates, the above results show that SiNSs are the potential electrode materials for Li-ion batteries application.

Chapter 8

Conclusions & Outlook

To summarize, detailed computational studies are performed which may serve as guidelines for the development of Si nanostructured anodes for Li-ion batteries. The calculations on total energy, atomic arrangement and electronic properties of Si clusters, Si/CNT hybrids, Si nanotubes and Si nanosheets offered detailed information about their structure and can be interesting to a general reader. The calculations on Li binding energies in the above nanomaterials provide knowledge about the occupied Li positions and Si host stability, and give insights, which are hard to get through experimental studies. As fast Li diffusion is desirable for high charge/discharge rate in practical Li-ion batteries, we studied the energy barrier for Li motion along typical diffusion paths in Si nanostructures. We reveal that Li mobility can be greatly enhanced in Si nanostructures and suggest the possible ways to control Li diffusivity through chemical modifications. The correlation between structural features, dimensional effects, surface functionalization and Li insertion characteristics are established. This study demonstrates the viability of using computations to design novel electrode materials with improved properties.

More specifically, in Chapter 5, the theoretical study on the structure and electronic properties of Si/CNT hybrids, as well as their ability for Li uptake, is presented. We reveal that in all adsorbed Si_n clusters, the structure of free-standing cluster is preserved, although slightly distorted. Once Si_n cluster becomes larger, the Si-C

interactions become weaker and the adsorbed Si cluster starts to favour 3D structures. The interaction between Si clusters and CNT support shows a strong dependence on the CNT surface chemistry. From our calculations, the interfacial bonding between Si and pristine, ammonia- or hydroxyl-functionalized CNTs is quite weak. In contrast, the bonding can be significantly improved by carboxyl-functionalization of the CNT. Both CNT and Si cluster in the hybrid Si/CNT structure preserve their Li uptake ability with the Li adsorption energies close to those in bulk Si and Si nanowires. More importantly, we show that Li insertion leads to the weakening of Si/CNT interface, which could be a main reason for the experimentally observed capacity fade in hybrid Si/CNT anode. Nevertheless, the structural integrity of Si/CNT hybrid upon lithiation is improved after the functionalization of CNT surface, potentially leading to the longer cycle life of the hybrid anode. The strengthening of Si/CNT interface through chemical functionalization may be very important in further practical applications.

In Chapter 6, we present the first-principles study on the structural and electronic properties of hexagonal and gearlike Si nanotubes (SiNTs). From the prospect of host stability, *g*-SiNTs are much more suitable than *h*-SiNTs for the Li-ion battery application. The binding between Li and *g*-SiNT has a positive ionic character with the electrons transferred from Li to the nanotube. This charge transfer subsequently leads to the shifting of the Fermi level to the conduction band in the total DOS, indicating that SiNT becomes metal-like, while the magnitude of the shift is proportional to the number of adsorbed Li atoms. We find that SiNT interior may serve as a fast diffusion pathway because of the low barrier of 0.10 eV, which is also common for CNTs and BC_3NTs. However, the important advantage of *g*-SiNTs is the significant reduction of energy barrier (nearly 7 times) for the penetration of Li atoms through the sidewall rings. Considering one of the key indications of a high performance anode is how easily Li

atoms can move into the tube interior, the above findings favorably distinguish Si nanotubes from its carbon-based counterparts.

In Chapter 7, the results of first-principles calculations on 2-D ultrathin silicon nanosheets (SiNSs) are presented. We find that the Li binding energy is negative in all studied Si nanosheets, and it shows a strong dependence on the thickness of nanosheets. Li insertion is energetically the most favorable at the surface of Si nanosheets. As a result, lithiation near the outer surface of Si nanosheet would proceed faster than near the core, in good agreement with the experimental studies. Using nudged elastic band technique, we have investigated possible Li diffusion pathways and the respective activation barriers in Si nanosheets. Our results show that Li diffusion on the surfaces of Si nanosheets is very fast as compared to the bulk case (the activation barrier is 0.4 eV smaller on the surface than in the bulk). Moreover, we have found that surface passivations (H, Cl, F, and I,) has a strong effect on the Li surface diffusion rate in Si nanosheets. Our results suggest H passivated SiNSs have the fastest Li diffusion rate. Considering the high surface-to-volume ratio of nanosheets and fast Li surface diffusion rates, our results show that SiNSs are the potential electrode materials for Li-ion batteries application.

Future Outlook

The search for alternative electrode materials for Li-ion batteries is necessary from the perspective of their emerging applications in electric vehicles and portable electronics. The theoretical studies, presented in this thesis, are novel and important. Below we would like to highlight potential future implications related to this thesis.

This thesis develops an understanding of Si/CNT interface interactions and suggests the use of rational interface functionalization for enhancing the properties, important for Li-ion battery application, such as structural stability. We expect that suggested functionalization strategy may be used to improve hybrid anodes in experimental studies.

Although the improved performance of 2D anode materials has been recently demonstrated, the studies on Si ultrathin nanosheets and nanotubes are still very rare. We expect that our theoretical study may inspire and guide further experimental investigations in this field.

Similar computational methodology can be applied in the future studies of alternative electrode materials (i.e. Ge, Sn, etc.). In the future research, we plan to add important dimensions to the research work, including other battery chemistries, such Na-ion and Mg-ion.

Appendix A

Benchmark Calculations

To determine the optimal simulation parameters, we firstly perform a series of benchmark ab initio investigations on Si and C. To determine the lattice constant in Quantum Espresso, the total energy of the given structure is calculated as a factor of the unit cell size. The lattice constant is then defined as a unit cell size, for which the total energy is minimal. We consider the effects of main simulation parameters, such as number of k-points, kinetic energy cutoffs for wavefunctions (ecutwfc) and charge density (ecutrho).

For the diamond crystal structure of Si, the experimentally measured lattice constant is 5.43 Å. Our simulations on Si diamond are performed in cubic simulation cell with 64 atoms. The k-points mesh is varied between 2x2x2, 5x5x5 and 8x8x8; ecutwfc is set as 28 Ry, 32 Ry, 37 Ry and 45 Ry; ecutrho is defined as 320 Ry and 370 Ry.

We perform benchmark calculations on two distinct C structures – diamond and graphene (sp^3 and sp^2 hybridizations, respectively). The experimental lattice constants of diamond and graphene are 3.57 and 2.46 Å, respectively. In our calculations, we use cubic diamond cell with 64 C atoms and graphene cell with 8 C atoms. For diamond, we set k-points mesh as 2x2x2, 5x5x5 and 8x8x8; ecutwfc is set as 28 Ry, 32 Ry, 37 Ry and 45 Ry; ecutrho is equal to 320 Ry and 370 Ry. For graphene, k-points mesh varies

between 3x3x1, 6x6x1, 12x12x1 and 20x20x1 with the choice of ecutwfc and ecutrho parameters, same to C diamond.

The obtained results (Figures A.1-A.6) demonstrate that a change of the simulation parameters (k-point mesh, ecutwfc and ecutrho) affects the numerical values of all total energies, but has no influence on the calculated lattice constants. The results of our calculations are in very good agreement with the experimental values, supporting our choice of pseudopotentials.

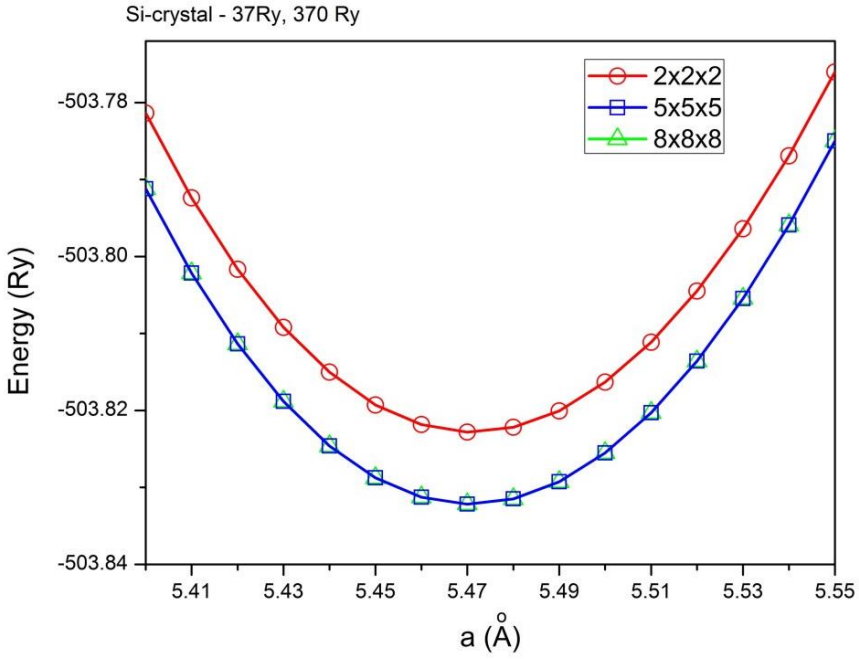

Figure A.1. Total energy of Si crystal as a function of k-points mesh. Simulation parameters: ecutwfc=37 Ry, ecutrho=370 Ry.

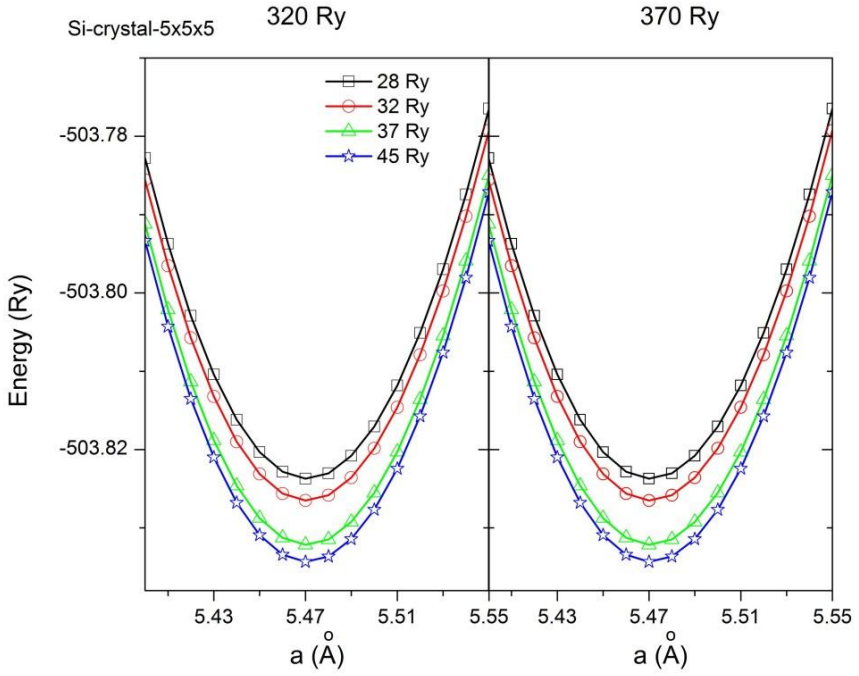

Figure A.2. Total energy of Si crystal as a function of kinetic energy cutoffs. Simulation parameters: 5x5x5 k-points mesh.

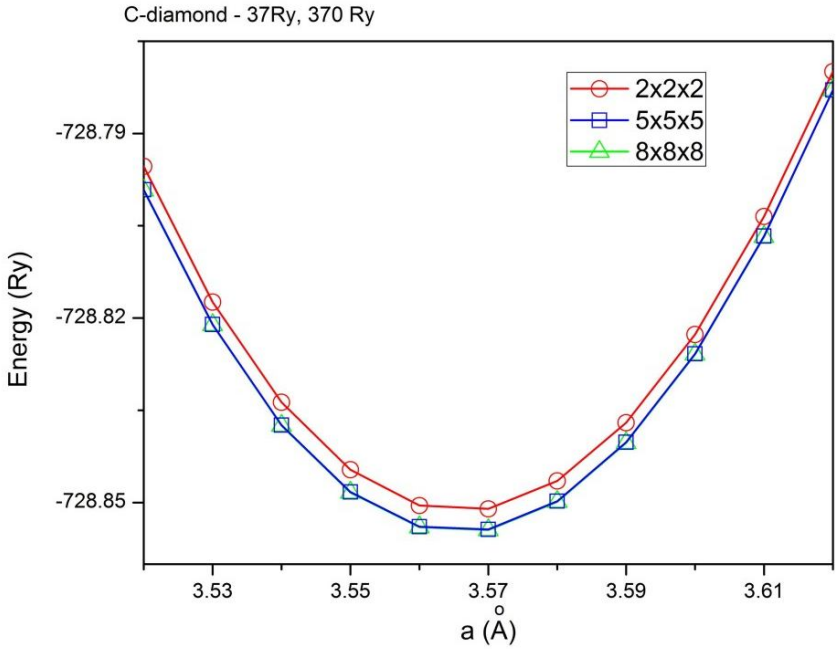

Figure A.3. Total energy of C diamond as a function of k-points mesh. Simulation parameters: ecutwfc=37 Ry, ecutrho=370 Ry.

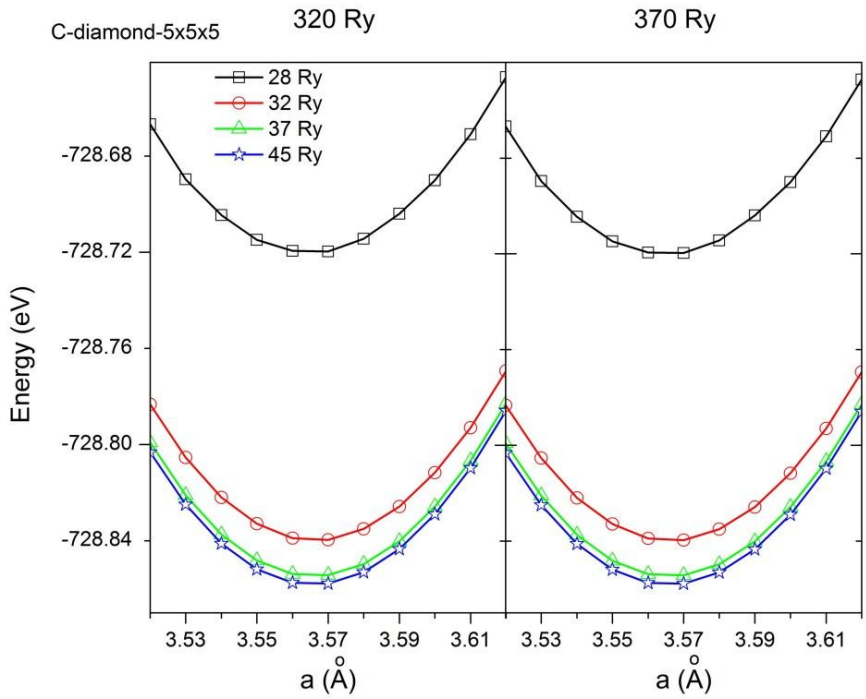

Figure A.4. Total energy of C diamond as a function of kinetic energy cutoffs. Simulation parameters: 5x5x5 k-points mesh.

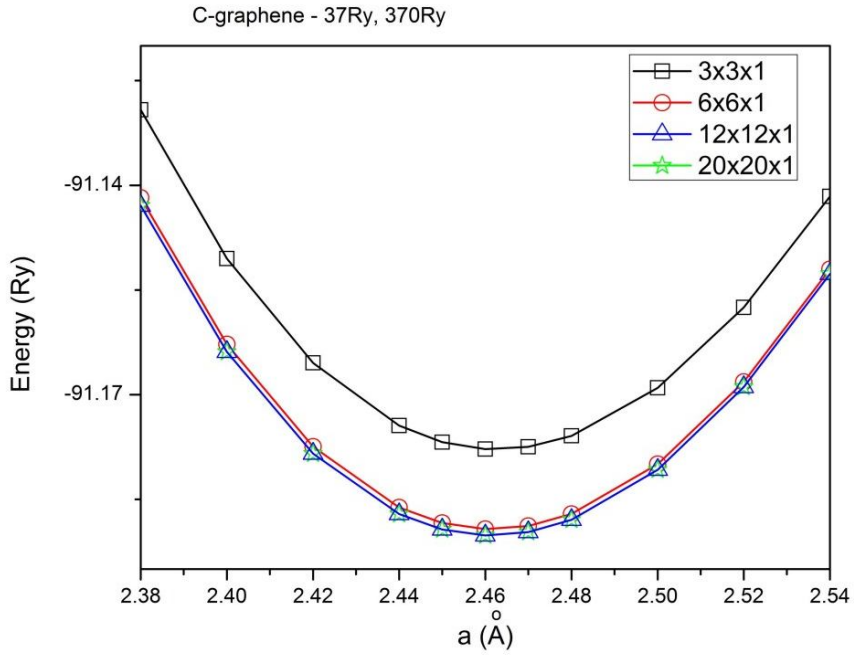

Figure A.5. Total energy of graphene as a function of k-points mesh. Simulation parameters: ecutwfc=37 Ry, ecutrho=370 Ry.

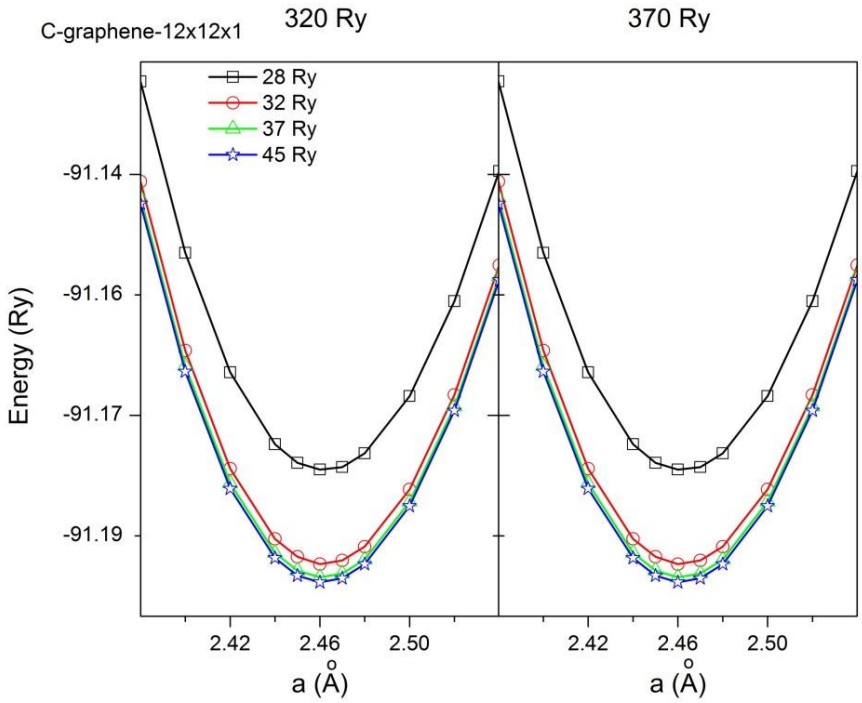

Figure A.6. Total energy of graphene as a function of of kinetic energy cutoffs. Simulation parameters: 12x12x1 k-points mesh.

List of Publications:

1. V.V. Kulish; O.I. Malyi; M.F. Ng; P. Wu; Z. Chen, *"Enhanced Li Adsorption and Diffusion in Silicon Nanosheets Based on First Principles Calculations"*, RSC Advances, 2013, *3* (13), 4231-4236.

2. V.V. Kulish; M.F. Ng; O.I. Malyi; P. Wu; Z. Chen, *"Improved Binding and Stability in Si/CNT Hybrid Nanostructures via Interfacial Functionalization: a First-Principles Study",* RSC Advances, 2013, *3* (22), 8446-8453.

3. V.V. Kulish; M.F. Ng; O.I. Malyi; P. Wu; Z. Chen, *"Enhanced Li Adsorption and Diffusion in Single-Walled Silicon Nanotubes: An Ab Initio Study"*, ChemPhysChem, 2013, *14* (6), 1161-1167.

4. O.I. Malyi, P. Wu, V.V. Kulish, K. Bai, and Z. Chen, *Formation and migration of oxygen and zirconium vacancies in cubic zirconia and zirconium oxysulfide,* Solid State Ionics, 2012, Vol. 212, pp. 117-122.

5. O.I. Malyi, K. Bai, V.V. Kulish, P. Wu, Z. Chen, *Density functional theory study of sulfur tolerance of copper: new copper-sulfur phase diagram,* Chemical Physics Letters, 2012, Vol. 533, pp. 20-24.

6. V.V. Kulish, O.I. Malyi, M.-F. Ng, P. Wu, and Z. Chen, *Do layered silicon nanomaterial have improved potential for sodium-ion batteries? A first-principles study,* submitted.

Conference Presentations:

2011 – "First Principles Study on Si/CNT Nanostructures as a Potential Anode Material for Li-ion Batteries" at International Conference on Materials and Advanced Technologies (ICMAT-2001), Singapore.

2011 – "Li Adsorption and Diffusion in Si Nanotubes: an Ab Initio Study" at The 6th Conference of the Asian Consortium on Computational Materials Science (ACCMS-6), Singapore.

References

1. Tarascon, J. M.; Armand, M., Issues and challenges facing rechargeable lithium batteries. *Nature* **2001,** *414* (6861), 359-367.

2. Armand, M.; Tarascon, J. M., Building better batteries. *Nature* **2008,** *451* (7179), 652-657.

3. Cheng, F. Y.; Liang, J.; Tao, Z. L.; Chen, J., Functional Materials for Rechargeable Batteries. *Advanced Materials* **2011,** *23* (15), 1695-1715.

4. Cairns, E. J.; Albertus, P., Batteries for Electric and Hybrid-Electric Vehicles. In *Annual Review of Chemical and Biomolecular Engineering, Vol 1*, 2010; Vol. 1, pp 299-320.

5. Ellis, B. L.; Lee, K. T.; Nazar, L. F., Positive Electrode Materials for Li-Ion and Li-Batteries. *Chem. Mat.* **2010,** *22* (3), 691-714.

6. Goodenough, J. B.; Kim, Y., Challenges for Rechargeable Li Batteries. *Chem. Mat.* **2010,** *22* (3), 587-603.

7. Landi, B. J.; Ganter, M. J.; Cress, C. D.; DiLeo, R. A.; Raffaelle, R. P., Carbon nanotubes for lithium ion batteries. *Energy Environ. Sci.* **2009,** *2* (6), 638-654.

8. Poizot, P.; Laruelle, S.; Grugeon, S.; Dupont, L.; Tarascon, J. M., Nano-sized transition-metaloxides as negative-electrode materials for lithium-ion batteries. *Nature* **2000,** *407* (6803), 496-499.

9. Armstrong, A. R.; Armstrong, G.; Canales, J.; Garcia, R.; Bruce, P. G., Lithium-ion intercalation into TiO_2-B nanowires. *Advanced Materials* **2005,** *17* (7), 862-+.

10. Chen, J.S.; Tan, Y.; Li, C.M.; Cheah, Y.L.; Luan, D.; Madhavi, S.; Boey, F.Y.C.; Archer, L.A.; Lou, X.W., Constructing Hierarchical Spheres from Large Ultrathin Anatase TiO_2 Nanosheets with Nearly 100% Exposed (001) Facets for Fast Reversible Lithium Storage. *Journal of the American Chemical Society* **2010,** *132* (17), 6124-6130.

11. Chen, J.; Xu, L. N.; Li, W. Y.; Gou, X. L., alpha-Fe_2O_3 nanotubes in gas sensor and lithium-ion battery applications. *Advanced Materials* **2005,** *17* (5), 582-+.

12. Li, W. Y.; Xu, L. N.; Chen, J., Co_3O_4 nanomaterials in lithium-ion batteries and gas sensors. *Adv. Funct. Mater.* **2005,** *15* (5), 851-857.

13. Chen, J. S.; Zhu, T.; Hu, Q. H.; Gao, J. J.; Su, F. B.; Qiao, S. Z.; Lou, X. W., Shape-Controlled Synthesis of Cobalt-based Nanocubes, Nanodiscs, and Nanoflowers and Their Comparative Lithium-Storage Properties. *Acs Applied Materials & Interfaces* **2010,** *2* (12), 3628-3635.

14. Cao, A. M.; Hu, J. S.; Liang, H. P.; Wan, L. J., Self-assembled vanadium pentoxide (V_2O_5) hollow microspheres from nanorods and their application in lithium-ion batteries. *Angew. Chem.-Int. Edit.* **2005,** *44* (28), 4391-4395.

15. Chan, C. K.; Peng, H. L.; Twesten, R. D.; Jarausch, K.; Zhang, X. F.; Cui, Y., Fast, completely reversible Li insertion in vanadium pentoxide nanoribbons. *Nano Lett.* **2007,** *7* (2), 490-495.

16. Park, C. M.; Kim, J. H.; Kim, H.; Sohn, H. J., Li-alloy based anode materials for Li secondary batteries. *Chemical Society Reviews* **2010,** *39* (8), 3115-3141.

17. Larcher, D.; Beattie, S.; Morcrette, M.; Edstroem, K.; Jumas, J.C.; Tarascon, J.M., Recent findings and prospects in the field of pure metals as negative electrodes for Li-ion batteries. *J. Mater. Chem.* **2007,** *17* (36), 3759-3772.

18. Flandrois, S.; Simon, B., Carbon materials for lithium-ion rechargeable batteries. *Carbon* **1999,** *37* (2), 165-180.

19. Maranchi, J. P.; Hepp, A. F.; Evans, A. G.; Nuhfer, N. T.; Kumta, P. N., Interfacial properties of the a-Si/Cu : active-inactive thin-film anode system for lithium-ion batteries. *J. Electrochem. Soc.* **2006,** *153* (6), A1246-A1253.

20. Arico, A. S.; Bruce, P.; Scrosati, B.; Tarascon, J. M.; Van Schalkwijk, W., Nanostructured materials for advanced energy conversion and storage devices. *Nat. Mater.* **2005,** *4* (5), 366-377.

21. Jiang, C. H.; Hosono, E.; Zhou, H. S., Nanomaterials for lithium ion batteries. *Nano Today* **2006,** *1* (4), 28-33.

22. Bruce, P. G.; Scrosati, B.; Tarascon, J. M., Nanomaterials for rechargeable lithium batteries. *Angew. Chem.-Int. Edit.* **2008,** *47* (16), 2930-2946.

23. Szczech, J. R.; Jin, S., Nanostructured silicon for high capacity lithium battery anodes. *Energy Environ. Sci.* **2011,** *4* (1), 56-72.

24. Li, H.; Huang, X. J.; Chen, L. Q.; Wu, Z. G.; Liang, Y., A high capacity nano-Si composite anode material for lithium rechargeable batteries. *Electrochem. Solid State Lett.* **1999,** *2* (11), 547-549.

25. Graetz, J.; Ahn, C. C.; Yazami, R.; Fultz, B., Highly reversible lithium storage in nanostructured silicon. *Electrochem. Solid State Lett.* **2003,** *6* (9), A194-A197.

26. Kim, H.; Seo, M.; Park, M. H.; Cho, J., A Critical Size of Silicon Nano-Anodes for Lithium Rechargeable Batteries. *Angew. Chem.-Int. Edit.* **2010,** *49* (12), 2146-2149.

27. Li, H.; Huang, X. J.; Chen, L. Q.; Zhou, G. W.; Zhang, Z.; Yu, D. P.; Mo, Y. J.; Pei, N., The crystal structural evolution of nano-Si anode caused by lithium insertion and extraction at room temperature. *Solid State Ionics* **2000,** *135* (1-4), 181-191.

28. Meduri, P.; Pendyala, C.; Kumar, V.; Sumanasekera, G. U.; Sunkara, M. K., Hybrid Tin Oxide Nanowires as Stable and High Capacity Anodes for Li-Ion Batteries. *Nano Lett.* **2009,** *9* (2), 612-616.

29. Wang, D. H.; Choi, D. W.; Li, J.; Yang, Z. G.; Nie, Z. M.; Kou, R.; Hu, D. H.; Wang, C. M.; Saraf, L. V.; Zhang, J. G.; Aksay, I. A.; Liu, J., Self-Assembled TiO_2-Graphene Hybrid Nanostructures for Enhanced Li-Ion Insertion. *ACS Nano* **2009,** *3* (4), 907-914.

30. Kim, S. W.; Seo, D. H.; Gwon, H.; Kim, J.; Kang, K., Fabrication of FeF_3 Nanoflowers on CNT Branches and Their Application to High Power Lithium Rechargeable Batteries. *Advanced Materials* **2010,** *22* (46), 5260-5264.

31. Chan, C. K.; Peng, H. L.; Liu, G.; McIlwrath, K.; Zhang, X. F.; Huggins, R. A.; Cui, Y., High-performance lithium battery anodes using silicon nanowires. *Nat. Nanotechnol.* **2008,** *3* (1), 31-35.

32. Chockla, A. M.; Harris, J. T.; Akhavan, V. A.; Bogart, T. D.; Holmberg, V. C.; Steinhagen, C.; Mullins, C. B.; Stevenson, K. J.; Korgel, B. A., Silicon Nanowire Fabric as a Lithium Ion Battery Electrode Material. *Journal of the American Chemical Society* **2011,** *133* (51), 20914-20921.

33. Liu, N. A.; Hu, L. B.; McDowell, M. T.; Jackson, A.; Cui, Y., Prelithiated Silicon Nanowires as an Anode for Lithium Ion Batteries. *ACS Nano* **2011,** *5* (8), 6487-6493.

34. Nguyen, H.T.; Yao, F.; Zamfir, M.R.; Biswas, C.; So, K.P.; Lee, Y.H.; Kim, S.M.; Cha, S.N.; Kim, J.M.; Pribat, D., Highly Interconnected Si Nanowires for Improved Stability Li-Ion Battery Anodes. *Advanced Energy Materials* **2011,** *1* (6), 1154-1161.

35. Ge, M. Y.; Rong, J. P.; Fang, X.; Zhou, C. W., Porous Doped Silicon Nanowires for Lithium Ion Battery Anode with Long Cycle Life. *Nano Lett.* **2012,** *12* (5), 2318-2323.

36. Liu, X. H.; Zhang, L. Q.; Zhong, L.; Liu, Y.; Zheng, H.; Wang, J. W.; Cho, J. H.; Dayeh, S. A.; Picraux, S. T.; Sullivan, J. P.; Mao, S. X.; Ye, Z. Z.; Huang, J. Y., Ultrafast Electrochemical Lithiation of Individual Si Nanowire Anodes. *Nano Lett.* **2011,** *11* (6), 2251-2258.

37. McDowell, M. T.; Lee, S. W.; Ryu, I.; Wu, H.; Nix, W. D.; Choi, J. W.; Cui, Y., Novel Size and Surface Oxide Effects in Silicon Nanowires as Lithium Battery Anodes. *Nano Lett.* **2011,** *11* (9), 4018-4025.

38. Chen, H. X.; Xiao, Y.; Wang, L.; Yang, Y., Silicon nanowires coated with copper layer as anode materials for lithium-ion batteries. *Journal of Power Sources* **2011,** *196* (16), 6657-6662.

39. McDowell, M. T.; Cui, Y., Single Nanostructure Electrochemical Devices for Studying Electronic Properties and Structural Changes in Lithiated Si Nanowires. *Advanced Energy Materials* **2011,** *1* (5), 894-900.

40. Liu, X. H.; Zheng, H.; Zhong, L.; Huan, S.; Karki, K.; Zhang, L. Q.; Liu, Y.; Kushima, A.; Liang, W.T.; Wang, J.W.; Cho, J.H.; Epstein, E.; Dayeh, S.A.; Picraux, S.T.; Zhu, T.; Li, J.; Sullivan, J. P.; Cumings, J.; Wang, C. S.; Mao, S. X.; Ye, Z. Z.; Zhang, S. L.; Huang, J. Y., Anisotropic Swelling and Fracture of Silicon Nanowires during Lithiation. *Nano Lett.* **2011,** *11* (8), 3312-3318.

41. Lee, S. W.; McDowell, M. T.; Choi, J. W.; Cui, Y., Anomalous Shape Changes of Silicon Nanopillars by Electrochemical Lithiation. *Nano Lett.* **2011,** *11* (7), 3034-3039.

42. Yang, H.; Huang, S.; Huang, X.; Fan, F. F.; Liang, W. T.; Liu, X. H.; Chen, L. Q.; Huang, J. Y.; Li, J.; Zhu, T.; Zhang, S. L., Orientation-Dependent Interfacial Mobility Governs the Anisotropic Swelling in Lithiated Silicon Nanowires. *Nano Lett.* **2012,** *12* (4), 1953-1958.

43. Lee, S. W.; McDowell, M. T.; Berla, L. A.; Nix, W. D.; Cui, Y., Fracture of crystalline silicon nanopillars during electrochemical lithium insertion. *Proceedings of the National Academy of Sciences of the United States of America* **2012,** *109* (11), 4080-4085.

44. Liu, X. H.; Liu, Y.; Kushima, A.; Zhang, S.; Zhu, T.; Li, J.; Huang, J. Y., In Situ TEM Experiments of Electrochemical Lithiation and Delithiation of Individual Nanostructures. *Advanced Energy Materials* **2012,** *2* (7), 722-741.

45. Liu, X. H.; Huang, J. Y., In situ TEM electrochemistry of anode materials in lithium ion batteries. *Energy Environ. Sci.* **2011,** *4* (10), 3844-3860.

46. Karki, K.; Epstein, E.; Cho, J. H.; Jia, Z.; Li, T.; Picraux, S. T.; Wang, C. S.; Cumings, J., Lithium-Assisted Electrochemical Welding in Silicon Nanowire Battery Electrodes. *Nano Lett.* **2012,** *12* (3), 1392-1397.

47. Liu, R.; Duay, J.; Lee, S. B., Heterogeneous nanostructured electrode materials for electrochemical energy storage. *Chemical Communications* **2011,** *47* (5), 1384-1404.

48. Cui, L. F.; Ruffo, R.; Chan, C. K.; Peng, H. L.; Cui, Y., Crystalline-Amorphous Core-Shell Silicon Nanowires for High Capacity and High Current Battery Electrodes. *Nano Lett.* **2009,** *9* (1), 491-495.

49. Chen, H.; Xu, J.; Chen, P.-c.; Fang, X.; Qiu, J.; Fu, Y.; Zhou, C., Bulk Synthesis of Crystalline and Crystalline Core/Amorphous Shell Silicon Nanowires and Their Application for Energy Storage. *ACS Nano* **2011,** *5* (10), 8383-8390.

50. Ben-Ishai, M.; Patolsky, F., Wall-Selective Chemical Alteration of Silicon Nanotube Molecular Carriers. *Journal of the American Chemical Society* **2011,** *133* (5), 1545-1552.

51. Ben Ishai, M.; Patolsky, F., Shape- and Dimension-Controlled Single-Crystalline Silicon and SiGe Nanotubes: Toward Nanofluidic FET Devices. *Journal of the American Chemical Society* **2009,** *131* (10), 3679-3689.

52. Park, M. H.; Kim, M. G.; Joo, J.; Kim, K.; Kim, J.; Ahn, S.; Cui, Y.; Cho, J., Silicon Nanotube Battery Anodes. *Nano Lett.* **2009,** *9* (11), 3844-3847.

53. Song, T.; Xia, J.L.; Lee, J.H.; Lee, D.H.; Kwon, M.S.; Choi, J.M.; Wu, J.; Doo, S.; Chang, H.; Il Park, W.; Zang, D. S.; Kim, H.; Huang, Y. G.; Hwang, K. C.; Rogers, J. A.; Paik, U., Arrays of Sealed Silicon Nanotubes As Anodes for Lithium Ion Batteries. *Nano Lett.* **2010,** *10* (5), 1710-1716.

54. Yoo, J.-K.; Kim, J.; Jung, Y. S.; Kang, K., Scalable Fabrication of Silicon Nanotubes and their Application to Energy Storage. *Advanced Materials* **2012**, *24* (40), 5452-5456.

55. Kim, H.; Han, B.; Choo, J.; Cho, J., Three-Dimensional Porous Silicon Particles for Use in High-Performance Lithium Secondary Batteries. *Angew. Chem.-Int. Edit.* **2008,** *47* (52), 10151-10154.

56. Yao, Y.; McDowell, M. T.; Ryu, I.; Wu, H.; Liu, N. A.; Hu, L. B.; Nix, W. D.; Cui, Y., Interconnected Silicon Hollow Nanospheres for Lithium-Ion Battery Anodes with Long Cycle Life. *Nano Lett.* **2011,** *11* (7), 2949-2954.

57. Liu, N.; Wu, H.; McDowell, M. T.; Yao, Y.; Wang, C.; Cui, Y., A Yolk-Shell Design for Stabilized and Scalable Li-Ion Battery Alloy Anodes. *Nano Lett.* **2012,** *12* (6), 3315-3321.

58. Wu, H.; Zheng, G.; Liu, N.; Carney, T. J.; Yang, Y.; Cui, Y., Engineering Empty Space between Si Nanoparticles for Lithium-Ion Battery Anodes. *Nano Lett.* **2012,** *12* (2), 904-909.

59. Hertzberg, B.; Alexeev, A.; Yushin, G., Deformations in Si−Li Anodes Upon Electrochemical Alloying in Nano-Confined Space. *Journal of the American Chemical Society* **2010,** *132* (25), 8548-8549.

60. Maranchi, J. P.; Hepp, A. F.; Kumta, P. N., High capacity, reversible silicon thin-film anodes for lithium-ion batteries. *Electrochem. Solid State Lett.* **2003,** *6* (9), A198-A201.

61. Ohara, S.; Suzuki, J.; Sekine, K.; Takamura, T., A thin film silicon anode for Li-ion batteries having a very large specific capacity and long cycle life. *Journal of Power Sources* **2004,** *136* (2), 303-306.

62. Li, J. C.; Dozier, A. K.; Li, Y. C.; Yang, F. Q.; Cheng, Y. T., Crack Pattern Formation in Thin Film Lithium-Ion Battery Electrodes. *J. Electrochem. Soc.* **2011,** *158* (6), A689-A694.

63. Yu, C.; Li, X.; Ma, T.; Rong, J.; Zhang, R.; Shaffer, J.; An, Y.; Liu, Q.; Wei, B.; Jiang, H., Silicon Thin Films as Anodes for High-Performance Lithium-Ion Batteries with Effective Stress Relaxation. *Advanced Energy Materials* **2012,** *2* (1), 68-73.

64. Kim, U.; Kim, I.; Park, Y.; Lee, K. Y.; Yim, S. Y.; Park, J. G.; Ahn, H. G.; Park, S. H.; Choi, H. J., Synthesis of Si Nanosheets by a Chemical Vapor Deposition Process and Their Blue Emissions. *ACS Nano* **2011,** *5* (3), 2176-2181.

65. Okamoto, H.; Kumai, Y.; Sugiyama, Y.; Mitsuoka, T.; Nakanishi, K.; Ohta, T.; Nozaki, H.; Yamaguchi, S.; Shirai, S.; Nakano, H., Silicon Nanosheets and Their Self-Assembled Regular Stacking Structure. *Journal of the American Chemical Society* **2010,** *132* (8), 2710-2718.

66. Sugiyama, Y.; Okamoto, H.; Mitsuoka, T.; Morikawa, T.; Nakanishi, K.; Ohta, T.; Nakano, H., Synthesis and Optical Properties of Monolayer Organosilicon Nanosheets. *Journal of the American Chemical Society* **2010,** *132* (17), 5946-+.

67. Okamoto, H.; Sugiyama, Y.; Nakano, H., Synthesis and Modification of Silicon Nanosheets and Other Silicon Nanomaterials. *Chemistry – A European Journal* **2011,** *17* (36), 9864-9887.

68. Lu, Z.; Zhu, J.; Sim, D.; Zhou, W.; Shi, W.; Hng, H. H.; Yan, Q., Synthesis of Ultrathin Silicon Nanosheets by Using Graphene Oxide as Template. *Chem. Mat.* **2011,** *23* (24), 5293-5295.

69. Ding, S.; Zhang, D.; Chen, J. S.; Lou, X. W., Facile synthesis of hierarchical MoS_2 microspheres composed of few-layered nanosheets and their lithium storage properties. *Nanoscale* **2012,** *4* (1), 95-98.

70. Chen, J. S.; Lou, X. W., Anatase TiO_2 nanosheet: An ideal host structure for fast and efficient lithium insertion/extraction. *Electrochemistry Communications* **2009,** *11* (12), 2332-2335.

71. Liu, J. H.; Chen, J. S.; Wei, X. F.; Lou, X. W.; Liu, X. W., Sandwich-Like, Stacked Ultrathin Titanate Nanosheets for Ultrafast Lithium Storage. *Advanced Materials* **2011,** *23* (8), 998-1002.

72. Wang, C.; Zhou, Y.; Ge, M. Y.; Xu, X. B.; Zhang, Z. L.; Jiang, J. Z., Large-Scale Synthesis of SnO_2 Nanosheets with High Lithium Storage Capacity. *Journal of the American Chemical Society* **2010,** *132* (1), 46-+.

73. Ding, S.; Wen Lou, X., SnO_2 nanosheet hollow spheres with improved lithium storage capabilities. *Nanoscale* **2011,** *3* (9), 3586-3588.

74. Kim, T. J.; Kirn, C.; Son, D.; Choi, M.; Park, B., Novel SnS_2-nanosheet anodes for lithium-ion batteries. *Journal of Power Sources* **2007,** *167* (2), 529-535.

75. Wilson, A. M.; Dahn, J. R., Lithium Insertion in Carbons Containing Nanodispersed Silicon. *J. Electrochem. Soc.* **1995,** *142* (2), 326-332.

76. Wang, G. X.; Ahn, J. H.; Yao, J.; Bewlay, S.; Liu, H. K., Nanostructured Si-C composite anodes for lithium-ion batteries. *Electrochemistry Communications* **2004,** *6* (7), 689-692.

77. Kim, I. S.; Kumta, P. N., High capacity Si/C nanocomposite anodes for Li-ion batteries. *Journal of Power Sources* **2004,** *136* (1), 145-149.

78. Niu, J. J.; Lee, J. Y., Improvement of usable capacity and cyclability of silicon-based anode materials for lithium batteries by sol-gel graphite matrix. *Electrochem. Solid State Lett.* **2002,** *5* (6), A107-A110.

79. Wang, W.; Kumta, P. N., Reversible high capacity nanocomposite anodes of Si/C/SWNTs for rechargeable Li-ion batteries. *Journal of Power Sources* **2007,** *172* (2), 650-658.

80. Yang, J.; Wang, B. F.; Wang, K.; Liu, Y.; Xie, J. Y.; Wen, Z. S., Si/C composites for high capacity lithium storage materials. *Electrochem. Solid State Lett.* **2003,** *6* (8), A154-A156.

81. Shu, J.; Li, H.; Yang, R. Z.; Shi, Y.; Huang, X. J., Cage-like carbon nanotubes/Si composite as anode material for lithium ion batteries. *Electrochemistry Communications* **2006,** *8* (1), 51-54.

82. Zhang, Y.; Zhang, X. G.; Zhang, H. L.; Zhao, Z. G.; Li, F.; Liu, C.; Cheng, H. M., Composite anode material of silicon/graphite/carbon nanotubes for Li-ion batteries. *Electrochimica Acta* **2006,** *51* (23), 4994-5000.

83. Grobert, N., Carbon nanotubes - becoming clean. *Materials Today* **2007,** *10* (1-2), 28-35.

84. Reddy, A. L. M.; Shaijumon, M. M.; Gowda, S. R.; Ajayan, P. M., Coaxial MnO_2/Carbon Nanotube Array Electrodes for High-Performance Lithium Batteries. *Nano Lett.* **2009,** *9* (3), 1002-1006.

85. Cao, F. F.; Guo, Y. G.; Zheng, S. F.; Wu, X. L.; Jiang, L. Y.; Bi, R. R.; Wan, L. J.; Maier, J., Symbiotic Coaxial Nanocables: Facile Synthesis and an Efficient and Elegant Morphological Solution to the Lithium Storage Problem. *Chem. Mat.* **2010,** *22* (5), 1908-1914.

86. Wang, G. X.; Wang, B.; Wang, X. L.; Park, J.; Dou, S. X.; Ahn, H.; Kim, K., Sn/graphene nanocomposite with 3D architecture for enhanced reversible lithium storage in lithium ion batteries. *J. Mater. Chem.* **2009,** *19* (44), 8378-8384.

87. Zhang, H.; Cao, G. P.; Wang, Z. Y.; Yang, Y. S.; Shi, Z. J.; Gu, Z. N., Growth of manganese oxide nanoflowers on vertically-aligned carbon nanotube arrays for high-rate electrochemical capacitive energy storage. *Nano Lett.* **2008,** *8* (9), 2664-2668.

88. Hu, L. B.; Wu, H.; Hong, S. S.; Cui, L. F.; McDonough, J. R.; Bohy, S.; Cui, Y., Si nanoparticle-decorated Si nanowire networks for Li-ion battery anodes. *Chemical Communications* **2011,** *47* (1), 367-369.

89. Zhao, X.; Hayner, C. M.; Kung, M. C.; Kung, H. H., In-Plane Vacancy-Enabled High-Power Si-Graphene Composite Electrode for Lithium-Ion Batteries. *Advanced Energy Materials* **2011,** *1* (6), 1079-1084.

90. Lee, J. K.; Smith, K. B.; Hayner, C. M.; Kung, H. H., Silicon nanoparticles-graphene paper composites for Li ion battery anodes. *Chemical Communications* **2010,** *46* (12), 2025-2027.

91. Wang, W.; Kumta, P. N., Nanostructured Hybrid Silicon/Carbon Nanotube Heterostructures: Reversible High-Capacity Lithium-Ion Anodes. *ACS Nano* **2010,** *4* (4), 2233-2241.

92. Chan, C. K.; Patel, R. N.; O'Connell, M. J.; Korgel, B. A.; Cui, Y., Solution-Grown Silicon Nanowires for Lithium-Ion Battery Anodes. *ACS Nano* **2010,** *4* (3), 1443-1450.

93. Zhao, J.; Buldum, A.; Han, J.; Lu, J. P., First-principles study of Li-intercalated carbon nanotube ropes. *Physical Review Letters* **2000,** *85* (8), 1706-1709.

94. Meunier, V.; Kephart, J.; Roland, C.; Bernholc, J., Ab initio investigations of lithium diffusion in carbon nanotube systems. *Physical Review Letters* **2002,** *88* (7), 4.

95. Nishidate, K.; Hasegawa, M., Energetics of lithium ion adsorption on defective carbon nanotubes. *Phys. Rev. B* **2005,** *71* (24).

96. Zhou, Z.; Zhao, J. J.; Gao, X. P.; Chen, Z. F.; Yan, J.; Schleyer, P. V.; Morinaga, M., Do composite single-walled nanotubes have enhanced capability for lithium storage? *Chem. Mat.* **2005,** *17* (5), 992-1000.

97. Zhao, J. J.; Wen, B.; Zhou, Z.; Chen, Z. F.; Schleyer, P. V., Reduced Li diffusion barriers in composite BC_3 nanotubes. *Chemical Physics Letters* **2005,** *415* (4-6), 323-326.

98. Koh, W.; Choi, J. I.; Lee, S. G.; Lee, W. R.; Jang, S. S., First-principles study of Li adsorption in a carbon nanotube-fullerene hybrid system. *Carbon* **2011,** *49* (1), 286-293.

99. Koh, W.; Choi, J. I.; Donaher, K.; Lee, S. G.; Jang, S. S., Mechanism of Li Adsorption on Carbon Nanotube-Fullerene Hybrid System: A First-Principles Study. *Acs Applied Materials & Interfaces* **2011,** *3* (4), 1186-1194.

100. Zheng, J. W.; Nai, S. M. L.; Ng, M. F.; Wu, P.; Wei, J.; Gupta, M., DFT Study on Nano Structures of Sn/CNT Complex for Potential Li-Ion Battery Application. *J. Phys. Chem. C* **2009,** *113* (31), 14015-14019.

101. Ng, M. F.; Zheng, J. W.; Wu, P., Evaluation of Sn Nanowire Encapsulated Carbon Nanotube for a Li-Ion Battery Anode by DFT Calculations. *J. Phys. Chem. C* **2010,** *114* (18), 8542-8545.

102. Cho, Y. J.; Kim, H. S.; Im, H.; Myung, Y.; Jung, G. B.; Lee, C. W.; Park, J.; Park, M. H.; Cho, J.; Kang, H. S., Nitrogen-Doped Graphitic Layers Deposited on Silicon Nanowires for Efficient Lithium-Ion Battery Anodes. *J. Phys. Chem. C* **2011,** *115* (19), 9451-9457.

103. Chi, D.H.; Cuong, N.T.; Tuan, N.A.; Kim, Y.T.; Bao, H.T.; Mitani, T.; Ozaki, T.; Nagao, H., Electronic structures of Pt clusters adsorbed on (5,5) single wall carbon nanotube. *Chemical Physics Letters* **2006,** *432* (1-3), 213-217.

104. Yoon, M.; Yang, S. Y.; Hicke, C.; Wang, E.; Geohegan, D.; Zhang, Z. Y., Calcium as the superior coating metal in functionalization of carbon fullerenes for high-capacity hydrogen storage. *Physical Review Letters* **2008,** *100* (20).

105. Sun, Q.; Jena, P.; Wang, Q.; Marquez, M., First-principles study of hydrogen storage on $Li_{12}C_{60}$. *Journal of the American Chemical Society* **2006,** *128* (30), 9741-9745.

106. Cuong, N. T.; Sugiyama, A.; Fujiwara, A.; Mitani, T.; Chi, D. H., Density functional study of Pt-4 clusters adsorbed on a carbon nanotube support. *Phys. Rev. B* **2009,** *79* (23).

107. Krishnan, S.; Yilmaz, H.; Vadapoo, R.; Marin, C., Selenium adsorbed single wall carbon nanotubes as a potential candidate for nanoscale interconnects. *Applied Physics Letters* **2010,** *97* (16).

108. Wan, W. H.; Zhang, Q. F.; Cui, Y.; Wang, E. G., First principles study of lithium insertion in bulk silicon. *J. Phys.-Condes. Matter* **2010,** *22* (41).

109. Kim, H.; Kweon, K. E.; Chou, C. Y.; Ekerdt, J. G.; Hwang, G. S., On the Nature and Behavior of Li Atoms in Si: A First Principles Study. *J. Phys. Chem. C* **2010,** *114* (41), 17942-17946.

110. Aggarwal, R. L.; Fisher, P.; Mourzine, V.; Ramdas, A. K., Excitation Spectra of Lithium Donors in Silicon and Germanium. *Physical Review* **1965,** *138* (3A), A882-A893.

111. Zhang, Q. F.; Zhang, W. X.; Wan, W. H.; Cui, Y.; Wang, E. G., Lithium Insertion In Silicon Nanowires: An ab Initio Study. *Nano Lett.* **2010,** *10* (9), 3243-3249.

112. Giannozzi, P.; Baroni, S.; Bonini, N.; Calandra, M.; Car, R.; Cavazzoni, C.; Ceresoli, D.; Chiarotti, G. L.; Cococcioni, M.; Dabo, I.; Dal Corso, A.; de Gironcoli, S.; Fabris, S.; Fratesi, G.; Gebauer, R.; Gerstmann, U.; Gougoussis, C.; Kokalj, A.; Lazzeri, M.; Martin-Samos, L.; Marzari, N.; Mauri, F.; Mazzarello, R.; Paolini, S.; Pasquarello, A.; Paulatto, L.; Sbraccia, C.; Scandolo, S.; Sclauzero, G.; Seitsonen, A. P.; Smogunov, A.; Umari, P.; Wentzcovitch, R. M., QUANTUM ESPRESSO: a modular and open-source software project for quantum simulations of materials. *J. Phys.-Condes. Matter* **2009,** *21* (39), 19.

113. Perdew, J. P.; Chevary, J. A.; Vosko, S. H.; Jackson, K. A.; Pederson, M. R.; Singh, D. J.; Fiolhais, C., Atoms, molecules, solids, and surfaces - applications of the generalized gradient approximation for excange and correlation. *Phys. Rev. B* **1992,** *46* (11), 6671-6687.

114. Perdew, J. P.; Burke, K.; Ernzerhof, M., Generalized gradient approximation made simple. *Physical Review Letters* **1996,** *77* (18), 3865-3868.

115. Henkelman, G.; Uberuaga, B. P.; Jonsson, H., A climbing image nudged elastic band method for finding saddle points and minimum energy paths. *Journal of Chemical Physics* **2000,** *113* (22), 9901-9904.

116. Jonsson, H.; Mills, G.; Jacobsen, K. W., Classical and Quantum Dynamics in Condensed Phase Simulations. Berne, B. J.; Ciccotti, G.; Coker, D. F., Eds. World Scientific: Singapore, 1998.

117. Zhang, Q. F.; Cui, Y.; Wang, E. G., Anisotropic Lithium Insertion Behavior in Silicon Nanowires: Binding Energy, Diffusion Barrier, and Strain Effect. *J. Phys. Chem. C* **2011,** *115* (19), 9376-9381.

118. Arrouvel, C.; Parker, S. C.; Islam, M. S., Lithium Insertion and Transport in the TiO_2−B Anode Material: A Computational Study. *Chem. Mat.* **2009,** *21* (20), 4778-4783.

119. Tibbetts, K.; Miranda, C. R.; Meng, Y. S.; Ceder, G., An ab initio study of lithium diffusion in titanium disulfide nanotubes. *Chem. Mat.* **2007,** *19* (22), 5302-5308.

120. Uthaisar, C.; Barone, V., Edge Effects on the Characteristics of Li Diffusion in Graphene. *Nano Lett.* **2010,** *10* (8), 2838-2842.

121. Tang, Q.; Zhou, Z.; Shen, P., Are MXenes Promising Anode Materials for Li Ion Batteries? Computational Studies on Electronic Properties and Li Storage Capability of Ti_3C_2 and $Ti_3C_2X_2$ (X = F, OH) Monolayer. *Journal of the American Chemical Society* **2012,** *134* (40), 16909-16916.

122. Suarez-Martinez, I.; Ewels, C.; Ke, X.; Van Tendeloo, G.; Thiess, S.; Drube, W.; Felten, A.; Pireaux, J. J.; Ghijsen, J.; Bittencourt, C., Study of the Interface between Rhodium and Carbon Nanotubes. *ACS Nano* **2010,** *4* (3), 1680-1686.

123. Eder, D.; Windle, A. H., Carbon-inorganic hybrid materials: The carbon-nanotube/TiO_2 interface. *Advanced Materials* **2008,** *20* (9), 1787-+.

124. Kim, K. T.; Il Cha, S.; Gemming, T.; Eckert, J.; Hong, S. H., The Role of Interfacial Oxygen Atoms in the Enhanced Mechanical Properties of Carbon-Nanotube-Reinforced Metal Matrix Nanocomposites. *Small* **2008,** *4* (11), 1936-1940.

125. Kou, R.; Shao, Y. Y.; Mei, D. H.; Nie, Z. M.; Wang, D. H.; Wang, C. M.; Viswanathan, V. V.; Park, S.; Aksay, I. A.; Lin, Y. H.; Wang, Y.; Liu, J., Stabilization of Electrocatalytic Metal Nanoparticles at Metal-Metal Oxide-Graphene Triple Junction Points. *Journal of the American Chemical Society* **2011,** *133* (8), 2541-2547.

126. Zhou, J. S.; Song, H. H.; Chen, X. H.; Huo, J. P., Diffusion of Metal in a Confined Nanospace of Carbon Nanotubes Induced by Air Oxidation. *Journal of the American Chemical Society* **2010,** *132* (33), 11402-11405.

127. Li, X. L.; Jia, Y.; Cao, A. Y., Tailored Single-Walled Carbon Nanotube-CdS Nanoparticle Hybrids for Tunable Optoelectronic Devices. *ACS Nano* **2010,** *4* (1), 506-512.

128. Zhou, J.; Song, H.; Ma, L.; Chen, X., Magnetite/graphene nanosheet composites: interfacial interaction and its impact on the durable high-rate performance in lithium-ion batteries. *RSC Advances* **2011**.

129. Liao, H.; Karki, K.; Zhang, Y.; Cumings, J.; Wang, Y., Interfacial Mechanics of Carbon Nanotube@Amorphous-Si Coaxial Nanostructures. *Advanced Materials* **2011,** *23* (37), 4318-4322.

130. Durgun, E.; Dag, S.; Ciraci, S.; Gulseren, O., Energetics and electronic structures of individual atoms adsorbed on carbon nanotubes. *Journal of Physical Chemistry B* **2004,** *108* (2), 575-582.

131. Gao, H. G.; Zhou, J. A.; Lu, M. H.; Fa, W.; Chen, Y. F., First-principles study of the IVA group atoms adsorption on graphene. *Journal of Applied Physics* **2010,** *107* (11).

132. Akturk, E.; Ataca, C.; Ciraci, S., Effects of silicon and germanium adsorbed on graphene. *Applied Physics Letters* **2010,** *96* (12).

133. Raghavachari, K.; Logovinsky, V., Structure and bonding in small silicon clusters. *Physical Review Letters* **1985,** *55* (26), 2853-2856.

134. Ballone, P.; Andreoni, W.; Car, R.; Parrinello, M., Equilibrium structures and finite temperature properties of silicon microclusters from ab initio molecular-dynamics calculations. *Physical Review Letters* **1988,** *60* (4), 271-274.

135. Jing, X. D.; Troullier, N.; Dean, D.; Binggeli, N.; Chelikowsky, J. R.; Wu, K.; Saad, Y., Ab initio molecular-dynamics simulations of Si clusters using the higher-order finite-difference-pseudopotential method. *Phys. Rev. B* **1994,** *50* (16), 12234-12237.

136. Yoo, S. H.; Zeng, X. C., Motif transition in growth patterns of small to medium-sized silicon clusters. *Angew. Chem.-Int. Edit.* **2005,** *44* (10), 1491-1494.

137. Sai, L. W.; Tang, L. L.; Zhao, J. J.; Wang, J.; Kumar, V., Lowest-energy structures and electronic properties of Na-Si binary clusters from ab initio global search. *Journal of Chemical Physics* **2011,** *135* (18).

138. Ma, L.; Zhao, J. J.; Wang, J. G.; Wang, B. L.; Lu, Q. L.; Wang, G. H., Growth behavior and magnetic properties of Si_nFe (n=2-14) clusters. *Phys. Rev. B* **2006,** *73* (12).

139. Ho, K. M.; Shvartsburg, A. A.; Pan, B. C.; Lu, Z. Y.; Wang, C. Z.; Wacker, J. G.; Fye, J. L.; Jarrold, M. F., Structures of medium-sized silicon clusters. *Nature* **1998,** *392* (6676), 582-585.

140. Honea, E. C.; Ogura, A.; Murray, C. A.; Raghavachari, K.; Sprenger, W. O.; Jarrold, M. F.; Brown, W. L., Raman-spectra of size-selected silicon clusters and comparison with calculated structures. *Nature* **1993,** *366* (6450), 42-44.

141. Bloomfield, L. A.; Freeman, R. R.; Brown, W. L., Photofragmentation of mass-resolved Si_{2-12}^+ clusters. *Physical Review Letters* **1985,** *54* (20), 2246-2249.

142. Raghavachari, K., Theoretical-study of small silicon clusters - equilibrium geometries and electronic-structures of Si_{2-7}, Si_{10}. *Journal of Chemical Physics* **1986,** *84* (10), 5672-5686.

143. Zhao, Q.; Nardelli, M. B.; Lu, W.; Bernholc, J., Carbon nanotube-metal cluster composites: A new road to chemical sensors? *Nano Lett.* **2005,** *5* (5), 847-851.

144. Zhou, M.; Zhang, A. H.; Dai, Z. X.; Zhang, C.; Feng, Y. P., Greatly enhanced adsorption and catalytic activity of Au and Pt clusters on defective graphene. *Journal of Chemical Physics* **2010,** *132* (19).

145. Allred, A. L., Electronegativity values from thermochemical data. *Journal of Inorganic & Nuclear Chemistry* **1961,** *17* (3-4), 215-221.

146. Tomanek, D.; Schluter, M. A., Calculation of magic numbers and the stability of small Si clusters. *Physical Review Letters* **1986,** *56* (10), 1055-1058.

147. Li, X. L.; Liu, Y. Q.; Fu, L.; Cao, L. C.; Wei, D. C.; Wang, Y., Efficient synthesis of carbon nanotube-nanoparticle hybrids. *Adv. Funct. Mater.* **2006,** *16* (18), 2431-2437.

148. Durgun, E.; Dag, S.; Bagci, V. M. K.; Gülseren, O.; Yildirim, T.; Ciraci, S., Systematic study of adsorption of single atoms on a carbon nanotube. *Phys. Rev. B* **2003,** *67* (20), 201401.

149. Gülseren, O.; Yildirim, T.; Ciraci, S., Tunable Adsorption on Carbon Nanotubes. *Physical Review Letters* **2001,** *87* (11), 116802.

150. Durgun, E.; Ciraci, S.; Yildirim, T., Functionalization of carbon-based nanostructures with light transition-metal atoms for hydrogen storage. *Phys. Rev. B* **2008,** *77* (8), 085405.

151. Chopra, N.; Majumder, M.; Hinds, B. J., Bifunctional carbon nanotubes by sidewall protection. *Adv. Funct. Mater.* **2005,** *15* (5), 858-864.

152. Friddle, R. W.; Lemieux, M. C.; Cicero, G.; Artyukhin, A. B.; Tsukruk, V. V.; Grossman, J. C.; Galli, G.; Noy, A., Single functional group interactions with individual carbon nanotubes. *Nat. Nanotechnol.* **2007,** *2* (11), 692-697.

153. Li, X. L.; Thompson, J. D.; Zhang, Y. Y.; Brady, C. I.; Zou, G. F.; Mack, N. H.; Williams, D.; Duque, J. G.; Jia, Q. X.; Doorn, S. K., Efficient synthesis of tailored magnetic carbon nanotubes via a noncovalent chemical route. *Nanoscale* **2011,** *3* (2), 668-673.

154. Zhang, J.; Zou, H.; Qing, Q.; Yang, Y.L.; Li, Q.W.; Liu, Z.; Guo, X.Y.; Du, Z.L., Effect of chemical oxidation on the structure of single-walled carbon nanotubes. *Journal of Physical Chemistry B* **2003,** *107* (16), 3712-3718.

155. Balasubramanian, K.; Burghard, M., Chemically functionalized carbon nanotubes. *Small* **2005,** *1* (2), 180-192.

156. Feller, D.; Dixon, D. A.; Nicholas, J. B., Binding Enthalpies for Alkali Cation−Benzene Complexes Revisited. *The Journal of Physical Chemistry A* **2000,** *104* (48), 11414-11419.

157. Zhao, X. Y.; Wei, C. M.; Yang, L.; Chou, M. Y., Quantum confinement and electronic properties of silicon nanowires. *Physical Review Letters* **2004,** *92* (23).

158. Ng, M. F.; Zhou, L. P.; Yang, S. W.; Sim, L. Y.; Tan, V. B. C.; Wu, P., Theoretical investigation of silicon nanowires: Methodology, geometry, surface modification, and electrical conductivity using a multiscale approach. *Phys. Rev. B* **2007,** *76* (15), 11.

159. Hochbaum, A. I.; Chen, R. K.; Delgado, R. D.; Liang, W. J.; Garnett, E. C.; Najarian, M.; Majumdar, A.; Yang, P. D., Enhanced thermoelectric performance of rough silicon nanowires. *Nature* **2008,** *451* (7175), 163-U5.

160. Buda, F.; Kohanoff, J.; Parrinello, M., Optical properties of porous silicon: A first-principles study. *Physical Review Letters* **1992,** *69* (8), 1272-1275.

161. Cui, Y.; Lieber, C. M., Functional nanoscale electronic devices assembled using silicon nanowire building blocks. *Science* **2001,** *291* (5505), 851-853.

162. Tian, B.Z.; Zheng, X.L.; Kempa, T.J.; Fang, Y.; Yu, N.F.; Yu, G.H.; Huang, J.L.; Lieber, C.M., Coaxial silicon nanowires as solar cells and nanoelectronic power sources. *Nature* **2007,** *449* (7164), 885-U8.

163. Barman, S.; Sen, P.; Das, G. P., Ti-Decorated Doped Silicon Fullerene: A Possible Hydrogen-Storage Material. *J. Phys. Chem. C* **2008,** *112* (50), 19963-19968.

164. Lan, J. H.; Cao, D. P.; Wang, W. C., $Li_{12}Si_{60}H_{60}$ Fullerene Composite: A Promising Hydrogen Storage Medium. *ACS Nano* **2009,** *3* (10), 3294-3300.

165. Cahangirov, S.; Topsakal, M.; Akturk, E.; Sahin, H.; Ciraci, S., Two- and One-Dimensional Honeycomb Structures of Silicon and Germanium. *Physical Review Letters* **2009,** *102* (23).

166. Guzman-Verri, G. G.; Voon, L., Electronic structure of silicon-based nanostructures. *Phys. Rev. B* **2007,** *76* (7).

167. Liu, C. C.; Feng, W. X.; Yao, Y. G., Quantum Spin Hall Effect in Silicene and Two-Dimensional Germanium. *Physical Review Letters* **2011,** *107* (7).

168. Chen, L.; Liu, C.-C.; Feng, B.; He, X.; Cheng, P.; Ding, Z.; Meng, S.; Yao, Y.; Wu, K., Evidence for Dirac Fermions in a Honeycomb Lattice Based on Silicon. *Physical Review Letters* **2012,** *109* (5), 056804.

169. Xu, C.; Luo, G.; Liu, Q.; Zheng, J.; Zhang, Z.; Nagase, S.; Gao, Z.; Lu, J., Giant magnetoresistance in silicene nanoribbons. *Nanoscale* **2012,** *4* (10), 3111-3117.

170. O'Hare, A.; Kusmartsev, F. V.; Kugel, K. I., A Stable "Flat″ Form of Two-Dimensional Crystals: Could Graphene, Silicene, Germanene Be Minigap Semiconductors? *Nano Lett.* **2012,** *12* (2), 1045-1052.

171. Ni, Z.Y.; Liu, Q.H.; Tang, K.C.; Zheng, J.X.; Zhou, J.; Qin, R.; Gao, Z.X.; Yu, D.; Lu, J., Tunable Bandgap in Silicene and Germanene. *Nano Lett.* **2012,** *12* (1), 113-118.

172. Drummond, N. D.; Zólyomi, V.; Fal'ko, V. I., Electrically tunable band gap in silicene. *Phys. Rev. B* **2012,** *85* (7), 075423.

173. Jose, D.; Datta, A., Structures and electronic properties of silicene clusters: a promising material for FET and hydrogen storage. *Physical Chemistry Chemical Physics* **2011,** *13* (16), 7304-7311.

174. Lu, N.; Li, Z. Y.; Yang, J. L., Electronic Structure Engineering via On-Plane Chemical Functionalization: A Comparison Study on Two-Dimensional Polysilane and Graphane. *J. Phys. Chem. C* **2009,** *113* (38), 16741-16746.

175. Feng, B.J.; Ding, Z.; Meng, S.; Yao, Y.; He, X.Y.; Cheng, P.; Chen, L.; Wu, K.H., Evidence of Silicene in Honeycomb Structures of Silicon on Ag(111). *Nano Lett.* **2012,** *12* (7), 3507-3511.

176. Fleurence, A.; Friedlein, R.; Ozaki, T.; Kawai, H.; Wang, Y.; Yamada-Takamura, Y., Experimental Evidence for Epitaxial Silicene on Diboride Thin Films. *Physical Review Letters* **2012,** *108* (24), 245501.

177. Vogt, P.; De Padova, P.; Quaresima, C.; Avila, J.; Frantzeskakis, E.; Asensio, M.; Resta, A.; Ealet, B.; Le Lay, G., Silicene: Compelling Experimental Evidence for Graphenelike Two-Dimensional Silicon. *Physical Review Letters* **2012,** *108* (15).

178. Tang, Y. H.; Pei, L. Z.; Chen, Y. W.; Guo, C., Self-assembled silicon nanotubes under supercritically hydrothermal conditions. *Physical Review Letters* **2005,** *95* (11).

179. Chen, Y. W.; Tang, Y. H.; Pei, L. Z.; Guo, C., Self-assembled silicon nanotubes grown from silicon monoxide. *Advanced Materials* **2005,** *17* (5), 564-+.

180. De Crescenzi, M.; Castrucci, P.; Scarselli, M.; Diociaiuti, M.; Chaudhari, P. S.; Balasubramanian, C.; Bhave, T. M.; Bhoraskar, S. V., Experimental imaging of silicon nanotubes. *Applied Physics Letters* **2005,** *86* (23).

181. Yamada, S.; Fujiki, H., Experimental evidence for nanostructural tube formation of silicon atoms. *Japanese Journal of Applied Physics Part 2-Letters & Express Letters* **2006,** *45* (29-32), L837-L839.

182. Mbenkum, B. N.; Schneider, A. S.; Schutz, G.; Xu, C.; Richter, G.; van Aken, P. A.; Majer, G.; Spatz, J. P., Low-Temperature Growth of Silicon Nanotubes and Nanowires on Amorphous Substrates. *ACS Nano* **2010,** *4* (4), 1805-1812.

183. Zhang, R. Q.; Lee, H. L.; Li, W. K.; Teo, B. K., Investigation of possible structures of silicon nanotubes via density-functional tight-binding molecular dynamics simulations and ab initio calculations. *Journal of Physical Chemistry B* **2005,** *109* (18), 8605-8612.

184. Durgun, E.; Tongay, S.; Ciraci, S., Silicon and III-V compound nanotubes: Structural and electronic properties. *Phys. Rev. B* **2005,** *72* (7).

185. Bai, J.; Zeng, X. C.; Tanaka, H.; Zeng, J. Y., Metallic single-walled silicon nanotubes. *Proceedings of the National Academy of Sciences of the United States of America* **2004,** *101* (9), 2664-2668.

186. Zhang, M.; Kan, Y. H.; Zang, O. J.; Su, Z. M.; Wang, R. S., Why silicon nanotubes stably exist in armchair structure? *Chemical Physics Letters* **2003,** *379* (1-2), 81-86.

187. Fagan, S. B.; Baierle, R. J.; Mota, R.; da Silva, A. J. R.; Fazzio, A., Ab initio calculations for a hypothetical material: Silicon nanotubes. *Phys. Rev. B* **2000,** *61* (15), 9994-9996.

188. Yang, X. B.; Ni, J., Electronic properties of single-walled silicon nanotubes compared to carbon nanotubes. *Phys. Rev. B* **2005,** *72* (19).

189. Singh, A. K.; Kumar, V.; Briere, T. M.; Kawazoe, Y., Cluster assembled metal encapsulated thin nanotubes of silicon. *Nano Lett.* **2002,** *2* (11), 1243-1248.

190. Singh, A. K.; Briere, T. M.; Kumar, V.; Kawazoe, Y., Magnetism in transition-metal-doped silicon nanotubes. *Physical Review Letters* **2003,** *91* (14).

191. Shan, G. C.; Wang, Y.; Huang, W., Electronic transport characteristics in silicon nanotube field-effect transistors. *Physica E-Low-Dimensional Systems & Nanostructures* **2011,** *43* (9), 1655-1658.

192. Lan, J. H.; Cheng, D. J.; Cao, D. P.; Wang, W. C., Silicon nanotube as a promising candidate for hydrogen storage: From the first principle calculations to grand canonical Monte Carlo simulations. *J. Phys. Chem. C* **2008,** *112* (14), 5598-5604.

193. Li, K. J.; Wang, W. C.; Cao, D. P., Novel Chemical Sensor for CO and NO: Silicon Nanotube. *J. Phys. Chem. C* **2011,** *115* (24), 12015-12022.

194. Sahin, H.; Cahangirov, S.; Topsakal, M.; Bekaroglu, E.; Akturk, E.; Senger, R. T.; Ciraci, S., Monolayer honeycomb structures of group-IV elements and III-V binary compounds: First-principles calculations. *Phys. Rev. B* **2009,** *80* (15).

195. Gao, B.; Kleinhammes, A.; Tang, X. P.; Bower, C.; Fleming, L.; Wu, Y.; Zhou, O., Electrochemical intercalation of single-walled carbon nanotubes with lithium. *Chemical Physics Letters* **1999,** *307* (3-4), 153-157.

196. Shimoda, H.; Gao, B.; Tang, X.; Kleinhammes, A.; Fleming, L.; Wu, Y.; Zhou, O., Lithium intercalation into opened single-wall carbon nanotubes: Storage capacity and electronic properties. *Physical Review Letters* **2002,** *88* (1).

197. Yang, J. L.; Liu, H. J.; Chan, C. T., Theoretical study of alkali-atom insertion into small-radius carbon nanotubes to form single-atom chains. *Phys. Rev. B* **2001,** *64* (8), art. no.-085420.

198. Geim, A. K., Graphene: Status and Prospects. *Science* **2009,** *324* (5934), 1530-1534.

199. Huang, X.Q.; Tang, S.H.; Mu, X.L.; Dai, Y.; Chen, G.X.; Zhou, Z.Y.; Ruan, F.X.; Yang, Z.L.; Zheng, N.F., Freestanding palladium nanosheets with plasmonic and catalytic properties. *Nat. Nanotechnol.* **2011,** *6* (1), 28-32.

200. Yu, T.; Lim, B.; Xia, Y. N., Aqueous-Phase Synthesis of Single-Crystal Ceria Nanosheets. *Angew. Chem.-Int. Edit.* **2010,** *49* (26), 4484-4487.

201. Yu, J.; Fan, J.; Lv, K., Anatase TiO_2 nanosheets with exposed (001) facets: improved photoelectric conversion efficiency in dye-sensitized solar cells. *Nanoscale* **2010,** *2* (10), 2144-2149.

202. Zeng, Z. Y.; Yin, Z. Y.; Huang, X.; Li, H.; He, Q. Y.; Lu, G.; Boey, F.; Zhang, H., Single-Layer Semiconducting Nanosheets: High-Yield Preparation and Device Fabrication. *Angew. Chem.-Int. Edit.* **2011,** *50* (47), 11093-11097.

203. Son, J. S.; Wen, X. D.; Joo, J.; Chae, J.; Baek, S. I.; Park, K.; Kim, J. H.; An, K.; Yu, J. H.; Kwon, S. G.; Choi, S. H.; Wang, Z. W.; Kim, Y. W.; Kuk, Y.; Hoffmann, R.; Hyeon, T., Large-Scale Soft Colloidal Template Synthesis of 1.4 nm Thick CdSe Nanosheets. *Angew. Chem.-Int. Edit.* **2009,** *48* (37), 6861-6864.

204. Nakano, H.; Mitsuoka, T.; Harada, M.; Horibuchi, K.; Nozaki, H.; Takahashi, N.; Nonaka, T.; Seno, Y.; Nakamura, H., Soft synthesis of single-crystal silicon monolayer sheets. *Angew. Chem.-Int. Edit.* **2006,** *45* (38), 6303-6306.

205. Spencer, M.J.S.; Morishita, T.; Mikami, M.; Snook, I.; Sugiyama, Y.; Nakano, H., The electronic and structural properties of novel organomodified Si nanosheets. *Physical Chemistry Chemical Physics* **2011,** *13* (34), 15418-15422.

206. Nakano, H.; Nakano, M.; Nakanishi, K.; Tanaka, D.; Sugiyama, Y.; Ikuno, T.; Okamoto, H.; Ohta, T., Preparation of Alkyl-Modified Silicon Nanosheets by

Hydrosilylation of Layered Polysilane (Si_6H_6). *Journal of the American Chemical Society* **2012,** *134* (12), 5452-5455.

207. Beaulieu, L. Y.; Eberman, K. W.; Turner, R. L.; Krause, L. J.; Dahn, J. R., Colossal reversible volume changes in lithium alloys. *Electrochem. Solid State Lett.* **2001,** *4* (9), A137-A140.

208. Gao, B.; Sinha, S.; Fleming, L.; Zhou, O., Alloy formation in nanostructured silicon. *Advanced Materials* **2001,** *13* (11), 816-+.

209. Choi, N. S.; Yao, Y.; Cui, Y.; Cho, J., One dimensional Si/Sn - based nanowires and nanotubes for lithium-ion energy storage materials. *J. Mater. Chem.* **2011,** *21* (27), 9825-9840.

210. Su, L.; Zhou, Z.; Ren, M., Core double-shell $Si@SiO_2@C$ nanocomposites as anode materials for Li-ion batteries. *Chemical Communications* **2010,** *46* (15), 2590-2592.

211. Su, L.; Jing, Y.; Zhou, Z., Li ion battery materials with core-shell nanostructures. *Nanoscale* **2011,** *3* (10), 3967-3983.

212. Yoo, E.; Kim, J.; Hosono, E.; Zhou, H.; Kudo, T.; Honma, I., Large reversible Li storage of graphene nanosheet families for use in rechargeable lithium ion batteries. *Nano Lett.* **2008,** *8* (8), 2277-2282.

213. Peng, B.; Cheng, F. Y.; Tao, Z. L.; Chen, J., Lithium transport at silicon thin film: Barrier for high-rate capability anode. *Journal of Chemical Physics* **2010,** *133* (3).

214. Chan, T. L.; Chelikowsky, J. R., Controlling Diffusion of Lithium in Silicon Nanostructures. *Nano Lett.* **2010,** *10* (3), 821-825.

215. Buriak, J. M., Organometallic Chemistry on Silicon and Germanium Surfaces. *Chem. Rev.* **2002,** *102* (5), 1271-1308.

216. Leu, P. W.; Shan, B.; Cho, K. J., Surface chemical control of the electronic structure of silicon nanowires: Density functional calculations. *Phys. Rev. B* **2006,** *73* (19).

217. Gao, N.; Zheng, W. T.; Jiang, Q., Density functional theory calculations for two-dimensional silicene with halogen functionalization. *Physical Chemistry Chemical Physics* **2012,** *14* (1), 257-261.